

8-2013

Evaluation Of Presage® Dosimeters For Brachytherapy Sources And The 3D Dosimetry And Characterization Of The New Agx100 125I Seed Model

Olivia Huang

Follow this and additional works at: https://digitalcommons.library.tmc.edu/utgsbs_dissertations



Part of the [Medical Biophysics Commons](#)

Recommended Citation

Huang, Olivia, "Evaluation Of Presage® Dosimeters For Brachytherapy Sources And The 3D Dosimetry And Characterization Of The New Agx100 125I Seed Model" (2013). *Dissertations and Theses (Open Access)*. 393.

https://digitalcommons.library.tmc.edu/utgsbs_dissertations/393

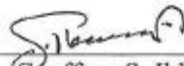
This Thesis (MS) is brought to you for free and open access by the MD Anderson UTHealth Houston Graduate School at DigitalCommons@TMC. It has been accepted for inclusion in Dissertations and Theses (Open Access) by an authorized administrator of DigitalCommons@TMC. For more information, please contact digcommons@library.tmc.edu.

**Evaluation of PRESAGE[®] dosimeters for brachytherapy
sources and the 3D dosimetry and characterization
of the new AgX100 ¹²⁵I seed model**

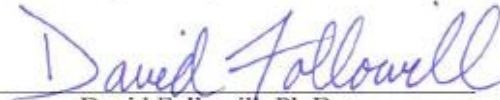
By

Olivia Y. Huang, B.S.

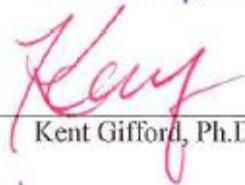
Approved:



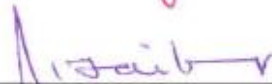
Geoffrey S. Ibbott, Ph.D.
Supervisory Professor



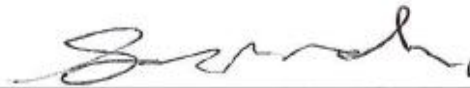
David Followill, Ph.D.



Kent Gifford, Ph.D.



Ramesh Tailor, Ph.D.



Shouhao Zhou, Ph.D.

APPROVED:

Dean, The University of Texas-Houston

The University of Texas-Houston M.D. Anderson Cancer Center

Graduate School of Biomedical Sciences

Evaluation of PRESAGE[®] dosimeters for brachytherapy

sources and the 3D dosimetry and characterization

of the new AgX100 ¹²⁵I seed model

A

THESIS

Presented to the faculty of

The University of Texas

M. D. Anderson Cancer Center

Graduate School of Biomedical Sciences

In Partial Fulfillment

Of the Requirements

For the Degree of

SPECIALIZED MASTER OF SCIENCE

By

Olivia Huang, B.S.

Houston, Texas

August 2013

Acknowledgements

First and foremost, I would like to acknowledge my advisor, Dr. Geoffrey Ibbott. Thank you for your patience, guidance, and encouragement throughout this project and these past two years of graduate school. I would also like to thank the members of my committee - Dr. David Followill, Dr. Kent Gifford, Dr. Shouhou Zhou, and Dr. Ramesh Tailor – for their expert advice and time invested in this project. I would like to also acknowledge Dr. John Adamovics for manufacturing the several batches of dosimeters used in this project. Furthermore, I would like to thank Ryan Grant, M.S. for teaching me how to use the PRESAGE[®]/DMOS system and for being the PRESAGE[®] guru of our lab group. To the rest of our lab group- Slade Klawikowski, Ph.D., Mitchell Carroll, M.S., and Yvonne Roed- thank you for all of their help and suggestions, especially during the troubleshooting phase of this project. I would also like to thank Theragenics Corporation for sending us a higher activity AgX100 seed for this project.

The staff members at the ADCL at M.D. Anderson Cancer Center - Stephanie Lampe, Charles Darcy-Clarke, and Regina Garcia – were amazingly kind and patient in helping me obtain sources and letting me into the LDR Brachytherapy room doors for each and every irradiation. I would also like to thank my fellow classmates at the RPC, particularly James Neihart, Christopher Pham, and Elizabeth McKenzie, for their support, encouragement, and their sense of humor, which helped keep me sane during stressful times.

Dedication

To Shuja-

Thank you for your patience and encouragement. These past two years in graduate school would have been terrifying without you.

To my parents-

Thank you both for always believing in me and for giving me all the tools in life to succeed.

Evaluation of PRESAGE[®] dosimeters for brachytherapy sources and the 3D dosimetry and characterization of the new AgX100 ¹²⁵I seed model

Publication No. _____

Olivia Huang, B.S.

Supervisory Professor: Geoffrey S. Ibbott, Ph.D.

With continuous new improvements in brachytherapy source designs and techniques, method of 3D dosimetry for treatment dose verifications would better ensure accurate patient radiotherapy treatment. This study was aimed to first evaluate the 3D dose distributions of the low-dose rate (LDR) Amersham 6711 Oncoseed[™] using PRESAGE[®] dosimeters to establish PRESAGE[®] as a suitable brachytherapy dosimeter. The new AgX100 ¹²⁵I seed model (Theragenics Corporation) was then characterized using PRESAGE[®] following the TG-43 protocol.

PRESAGE[®] dosimeters are solid, polyurethane-based, 3D dosimeters doped with radiochromic leuco dyes that produce a linear optical density response to radiation dose. For this project, the radiochromic response in PRESAGE[®] was captured using optical-CT scanning (632 nm) and the final 3D dose matrix was reconstructed using the MATLAB software. An Amersham 6711 seed with an air-kerma strength of approximately 9 U was used to irradiate two dosimeters to 2 Gy and 11 Gy at 1 cm to evaluate dose rates in the r=1 cm to r=5 cm region. The dosimetry parameters were compared to the values published in the updated AAPM Report No. 51 (TG-43U1). An AgX100 seed with an air-kerma strength

of about 6 U was used to irradiate two dosimeters to 3.6 Gy and 12.5 Gy at 1 cm. The dosimetry parameters for the AgX100 were compared to the values measured from previous Monte-Carlo and experimental studies[1,2].

In general, the measured dose rate constant, anisotropy function, and radial dose function for the Amersham 6711 showed agreements better than 5% compared to consensus values in the $r=1$ to $r=3$ cm region. The dose rates and radial dose functions measured for the AgX100 agreed with the MCNPX and TLD-measured values within 3% in the $r=1$ to $r=3$ cm region. The measured anisotropy function in PRESAGE[®] showed relative differences of up to 9% with the MCNPX calculated values. It was determined that post-irradiation optical density change over several days was non-linear in different dose regions, and therefore the dose values in the $r=4$ to $r=5$ cm regions had higher uncertainty due to this effect. This study demonstrated that within the radial distance of 3 cm, brachytherapy dosimetry in PRESAGE[®] can be accurate within 5% as long as irradiation times are within 48 hours.

Table of Contents

Signature Page	i
Title Page	ii
Acknowledgements.....	iii
Dedications	iv
Abstract.....	v
Table of Contents.....	vii
List of Figures.....	x
List of Tables	xii
Chapter 1- Introduction.....	1
1.1 Statement of Problem	1
1.1.1 General Problem Area	1
1.1.2 Specific Problem Area.....	2
1.2 Background.....	2
1.2.1 Brachytherapy.....	2
1.2.1.1 Amersham 6711.....	6
1.2.1.2 AgX100.....	7
1.2.2 History of Gel Dosimetry	9
1.2.3 PRESAGE [®] Dosimeters	12
1.2.3.1 Characteristics of PRESAGE [®]	12
1.2.3.2 Optical-CT Imaging.....	15
1.2.3.2.1 The OCTOPUS.....	15
1.2.3.2.2 Duke Mid-sized Optical-CT Scanner	16
1.2.3.3. Drawbacks of PRESAGE [®]	18
1.2.3.4 Previous work with PRESAGE [®]	19

1.3 Hypothesis and Specific Aim	21
Chapter 2- Materials and Methods	21
2.1 Dosimeter Design	21
2.2 Treatment Set-up and Delivery.....	27
2.2.1 Pre-Irradiation.....	27
2.2.2 Dose Calibration	28
2.2.3 Treatment Delivery.....	30
2.3 Imaging and Analysis	33
2.3.1 Optical-CT Imaging.....	33
2.3.2 Data Acquisition in CERR.....	34
2.4 TG-43 Formalism	37
2.4.1 Air-kerma Strength	39
2.4.2 Dose Rate.....	40
2.4.3 Dose Rate Constant.....	42
2.4.4. Geometry Function	43
2.4.5 Anisotropy Function	44
2.4.6 Radial Dose Function	46
Chapter 3- Results and Discussion for the Amersham 6711.....	48
3.1 Dose Rate.....	48
3.2 Dose Rate Constant.....	51
3.3 Anisotropy Function	52
3.4 Radial Dose Function	56
Chapter 4- Results and Discussion for the AgX100.....	58
4.1 General Discussion of Results	58
4.2 Dose Rate	60

4.3 Dose Rate Constant.....	61
4.4 Anisotropy Function	62
4.5 Radial Dose Function	66
Chapter 5- Discussion of the over-response in PRESAGE[®] at low doses.....	68
5.1 Post-irradiation OD change over time	68
5.2 Method of correction	75
Chapter 6- Uncertainty Analysis.....	78
6.1 Uncertainty in the Dose Rate Constant.....	78
6.2 Uncertainty in Anisotropy Function	80
6.3 Uncertainty in Radial Dose Function	80
Chapter 7- Conclusion.....	80
Appendix A.....	83
Appendix B.....	86
References.....	97
Vita	103

List of Figures

Figure 1. Amersham 6711 OncoSeed model design[14]	6
Figure 2. Dimensions of the Theragenics AgX100	8
Figure 3 Example of an irradiated PRESAGE [®] dosimeter.....	12
Figure 4. Example of a Calibration Curve for PRESAGE [®]	14
Figure 5. Diagram illustrating main components of the DMOS.....	17
Figure 6. The o-MeO-LMG PRESAGE [®] formulation	22
Figure 7. PRESAGE [®] dosimeter with 0.4 cm diameter channel	24
Figure 8. PRESAGE [®] dosimeter with 1.5 cm diameter channel	25
Figure 9 PRESAGE [®] plugs for 0.4 cm diameter channel.....	26
Figure 10 PRESAGE [®] plugs for 1.5 cm diameter channels	26
Figure 11. Catheter inserted into the 0.4 cm diameter PRESAGE [®] plug.....	27
Figure 12. PRESAGE [®] cuvettes for dose calibration	28
Figure 13. PRESAGE [®] cuvette setup at orthovoltage unit for calibration	29
Figure 14. Dosimeter (shielded from light) positioned in rice tank for backscatter	31
Figure 15. Dosimeter with plug, catheter, and 6711 seed.....	32
Figure 16. Screen capture of the Duke 3D Dosimetry Lab interface for reconstruction ..	34
Figure 17. Sagittal, Transverse and Coronal views of reconstructed dose cube in CERR36	
Figure 18. Dose line profile generated in CERR	36
Figure 19. Coordinate system for brachytherapy dosimetry as defined from TG-43	37
Figure 20. Transverse bisecting plane determined in CERR.....	39
Figure 21. Diagram illustrating the 12 measurement points in PRESAGE [®] for each point of interest for dose rate, anisotropy function, and radial dose function calculations.....	41

Figure 22. Amersham 6711: Dose Rate Comparison	49
Figure 23. Isodose lines in a large dosimeter displayed in CERR.....	50
Figure 24. AgX100 Anisotropy functions for $r = 1$ cm.	54
Figure 25. AgX100 Anisotropy functions for $r = 2$ cm.	54
Figure 26. AgX100 Anisotropy functions for $r = 3$ cm.	55
Figure 27. AgX100 Anisotropy functions for $r = 4$ cm.	55
Figure 28. AgX100 Anisotropy functions for $r = 5$ cm.	56
Figure 29. Comparison of AgX100 radial dose functions.	58
Figure 30. AgX100 Dose Rate Comparison.	61
Figure 31. AgX100 Anisotropy Function at $r = 1$ cm.....	65
Figure 32. AgX100 Anisotropy Function at $r = 2$ cm.....	65
Figure 33. AgX100 Anisotropy Function at $r = 3$ cm.....	66
Figure 34. AgX100: Radial Dose Function Comparison.....	67
Figure 35. Calibration curve demonstrating linearity in dose response.....	69
Figure 36. OD change over time for PRESAGE® at 0 Gy	70
Figure 37. OD change over time for PRESAGE® at 1 Gy	71
Figure 38. OD change over time for PRESAGE® at 3 Gy	71
Figure 39. OD change over time for PRESAGE® at 5 Gy	72
Figure 40. OD change over time for PRESAGE® at 7 Gy	72
Figure 41. Isodose lines of AgX100-irradiated large channel dosimeter	75

List of Tables

Table 1: Categories of brachytherapy as defined in ICRU Report 38[13]	4
Table 2: List of radionuclides and their characteristics[14,15,16].....	5
Table 3. Doses calculated for 20 cGy at 5 cm	23
Table 4. Dose rate using 2D formalism for the Amersham 6711	40
Table 5. Dose rates using 2D formalism for the AgX100	40
Table 6. Dose rate constants for both ^{125}I seed models.....	43
Table 7. Geometry Factors for L=3 mm	44
Table 8. Geometry Factors for L=3.5 mm	44
Table 9. Anisotropy Function Table for Amersham 6711	45
Table 10. Radial Dose Functions for the Amersham 6711	47
Table 11. Amersham 6711: Dose Rate Comparison.....	48
Table 12. Amersham 6711: Comparison of the doses delivered	50
Table 13. Amersham 6711: Comparison of the dose rate constant	51
Table 14. Amersham 6711: Anisotropy Functions measured in PRESAGE [®]	52
Table 15. Amersham 6711 Anisotropy Functions: Relative Differences (%)	53
Table 16. Amersham 6711: Radial Dose Function Comparison	57
Table 17. Dose Comparison in 0.4 cm channel dosimeter	58
Table 18. Dose Comparison in 1.5 cm channel dosimeter	59
Table 19. AgX100: Dose Rate Comparison	60
Table 20. Dose Rate constants of the AgX100.....	62
Table 21. Dose Rate Constant Comparison	62
Table 22. AgX100: Anisotropy Function measured in PRESAGE [®]	63

Table 23. AgX100: TLD-measured Anisotropy Functions[2].....	63
Table 24. AgX100: Monte-Carlo calculated Anisotropy Functions[1]	64
Table 27. AgX100- Radial Dose Function Comparison.....	66
Table 28. OD change at several time points post-irradiation.....	69
Table 29. OD change at several time points post-irradiation (continued)	69
Table 30. Table describing dose deposited on Day 1 at r=4cm and the calculated OD- Ratio.....	76
Table 31. “Corrected” doses at each radial distance for the 6711-irradiated dosimeter...	77
Table 32. Uncertainty in PRESAGE [®] measurements of the dose rate constant.....	79

1 Introduction

1.1 Statement of Problem

1.1.1 General Problem Area

Radiation therapy has advanced dramatically in complexity since the first paper on the concept of Intensity Modulated Radiation Therapy (IMRT) was published in 1994[3]. Cutting-edge technology allows for radiotherapy methods to continuously improve conformality to the target volume, which can result in higher radiation doses administered to the tumor site to eradicate cancer while keeping normal tissue toxicity low. However, with such rapid advances it is imperative to balance the complex radiation therapy techniques with suitable quality assurance (QA) methods to ensure accurate clinical patient treatment and patient safety.

Currently, three dimensional (3D) IMRT dosimetric verification for commissioning and patient-specific QA is generally performed with the combination of absolute point dose measurements using a calibrated ion chamber and a two dimensional (2D) planar dosimetric analysis with radiochromic film or a diode array[4]. These methods provide a dosimetric check of volumetric sampling. However, the complexity of multiple beams with high doses and steep dose gradients make it very difficult to accurately and comprehensively verify the actual 3D dose distributions. With radiation doses as high as 40 Gy per treatment fraction in stereotactic radiosurgery, it is clear that an accurate method of comprehensive 3D dose verification through actual measurements is the next step in QA techniques to keep up with radiotherapy advancements and to ensure accurate patient treatment.

1.1.2 Specific Problem Area

More specifically among the variety of radiation therapy techniques, an accurate method of 3D dosimetry in brachytherapy is needed. Both high dose rate (HDR) and low dose rate (LDR) brachytherapy are commonly used modalities in radiation oncology centers worldwide. Methods in positioning sources in a designed formation to shape the dose distribution are advancing in brachytherapy, such as the COMS eye plaque for LDR treatment of choroidal melanoma[5] or various HDR applicator devices like the SAVI device for accelerated partial breast irradiation[6]. For the COMS eye plaque in particular, only a select few have carefully evaluated the COMS eye plaque dosimetry[7] and biological effective dose[8] through Monte Carlo simulations. 3D dosimetric verifications through experimental methods have yet to be published.

The success of LDR multi-source irradiations relies heavily on the rapid dose fall-off beyond the tumor volume, and typically doses as high as 85 Gy (typical eye plaque prescription dose) are delivered to the target. With high doses delivered to small volumes, a reliable QA method of 3D dosimetry for these brachytherapy devices is important for patient treatment. Additionally, a method of 3D dosimetry for LDR sources would greatly simplify the experimental methods in obtaining data for dosimetric characterization of new radioactive seed models.

1.2 Background

1.2.1 Brachytherapy

Brachytherapy is a technique in radiation therapy where one or several sealed radioactive sources are placed in close proximity to the tumor or treatment site using

interstitial, intracavitary, intravascular, or surface applicator methods. From its Greek derivation “*brachy*,” brachytherapy literally means ‘short range therapy,’ which refers to the short therapeutic range of the emitted radiation from the decay of the radioisotope.

Brachytherapy seeds are commonly used in oncology centers worldwide for radiation therapy, typically in prostate, cervical, breast, and eye plaque brachytherapy treatments.

Not long after Marie Curie’s discovery of Radium-226 in 1898, the concept of inserting a radium-filled tube into a tumor for clinical treatment of cancer followed in 1901 by Pierre Curie[9]. By 1904, small amounts of radium encapsulated in glass tubes were used clinically through applications on the skin surface and intratumoral implantations[9]. However, high costs for radium and difficulties in establishing an effective treatment method resulted in the decline of brachytherapy use until the discovery of the method to create artificial radionuclides in 1934, by Irene and Frederic Joliot-Curie[10]. Man-made radionuclides allowed for more control over the amount of administered radioactivity and the sizes and shapes of the encapsulated radioactivity. More options in the emitted energy range and half-life also became available and the start of a modern age of brachytherapy began. Remote afterloading technology, which greatly reduced personnel exposure to high activity sources, was introduced by Walstam and Henschke *et al* in the early 1960s, ultimately paving the way for HDR brachytherapy[11].

The main advantage of brachytherapy is the ability to manually position radioactive sources within or near the cancer site for exceptionally high doses to be delivered to the tumor volume. Since radiation dose falls off rapidly with distance according to the inverse square law, only the immediate region surrounding the treatment site is irradiated, while most normal tissue, particularly organs at risk, is spared of dose. Additionally, the dose rate

is much lower in brachytherapy, especially in LDR brachytherapy, compared to external beam radiation therapy. A lower dose rate renders a higher radiobiological advantage since longer periods of time between damaging “hits” allows for increased probability of repair of sublethally damaged DNA[9]. Furthermore, HDR and LDR brachytherapy typically have relatively short treatment times of less than 55 days, which advantageously hinders tumor repopulation[12].

The three main categories of dose rates defined in the International Commission on Radiation Units and Measurements Report 38[13] are shown in Table 1 below.

Category	Dose Rate
Low Dose Rate (LDR)	0.4 to 2 Gy per hour
Medium Dose Rate (MDR)	2 to 12 Gy per hour
High Dose Rate (HDR)	Greater than 12 Gy per hour

Table 1: Categories of brachytherapy as defined in ICRU Report 38[13]

Clinically-used sources for LDR brachytherapy currently include ^{125}I , ^{103}Pd , and ^{131}Cs , while sources used in HDR brachytherapy include ^{137}Cs , ^{60}Co , and ^{192}Ir . In the United States, ^{192}Ir is the only source used for HDR brachytherapy. However, ^{60}Co and ^{137}Cs are still used for HDR brachytherapy in other countries. Table 2 below lists the basic characteristics of each radionuclide.

Radionuclide	Dose rate	Half-life	Mean energy (gamma and x-rays)
¹²⁵ I	LDR	59.40 days	28.37 keV
¹⁰³ Pd	LDR	16.99 days	20.74 keV
¹³¹ Cs	LDR	9.7 days	30.4 keV
¹³⁷ Cs	HDR	30.08 years	661.7 keV
⁶⁰ Co	HDR	5.27 years	1252.9 keV
¹⁹² Ir	HDR	73.81 days	380.0 keV

Table 2: List of radionuclides and their characteristics[14,15,16]

LDR brachytherapy procedures typically require permanent implants of the sources, where dose delivery continues over the lifetime of the radioactivity. LDR brachytherapy has a great radiobiological benefit over HDR brachytherapy because it allows for increased time for DNA repair[9] and tumor cell reoxygenation[17] and more liberty to deliver higher overall radiation dose to the treatment volume. Furthermore, the manual insertions of individual LDR sources are advantageous for irregularly shaped target volumes compared to the less flexible catheters for HDR brachytherapy[18]. On the other hand, HDR brachytherapy offers drastically shorter irradiation times- typically ranging from less than a minute to a few minutes. This is not only very time-efficient for both the hospital and the patient, but greatly reduces cost for the patient as well[19]. Also, the remote afterloader device used for automatic insertion of the HDR source allows control from a separate room, which significantly reduces exposure to the hospital staff. Radiation exposure to the general public decreases as well, since no radioactivity remains in the patient after he or she leaves after each treatment.

1.2.1.1 Amersham model 6711 ^{125}I sources

^{125}I has a half-life of 59.43 days and decays by electron capture with emission of characteristic x-rays and gamma rays. The weighted mean energy of the photons emitted is 28.37 keV, and the highest photon energy emitted is 35.492 keV weighted at 0.0668 photons per disintegration[14]. The most commonly emitted photon energies are at 27.202 keV (0.406 photons per disintegration) and 27.472 keV (0.757 photons per disintegration), which are also the two lowest photon energies. The Amersham Health 6711 OncoSeed model (GE Healthcare, IL) of the ^{125}I source is the most extensively used source model for LDR brachytherapy since it became available in 1983. Figure 1 depicts the dimensions and structure of the source.

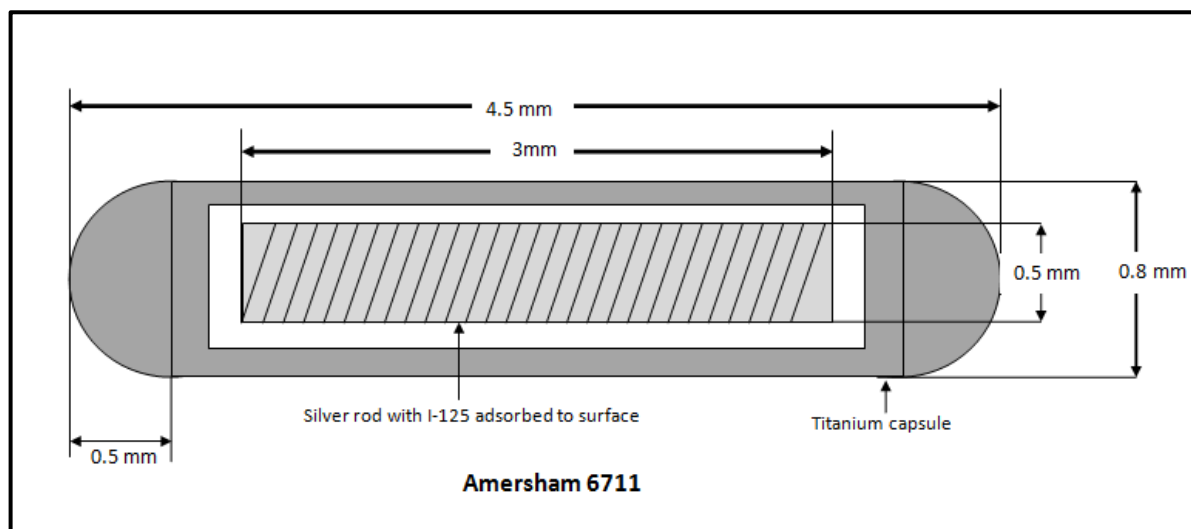


Figure 1. Amersham 6711 OncoSeed model design[14]

^{125}I is adsorbed onto a 3.0 mm long, 0.5 mm diameter silver rod. The rod is placed in a titanium capsule – with outer dimensions 4.5 mm in length and 0.8 mm in diameter – and is welded on both ends. The silver rod serves as a helpful x-ray marker visible in CT scans for proper positioning and patient dosimetry. Typical apparent activities for permanent

interstitial implants with ^{125}I seeds are within the range of 0.19 to 1.016 mCi or 0.243 to 1.291 U[20].

The Amersham 6711 seed model has been thoroughly evaluated by numerous researchers in the past few decades. The American Association for Physicists in Medicine (AAPM) published an Update of the Task Group No. 43 Report (TG-43U1) for brachytherapy dose calculations, which includes the general consensus dosimetry parameters of the Amersham 6711 widely followed for clinical use today[14]. The dosimetry parameters include the dose-rate constant, geometry function, radial dose function, and anisotropy function. These parameters were established and published in the TG-43U1 report to serve as the recommended standards for accurate brachytherapy dosimetry in the United States and internationally. Each parameter depends on the specific design of the radioactive source, and the consensus values were agreed upon by the members of the Brachytherapy Subcommittee through careful evaluation of the strengths and limitations of the techniques used for dosimetric characterization.

1.2.1.2 Theragenics model AgX100 ^{125}I source

In 2010, Theragenics Corporation (Buford, GA) introduced the AgX100 ^{125}I seed model. This model design was based on the Amersham 6711 seed model and has an almost identical design. The dimensions of the AgX100 are shown in Figure 2.

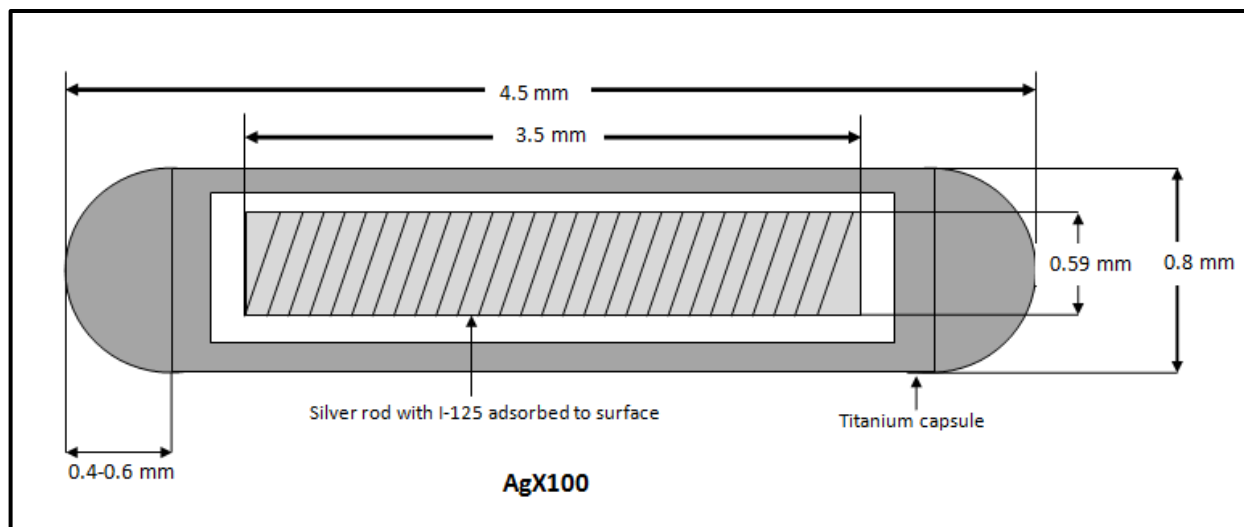


Figure 2. Dimensions of the Theragenics AgX100

Similar to the 6711 model, the AgX100 ^{125}I source is encapsulated in a titanium capsule welded on both ends. The seed has an outer length of 4.5 mm and a diameter of 0.8 mm. The main difference lies in the dimensions of the ^{125}I covered silver rod. The active length of the AgX100 is approximately 3.5 mm with a diameter of 0.59 mm, which is slightly larger than the active dimensions of the Amersham 6711 source. The AgX100 seed still remains to be a new source model to radiation oncology clinics and little work has been invested in the evaluation of this seed.

The AAPM TG-43U1 recommends “independent and redundant dosimetric characterizations” for any new seed models manufactured for clinical use[14]. Two main studies have evaluated and characterized the AgX100 seed model following TG-43 formalism. In 2012, Mourtada *et al* determined the dosimetric parameters of the AgX100 through Monte Carlo calculations[1]. Comparing the dose distributions surrounding the AgX100 in liquid water versus the 6711 model, the authors determined that the TG-43U1 dosimetric parameters for the two models were very similar except in the regions closest in proximity to the seed. These findings are expected since the active length of the new seed

model is much longer than the one in the 6711 model. Thus, Mourtada *et al* recommended separate TG-43U1 parameters to be established to account for these geometrical differences. Chen *et al* also determined the dosimetric parameters of the AgX100 model in 2012[2]. The authors used a germanium spectrometer to determine the photon energies emitted by the seed and LiF thermoluminescent dosimeters (TLDs) in a solid water phantom to determine the dosimetric parameters. The photon energy spectrum emitted from the AgX100 was almost indistinguishable from the spectrum published in TG-43U1 for the Amersham 6711. In comparison to the Monte Carlo-derived values by Mourtada *et al*, the measured dose rate constant, radial dose functions, and anisotropy functions were generally within 5%. The anisotropy functions for $\Theta < 10^\circ$, however, showed a rather large disagreement of up to 20.5% compared to the Monte Carlo-calculated anisotropy functions. The authors believe that the discrepancies may be due to intrinsic uncertainties in TLDs and the confined area of TLDs for dose measurements. Following the recommendations of these authors and TG-43, further evaluation of the dosimetric parameters of the AgX100 seed model is necessary for accurate dosimetry and optimal clinical use for patients.

1.2.2 History of Gel Dosimetry

Gel dosimetry has continuously been a topic of interest in medical physics since Andrews *et al* first investigated radiation depth doses in chloral hydrate diffused agar gel with spectrophotometry and pH probes in 1957[21]. The appealing offer of a direct method of capturing high spatial resolution 3D dose distributions over the complex and computationally intensive methods in calculating and verifying dose distributions has advanced several important accomplishments in the last few decades.

In 1984, Gore et al. presented the first method of imaging radiation dose distributions using magnetic resonance imaging (MRI) in Fricke gels, a ferrous sulphate chemical dosimeter (developed by Fricke and Morse in 1927) that undergoes an oxidative conversion from ferrous ion (Fe^{2+}) to ferric ion (Fe^{3+}) when exposed to radiation. It was demonstrated that the relaxation time of the protons in ferric ions was longer than ferrous ions, and thus a higher resulting concentration of ferric ions rendered a longer total relaxation rate, which allowed for dose estimations in Fricke gels[22]. Unfortunately, unreliable spatial accuracy due to the diffusion of ions in Fricke gel[23] resulted in difficulties yet to be resolved despite various attempts with chelating agents[24] and gelling agents to minimize the diffusion.

The focus of gel dosimetry then turned to polymer gels. In 1992, Maryanski *et al.* developed an agarose-based polymer gel called BANANA, which is an acronym for the chemical components: Bis, Acrylamide, Nitrous oxide, AND Agarose. This gel undergoes radiation-induced polymerization and cross-linking of polymer chains which produces a stable dose response over time- a great advantage over the ion diffusion problem in Fricke gel[25]. Changes in proton relaxation rates in the polymers due to the polymerization and cross-linking still allowed for the MRI imaging capability for dose analysis. In 1993, Maryanski *et al* improved the polymer gel by using gelatin instead of agarose and thus giving it the new name, BANG (acronym for Bis, Acrylamide, Nitrogen and aqueous Gelatin)[26]. The relaxation rate of water in gelatin gel is substantially lower than in agarose gels, therefore the background signal of the polymer gel is minimized and the dynamic range of the gel dosimeter increased[27]. A succession of further improvements in BANG gel

formulations led to several investigations of the clinical applications of polymer gels demonstrating great potential for clinical use.

Gore *et al*[28] and Maryanski *et al*[29] presented in 1996 the method of optical computed tomography (optical-CT) imaging as a more efficient and sensitive technique compared to MRI for imaging gel dosimeters. Oldham *et al* advanced the optical-CT technique in the 2003-2004[30,31], eventually leading to the design and manufacture of the optical-CT scanner used in this project.

Although polymer gel dosimetry has high potential as a 3D dosimeter, several drawbacks limit the practical clinical use of these gels. The greatest disadvantage of polymer gels is the high sensitivity to atmospheric oxygen. Oxygen acts as a free-radical inhibitor in polymer gels and results in the inhibition of polymerization response to radiation[26]. The polymer gels need to be synthesized and stored in an oxygen-free environment, which presents complications in the manufacturing process and clinical-use. Additionally, radiation dose response in polymer gel relies on light scattering effects that generate a change in the optical density. The scattered light photons have been shown to cause scatter artifacts within the gel which affect the accuracy of the dose response. The external container required to hold the gel also introduces large edge artifacts with optical-CT due to the differences in refractive indices of the container, gel, and the matching fluid[32]. Thus, PRESAGE[®] dosimeters were introduced in 2003 by J. Adamovics and M. J. Maryanski[33].

1.2.3 PRESAGE[®] Dosimeters

1.2.3.1 Characteristics of PRESAGE[®]

PRESAGE[®] dosimeters are polyurethane-based dosimeters manufactured by Heuris Pharma, LLC. The optically clear polyurethane matrix is solid, as opposed to gel, and is doped with Leuco Malachite Green (LMG) dye. Oxidation of LMG by free radicals induced by radiation produces malachite green. Upon exposure to radiation, a linear optical density response (or color change) to radiation dose is generated[32,34]. Several types of PRESAGE[®] formulations composed of varying amounts of LMG and free radical initiators are available, depending on the type of radiation used.



Figure 3 Example of an irradiated PRESAGE[®] dosimeter

There are several advantages in PRESAGE[®] over the previously mentioned gel dosimeters. The response to radiation occurs by the absorption of light rather than the scatter of light, which is a great improvement over gels to reduce spectral artifacts. PRESAGE[®] is

not sensitive to atmospheric gases, which removes any potential oxygen-induced inaccuracies and makes it much more convenient to use. An external container for support is also not necessary, which greatly reduces edge artifacts from optical-CT imaging[35]. This also allows for PRESAGE[®] to be easily synthesized into any desirable shape and size.

From 2006 to 2008, Guo *et al*, J. Adamovics *et al*, and Sakhalkar *et al* paved the way for PRESAGE[®] by thoroughly evaluating and characterizing the dosimeter response to radiation. The PRESAGE[®] dose response does not demonstrate any dependence on external beam photon energy nor dose rate. Irradiations with the photon energies of 1.25 MeV (Co-60), 6 MV, 10 MV, and 18 MV all displayed linear dose responses[34,35]. Electrons at the specific energy of 16 MeV were also evaluated and shown to demonstrate a linear response in PRESAGE[®][32]. Dose rates ranging from 0.66 Gy min⁻¹ to 10 Gy min⁻¹ showed linearity in OD change up to doses as high as 50 Gy[34].

Unlike Fricke gel, diffusion of the malachite green does not occur in the polyurethane[34]. The dose response in PRESAGE[®] is stable within the first few hours post-irradiation, although certain formulations have shown that the signal can fade over time[35] or increase in response (color bleaching) by about 4% per 24 hour period post-irradiation[34,35]. To account for any signal deviation post-irradiation, a calibration curve for the change in OD to absolute dose is typically generated through irradiating several PRESAGE[®] cuvettes (from the same manufactured batch of PRESAGE[®] dosimeters) to a range of known doses. The cuvettes are read-out following the same irradiation to dose read-out time scale as used for the experimental dosimeters. This not only accounts for any signal changes post-irradiation, but also quantifies the sensitivity of PRESAGE[®] for each batch

manufactured. Below is an example of a calibration curve from one batch of PRESAGE[®] demonstrating the linearity of dose response and the sensitivity.

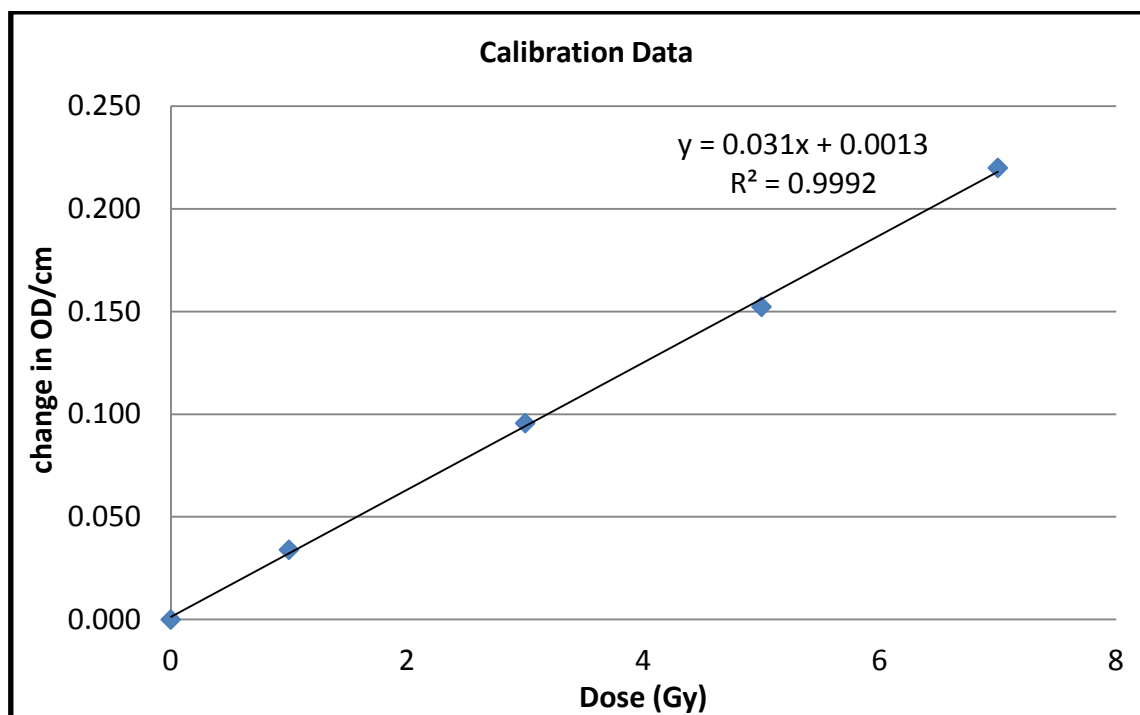


Figure 4. Example of a Calibration Curve for PRESAGE[®]

PRESAGE[®] has also been shown to have high reproducibility in radiochromic response between dosimeters. Guo *et al* demonstrated signal reproducibility among small volume PRESAGE[®] cuvettes (for readout through spectrophotometry) with a root mean square uncertainty of less than 2% [35] in OD response. Salkhalkar *et al* demonstrated reproducibility in large volume PRESAGE[®] dosimeters using a 3D gamma analysis (2% dose difference, 2 mm DTA) resulting in an excellent pass rate of 98% [36].

1.2.3.2 Optical-CT Imaging

1.2.3.2.1 The OCTOPUS®

The first scanning system coupled with the introduction of the PRESAGE® dosimetry system was the OCTOPUS, an optical tomographic system designed by Gore *et al.* in 1995. The scanner is available commercially (MGS Research Inc., Madison, CT) and provides a more time-efficient and cost-effective method of imaging both polymer gels and PRESAGE® dosimeters over the use of MRI for dosimeter readout. The basic setup of the scanner includes several mirrors that direct the 633 nm He-Ne laser beam (approximately 1 mm in diameter) to a reference photodiode for the initial light intensity, projections through the imaging tank, and finally to the photodiode array where the resulting light intensities are captured. The OCTOPUS was designed to produce linear scans so that one projection represents the intensities of one horizontal line across the dosimeter. Once all the line projections are acquired for one slice, the dosimeter is mechanically shifted vertically to a different level for acquisition of the next slice. Line projection acquisitions for each slice is repeated until the dosimeter has made a full 360° rotation[32]. The final 3D OD distribution is then reconstructed using filtered backprojection in MATLAB (The Math Works, Natick, MA).

The basic principles of using optical-CT to readout dose response in gel or PRESAGE® dosimeters can be understood with the basic equation[28]:

$$I(x) = I_o e^{-\int \mu(x,y) dy}$$

The laser beam is attenuated exponentially by $\mu(x,y)$, the optical attenuation coefficient per path length (y) at position (x) in the dosimeter. I_o is the intensity of the incident

monochromatic laser beam and $I(\mathbf{x})$ is the final intensity of the laser beam captured by the photodiode detector array. By measuring the initial and final intensities of the laser beam, the OD (or absorbance) can be calculated with the following equation:

$$OD = -\log(I/I_0)$$

While the OCTOPUS is a convenient, commercially-available scanner for 3D dosimeters, the line-by-line raster scanning is still time consuming. For example, it takes approximately 7 minutes to scan 150 line projections over one slice[32]. Assuming a slice is acquired every 2 degrees, it takes approximately 21 hours to scan one dosimeter. In 2010, Andrew Thomas and Mark Oldham introduced a faster and improved optical-CT design[37].

1.2.3.2.2 Duke Mid-Sized Optical-CT Scanner (DMOS)

The DMOS at the Radiological Physics Center was modeled after the Duke Large Field-of-view Optical-CT Scanner (DLOS), manufactured by Thomas *et al.* from Duke University Medical Center. The scanner was specifically designed for scanning PRESAGE[®] dosimeters. Instead of scanning one line at a time, this broad beam scanner is designed to capture all line-integrals at one projection angle simultaneously. Each projection angle can be acquired within seconds, thus reducing the scan time from several hours to just 10-20 minutes.

The DLOS/PRESAGE[®] system has been commissioned to be a 3D dosimetry system, demonstrating the highest spatial resolution at 0.5 mm size voxels with an MTF of 15%, good contrast up to 1 lp/mm, a dynamic range of at least 60 dB (corresponding to an

optical density up to 3 cm^{-1}), and low image noise after flood and dark corrected projection images[38].

The main components of the DMOS system are: two matching telecentric imaging lens, a LED light source, optical diffuser, bandpass filter, fluid bath, an aperture stop, and a CCD based camera. The figure below illustrates the main components in the DMOS.

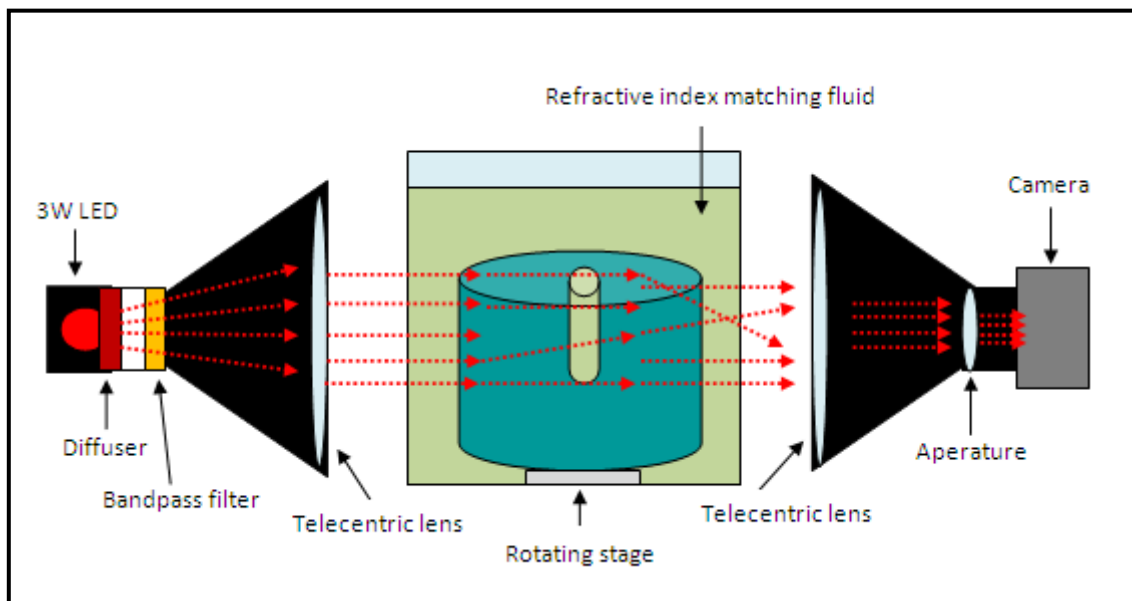


Figure 5. Diagram illustrating main components of the DMOS

The 3 Watt red LED source emits light first through the optical diffuser to create a more uniform light projection field. Schlieren bands are optical-CT imaging artifacts created from inconsistent amounts of light absorption at different wavelengths in PRESAGE[®][38]. To minimize this, Thomas and Newton *et al.* included a 10 nm bandpass filter to narrow the response profile of PRESAGE[®] to within the $632 \pm 5 \text{ nm}$ wavelength spectrum. To reduce edge artifacts caused by reflections and refractions at the dosimeter surface, dosimeters are placed in a tank filled with a fluid composed of a mixture of octyl salicylate, octyl

cinnamate, and light mineral oil. This fluid is properly adjusted to best match the RI of each specific batch of PRESAGE[®]. With a close RI match between the fluid and dosimeter, edge artifacts can be minimized to about 3 mm from the surface of the dosimeter in the reconstructed dose matrix.

A docking piece is permanently attached to the bottom of the dosimeter to allow for secure rotation of the dosimeter with the stage and image registration. By co-registering the pre-irradiation and post-irradiation images, any flaws or solid artifacts in the dosimeter can be subtracted out of the final image. Behind the imaging tank is another telecentric lens, and an aperture stop is positioned behind the lens at the focal point. The light is collimated with a tolerance of 0.1° to create projections from only the light parallel to the optical axis. The light projections are captured with a 12-bit monochromatic Basler camera with a 1040 × 1392 pixel CCD array.

1.2.3.3 Drawbacks of PRESAGE[®]

Despite the numerous advantages, there are two main drawbacks of PRESAGE[®] that require careful consideration. Firstly, UV light can initiate the oxidation reaction of LMG, which also induces OD change. Adamovics *et al* measured an OD change of approximately 1.373 cm⁻¹ in PRESAGE[®] dosimeters after 24 hours of room light exposure[39]. Therefore, the dosimeters must be shielded from as much UV exposure as possible to maintain low levels of noise in the dosimeters and prevent non-radiation induced chemical reactions in PRESAGE[®]. This is typically achieved by wrapping the dosimeters in black plastic bags and storing them in areas shielded from room light. PRESAGE[®] has also been shown to be fairly sensitive to temperature. Guo *et al* evaluated dose response in PRESAGE[®] at various

temperatures and concluded that the change in OD versus irradiation temperature is non-linear. PRESAGE[®] response increases with temperature due to higher radiochromic activity at elevated temperatures. To minimize background noise and non-linear radiochromic effects, the dosimeters are stored at 4°C until time of use. The dosimeters are also maintained at a constant temperature as best as possible throughout the pre-irradiation optical-CT scanning, irradiations, and post-irradiation optical-CT scanning processes. For absolute dose measurements, it is crucial to scan and irradiate PRESAGE[®] cuvettes at the same constant temperature the dosimeters were maintained at during the experimental process to preserve the OD changes as accurately as possible.

1.2.3.4 Previous work with PRESAGE[®]

Several studies have verified the feasibility and accuracy of PRESAGE[®] in capturing the 3D dosimetry of simple to complex IMRT treatment plans. In 2006, Guo *et al* demonstrated the feasibility of capturing 3D dose distributions in PRESAGE[®] by irradiating EBT film and PRESAGE[®] dosimeters with basic 5-beam open-field treatments with 6 MV photons. Their initial findings through 2D and 3D gamma analysis with the film and the ECLIPSE[®] treatment planning system (TPS) resulted in high passing rates for doses above 20% of 15 Gy prescribed to isocenter with a gamma criteria of 4% dose difference and 4 mm distance-to-agreement (DTA)[32]. In 2008, Oldham *et al* published comprehensive experimental data which verified the high precision and accuracy of PRESAGE[®] for complex IMRT plans. The authors created an 11 field coplanar plan with six small planning tumor volumes (PTVs) and a large organ-at-risk (OAR) region surrounding the PTVs. The resulting pass rates of 96% for the 3D gamma analysis with the ECLIPSE[®] TPS (3%, 3 mm DTA) and 91.4% for the 3D gamma analysis with EBT film (3%, 3 mm DTA) proved

PRESAGE[®] to be a better dosimeter for IMRT treatments[4]. Sakhalkar and Sterling *et al* published comparable gamma analysis results in cylindrical PRESAGE[®] inserts for the Radiological Physics Center (RPC) Head and Neck (H&N) IMRT phantom used for clinical trial credentialing purposes[40]. In 2010, Clift *et al* demonstrated good reproducibility (up to 4%) of radiosurgery field commissioning data in PRESAGE[®] with respect to film and mini-ion chambers[41].

3D dosimetry studies in PRESAGE[®] for proton therapy and brachytherapy have been ongoing as well, although conclusive quantitative results for dosimeter characterizations have yet to be published. Heard *et al* and Al-Nowais *et al* have investigated the dependence on LET in PRESAGE[®] for proton beams[42,43] and future characterization of the dosimeter for proton therapy is expected. In 2009, Wai *et al* compared anisotropy functions for distances at $r = 1$ cm and $r = 2$ cm of an HDR ¹⁹²Ir source measured in PRESAGE[®] to MCNP Monte Carlo calculations and EBT film[44]. The results showed agreement within 3% at 1 cm for anisotropy functions measured in PRESAGE[®] compared to their Monte Carlo study for a Nucletron microSelectron-HDR source. More extensive work for the characterization of PRESAGE[®] dosimeters for brachytherapy is necessary, especially for LDR sources. With established accuracy of PRESAGE[®] in measuring brachytherapy sources, new brachytherapy sources can be characterized through 3D dosimetry in PRESAGE[®].

1.3 Hypothesis and Specific Aims

The hypothesis of this study is that PRESAGE[®] dosimeters can reliably measure the 3D dosimetry of brachytherapy sources within $\pm 5\%$ to characterize the dosimetric parameters of the new AgX100 ¹²⁵I seed following the protocol specified by TG43-U1.

The specific aims for testing this hypothesis:

1. Develop a suitable PRESAGE[®] design for single brachytherapy source dosimetry, determine a suitable set-up for irradiation, and create a method for dose analysis.
2. Compare the measured and published consensus dosimetric parameters in AAPM TG-43U1 for the Amersham 6711 ¹²⁵I seed to establish PRESAGE[®] as a brachytherapy dosimeter.
3. Measure the delivered dose distribution and dosimetric parameters in PRESAGE[®] following the TG-43 formalism for the AgX100 ¹²⁵I source model.

2 Materials and Methods

2.1 Dosimeter Design

The PRESAGE[®] formulation used in this study was bis-(3-dimethylamino-phenyl)-(2-methoxy-phenyl)-methane (*o*-MeO-LMG). This formulation was chosen for its increased sensitivity, or higher dose response, which is appropriate for the low doses at farther distances from the brachytherapy sources.

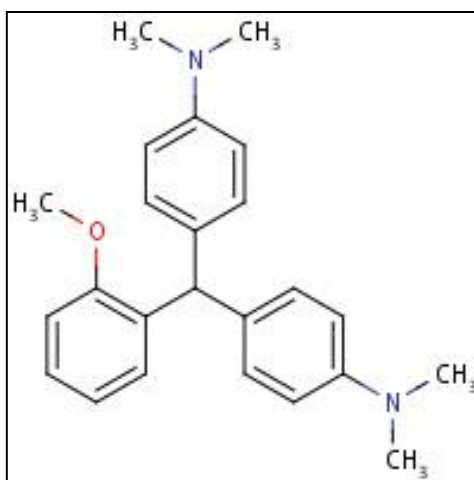


Figure 6. The o-MeO-LMG PRESAGE[®] formulation

The approximate mass density and electron density of this PRESAGE[®] formulation is 5.3% and 2.9% higher than the densities of water[45]. The effective atomic number (Z) of this formulation is 7.6, as reported by the manufacturer. This value is close to the effective Z of water at 7.42. PRESAGE[®] is therefore water-equivalent at MV energies, but may not be water-equivalent at the photon energies of ¹²⁵I. The uncertainty in the potentially increased photoelectric absorption (due to the higher effective Z) is included in the uncertainty analysis in Chapter 6.

Although TG-43U1 recommends dose measurements up to 10 cm away from the source reference point ($r = 0.5$ cm to $r = 10$ cm) for brachytherapy source characterization, the physical dimensions of the Duke Mid-size Optical-CT Scanner tank limit the size of the PRESAGE[®] dosimeters used for this project. The dosimeters were manufactured into a cylindrical shape made of approximately 1 kg of PRESAGE[®] with dimensions of approximately 12 cm in height and 11.4 cm in diameter.

Since the optical density of PRESAGE[®] increases linearly with dose and the radiation dose is a function of the inverse square of distance, doses up to several hundred

gray in the immediate vicinity of the source will result in a very large dose response (ie. the dye in the PRESAGE[®] matrix becomes very dark in color), which may affect the amount of light transmittance through the dosimeter in the optical-CT scanner. The minimum relative dose value that still produces an approximate dose response in PRESAGE[®] was estimated in this study to be at approximately 20 cGy based on preliminary experiments. The maximum dose that produces an accurate dose response has been estimated to be around 50 Gy based on previous studies[34]. Since the dosimeters are approximately 11.4 cm in diameter, dose measurements at $r = 5$ cm is the farthest distance away from the source that can be measured in the dosimeters used in this project. For the dose to be 20 cGy at 5 cm, the dose at 1 cm must be approximately 10.5 Gy or 181 Gy at 0.25 cm.

To eliminate potential imaging artifacts caused by such high optical density changes in the immediate vicinity of the source, the dosimeters were cast with a channel, or opening, in the center to remove the high dose gradient region altogether. The PRESAGE[®] channels were cast to be about 5.5 cm deep, with the bottom of the channel at the approximate center of the dosimeter. To evaluate the dose response in PRESAGE[®] and to ensure dose response accuracy, two different sized channels were designed. Table 3 provides approximate dose values necessary for the dose at 5 cm to be above 20 cGy.

Distance away from source (cm)	0.25	0.5	1	1.5	2	3	4	5
Dose (Gy)	196.5	49.1	11.4	4.6	2.3	0.8	0.4	0.2

Table 3. Doses calculated for 20 cGy at 5 cm

Large channels 1.5 cm in diameter were used to eliminate the high dose region from $r = 0$ cm to $r = 0.75$ cm and were irradiated to approximately 10.5 Gy at 1 cm. Imaging artifacts 3-4 mm from the edge of the PRESAGE[®] dosimeters caused by reflections and refractions on the PRESAGE[®] dosimeter surface limited dose measurements to the region 1 cm and beyond from the source. To include dose measurements closer to the source, smaller channels (0.4 cm in diameter) were designed and irradiated to much lower doses. The 0.4 cm channel eliminated high dose regions ($r = 0$ cm to $r = 0.2$ cm) allowed for accurate dose measurements from $r = 0.75$ cm to $r = 1.5$ cm. Therefore, with the combination of the two different sized channel dosimeters, dose measurements in the range of $r = 0.75$ cm to $r = 5$ cm could be acquired.

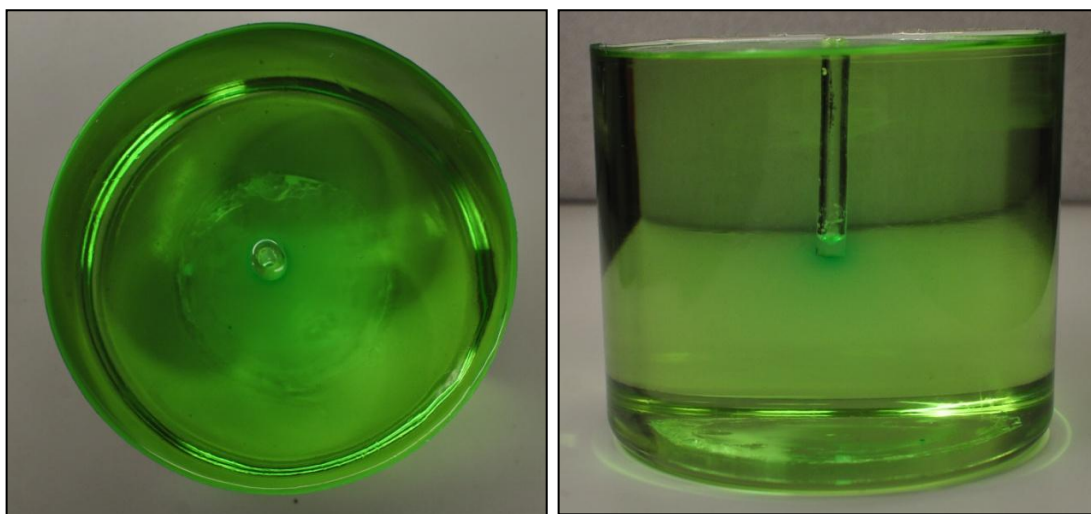


Figure 7. PRESAGE[®] dosimeter with 0.4 cm diameter channel

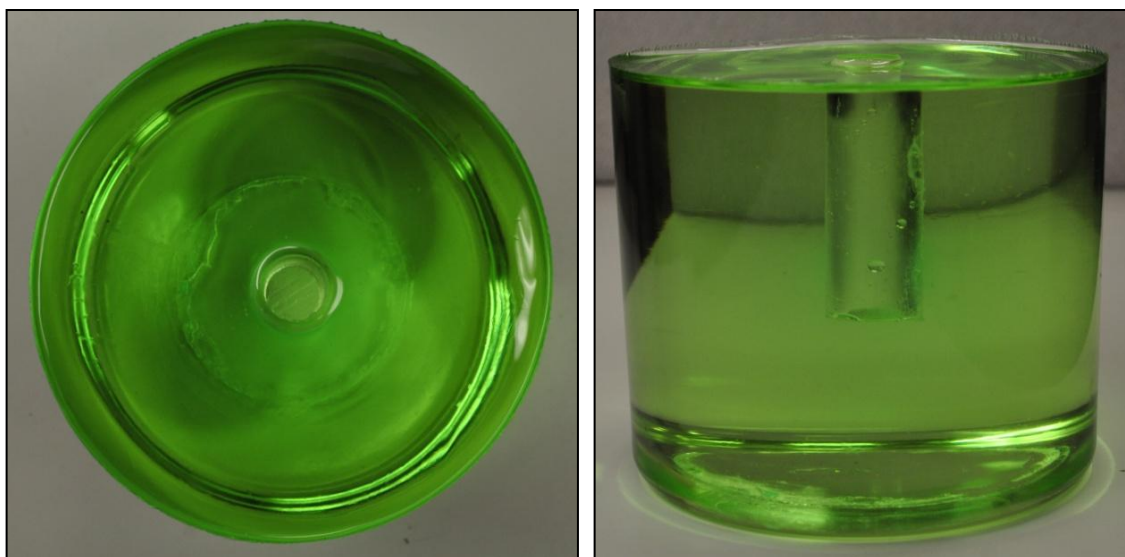


Figure 8. PRESAGE® dosimeter with 1.5 cm diameter channel

PRESAGE® plugs, or inserts, with the same dimensions as the channels were manufactured for insertion into the dosimeter channels during irradiation to provide a homogeneous photon attenuating medium. The plugs were then removed during the pre-scans and post-scans of the dosimeters. During optical-CT scanning, the channels were filled with refractive index matching fluid which resulted in an optical density change of zero after the pre-irradiation reconstructed image was subtracted from the post-irradiation reconstructed image. 0.2 cm diameter channels were drilled through the center of each plug to allow for a seed positioning catheter to be inserted tightly into the channel.

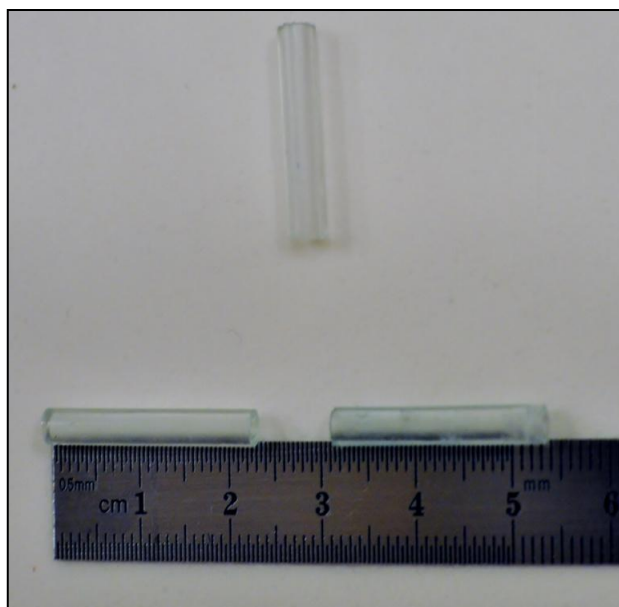


Figure 9 PRESAGE® plugs for 0.4 cm diameter channel



Figure 10 PRESAGE® plugs for 1.5 cm diameter channels

For both ^{125}I irradiations, a single seed was positioned at the bottom of a 1 mm diameter thin, plastic catheter. The main purposes of the catheter were to allow for secure insertion of the radioactive seed, easy removal of the seed from the bottom of the channel, and to ensure consistent positioning of the seed for each irradiation.

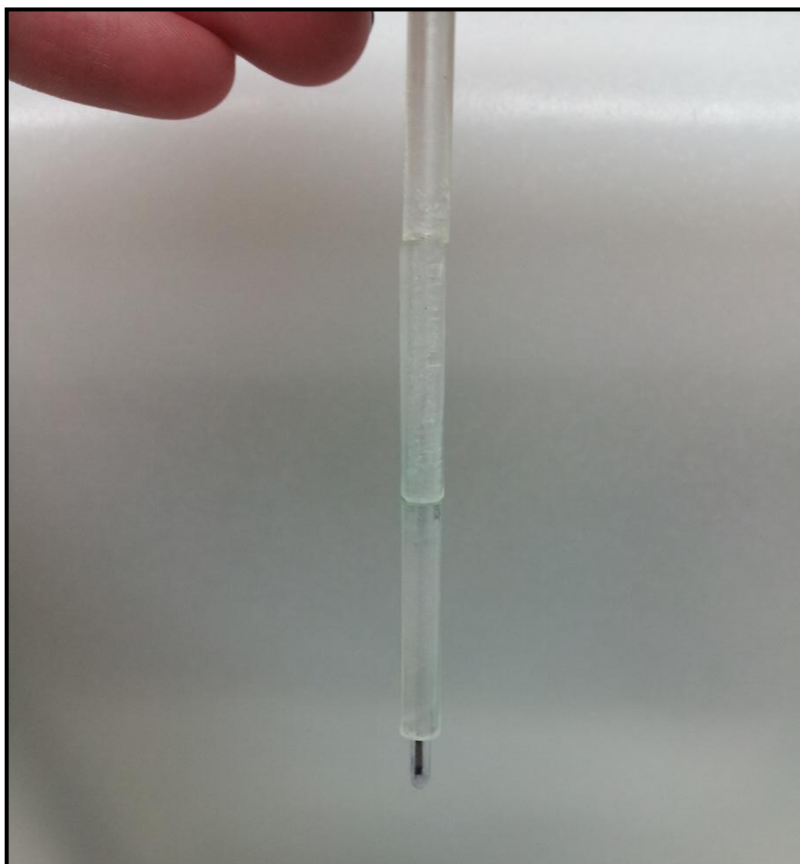


Figure 11. Catheter inserted into the 0.4 cm diameter PRESAGE[®] plug with bottom portion extended out for visualization purposes

2.2 Treatment Set-up and Delivery

2.2.1 Pre-Irradiation

Upon receiving the dosimeters shipped from Heuris Pharma, LLC, the PRESAGE[®] dosimeters were stored at 4° C and concealed from direct light exposure to reduce background radiochromic response[34]. Prior to pre-irradiation optical-CT scanning, the dosimeters were removed from the refrigerator and stored at room temperature for a minimum of four hours to allow for the dosimeters to thaw back to room temperature. Maintaining the dosimeters at a constant temperature from the start of the pre-irradiation scans to the end of the post-irradiation scans is believed to be crucial for consistency in dose

response. Dosimeters were scanned using the DMOS twenty-four hours prior to irradiation to capture background signal.

2.2.2 Dose Calibration

Several $1 \times 1 \times 4.3 \text{ cm}^3$ plastic cuvettes filled with PRESAGE[®] from the same batch as the dosimeters were used for dose calibration.



Figure 12. PRESAGE[®] cuvettes for dose calibration

Although radiochromic response in PRESAGE[®] has been shown to be independent of dose rate and photon energy at clinically relevant doses[34], the low photon energy range emitted by ¹²⁵I sources has not been thoroughly evaluated in previous studies. To maintain accurate calibration, the PRESAGE[®] cuvettes were irradiated with an orthovoltage unit at 75 kVp (mean energy around 25 keV) to mimic the weighted mean photon energy of 28 keV emitted by the ¹²⁵I radioactive decay.

Prior to irradiation, the absorbance of each cuvette was determined at 633 nm using a Genesys 20 spectrophotometer (Thermo Scientific, Waltham, MA) to measure the background optical density. Four cuvettes were irradiated to 1, 3, 5, and 7 Gy. A fifth cuvette was left un-irradiated to measure change in optical density over the time duration. The setup for the cuvette irradiation is shown in Figure 13.



Figure 13. PRESAGE[®] cuvette setup at orthovoltage unit for calibration

Solid water slabs were stacked to create a total thickness of 10 cm to account for backscatter radiation. Since the depth of maximum dose at 75 kVp is at the surface (SSD=50 cm), the cuvettes were placed on the top of the solid water setup in the center of an acrylic piece manufactured by the MDACC machine shop. Any air gaps between the cuvette and acrylic

were filled with old PRESAGE[®] cuvettes and water for consistent material electron densities.

After irradiation, the absorbance of each cuvette at 633 nm was measured again with a spectrophotometer. The change in optical density per cm (OD/cm) was determined by calculating the difference between the pre- and post-irradiation spectrophotometer readings. The calibration curve was used to convert the OD (per cm) values to the approximate radiation dose in Gray.

2.2.3 Treatment Delivery

To include backscatter radiation in PRESAGE[®] dosimetry, an appropriate water-equivalent material was investigated. Ideally, a dosimeter positioned in the center of a large water-filled tank for the duration of the irradiation would be the simplest and more accurate method of capturing the backscatter radiation. However, since PRESAGE[®] is partially soluble in water, white rice grains were selected as the backscatter material instead for its easier manageability and effectiveness.

Dosimeters were first wrapped in a black plastic zip-lock bag to shield the PRESAGE[®] from room light and to also serve as an outer protective cover for the dosimeter to prevent potential scratches on the surface of the dosimeter from the dry rice grains. The dosimeter was then placed in the center of plastic tank, and the tank was filled to the top with the rice grains. The rice grains created approximately 5 cm of backscatter material around the dosimeter.



Figure 14. Dosimeter (shielded from light) positioned in rice tank for backscatter

An Amersham 6711 seed with an activity of approximately 9 U was inserted into the catheter, and the catheter was positioned in the PRESAGE[®] plug such that the end of the catheter and the bottom of the seed were both as close to the bottom edge of the plug as possible. The plug was then fully inserted into the PRESAGE[®] channel for the duration of the irradiation. Figure 15 illustrates this configuration.



Figure 15. Dosimeter with plug, catheter, and 6711 seed

Dosimeters with 0.4 cm diameter channels were irradiated to 2.5 Gy at 1 cm for dose values in the range $r = 0.75$ to 1.5 cm. Dosimeters with 1.5 cm diameter channels were irradiated to 10.5 Gy at 1 cm for dose measurements in the range $r = 1.5$ to 5.0 cm. The irradiation times were approximately 25 hours and 138 hours for the small and large channel dosimeters respectively. The dosimeters were imaged within 4 hours post-irradiation.

An AgX100 source of approximately 6 U in air kerma strength provided by Theragenics Corporation (Buford, GA) was used for the small channel and large channel irradiation experiments using the same set-up as the experiments for the Amersham 6711. Since the seed has only been commercially-available for less than two years, seed strengths above 2 U are still in the experimental phase (not yet available for purchase). In an attempt to produce a higher activity seed, the manufacturer, for this project, used a 7 μm plating

thickness compared to the routine plating thickness of about 2 μm for the seed. The irradiation set-up was identical to the Amersham 6711 set-up. Radiation doses were increased to 3.6 Gy and 12.5 Gy at 1 cm for the small and large channel dosimeters in an attempt to improve dose response at larger radial distances. The time durations for the small and large channel dosimeter irradiations were approximately 45 hours (1.9 days) and 237 hours (9.9 days).

2.3 Imaging and Analysis

2.3.1 Optical-CT Imaging

To capture the change in optical density, each dosimeter was scanned prior to and post-irradiation to capture the background and final OD in the dosimeter. The dosimeters were imaged with a total of 720 projection images, with projection images taken every 0.5° rotation. Flood images were taken prior to imaging the dosimeter to capture inhomogeneities in the matching fluid and LED light field. Dark field images were also captured to correct for electronic noise.

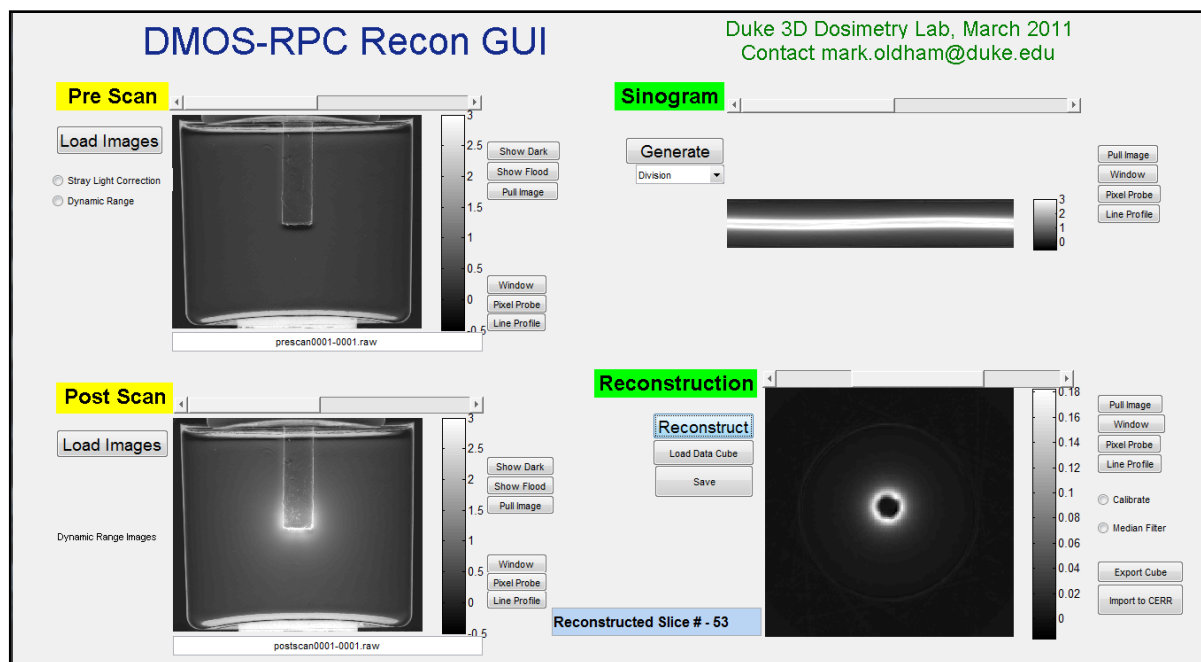


Figure 16. Screen capture of the Duke 3D Dosimetry Lab interface for reconstruction

The DMOS Matlab program (Duke University, NC) was used to reconstruct the change in OD in each of the 720 projection images of the PRESAGE[®] dosimeter. The combined reconstructed images together are referred to as a ‘dose cube’. The pre-irradiation and post-irradiation images were first loaded into the DMOS and corrected for imaging background noise using the flood and dark images. A 5×5 kernel median filter was applied to each pre-irradiation and post-irradiation projection image to reduce noise. The pre-irradiation images were then subtracted from the corresponding post-irradiation images and a resulting series of 2D sinograms were generated from the projection data, as shown in the upper right in the figure above. For the data image reconstruction, the “iradon” function in Matlab coupled with the Ram-lak filter was used to backproject the final dose cube from the sinograms. The dose cube was reconstructed to 1 mm voxel lengths.

2.3.2 Data Acquisition in CERR

The reconstructed dose cube showing the resulting radiation-induced optical density changes were imported from the DMOS program into the Computational Environment for Radiotherapy Research (CERR) platform. CERR is a widely-used and free Matlab software used to display and analyze treatment plans in radiation therapy research[46]. Once loaded into CERR, the change in OD values were scaled to dose values using the scale factor obtained from the calibration curve.

PRESAGE[®] is suspected to have volume effects that may affect the accuracy of dose values when the conversion factor for pixel to dose values, obtained from small volume PRESAGE[®], is applied to large 1 kg PRESAGE[®] dosimeters. Therefore, the converted dose values in CERR are re-normalized to the dose at $r = 1.5$ cm on the transverse bisecting plane of the seed. The relative dose values in PRESAGE[®] are measured in CERR using the “Dose Line Profile” tool. This tool function captures each dose pixel value along the user-selected line in the dosimeter and creates a plot of dose versus distance. Figure 17 below is an example of a reconstructed PRESAGE[®] dosimeter with a 1.5 cm channel displayed in CERR. Figure 18 is the dose line profile CERR projects from the line of data shown in Figure 17.

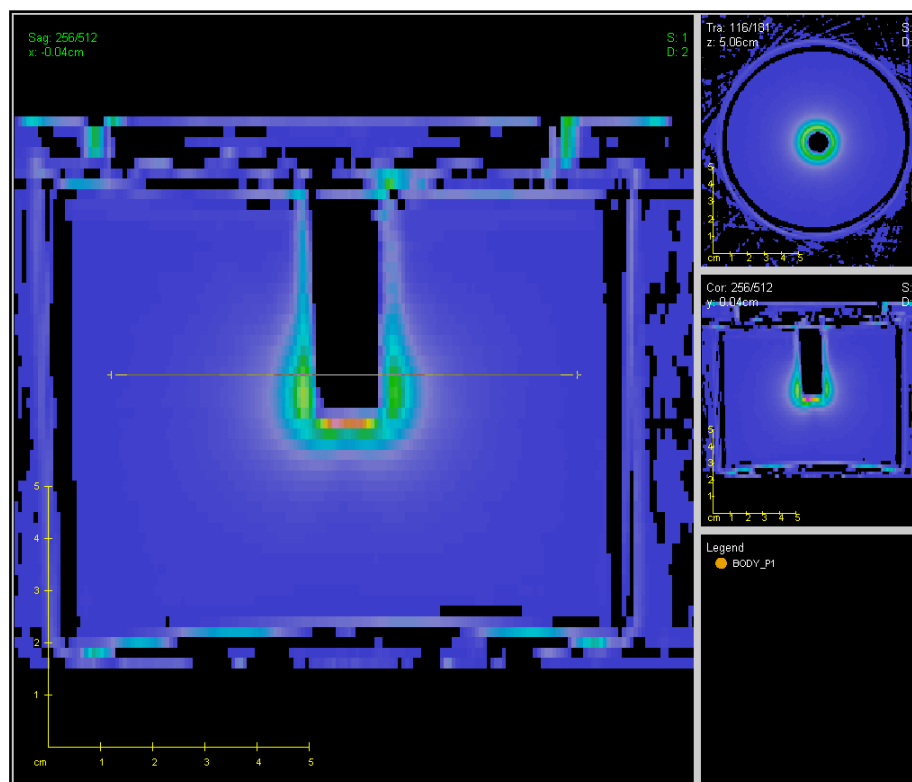


Figure 17. Sagittal, Transverse and Coronal views of reconstructed dose cube in CERR

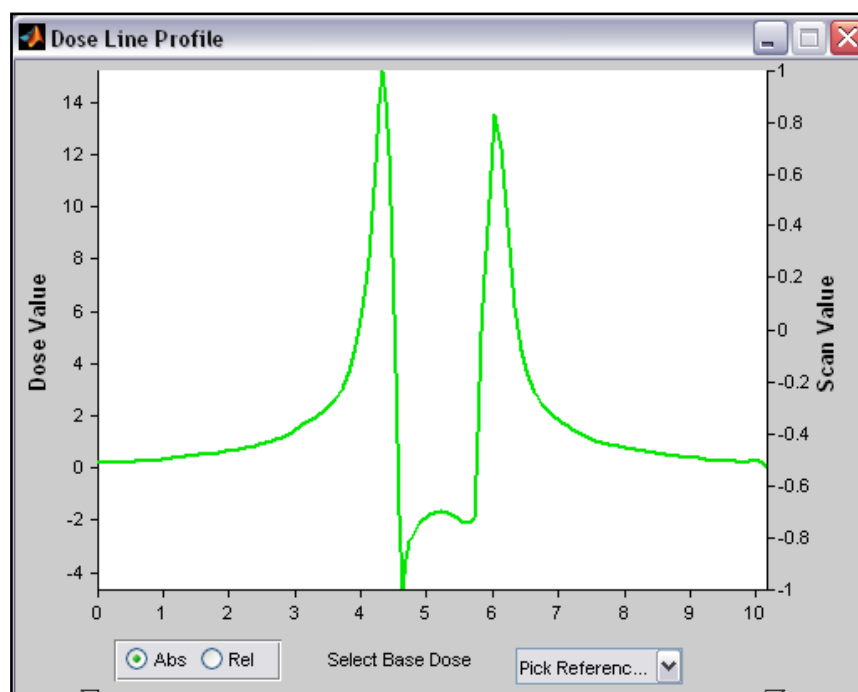


Figure 18. Dose line profile generated in CERR

For the purposes of this study, dose values with the corresponding distances from the dose-line profile were then exported into an Excel workbook for further dose and analysis.

2.4 TG-43 Formalism

The recommended formalism established in the AAPM TG-43 report and followed by the TG-43U1 report is defined here for purposes of clarification and easier understanding of the methods for PRESAGE[®] dosimetry analysis. The polar coordinate system used for brachytherapy calculations is shown in the figure below, reflecting the seed orientation used in this project.

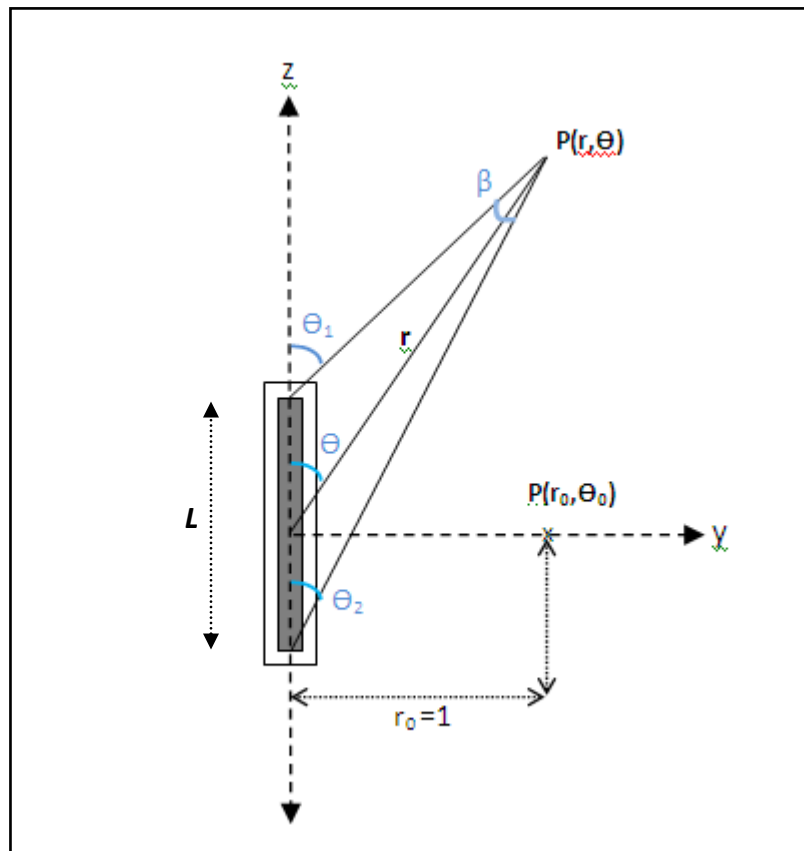


Figure 19. Coordinate system for brachytherapy dose calculations as defined from TG-43

L is the active length of the seed in centimeters. r is defined as the distance in centimeters from the center of the source to the point of interest and Θ is the polar angle created between r and the longitudinal bisecting plane of the seed. Therefore, $P(r, \theta)$ denotes the coordinates for the point of interest. TG-43 defines the reference point $P(r_0, \theta_0)$ at the distance of $r = 1$ cm and $\Theta = 90^\circ$ or $\pi/2$ radians, as shown in the Figure 17. The accuracy of the reference point in measurements is crucial because the anisotropy and radial dose function values are dependent on the dose rate at this point.

The transverse bisecting planes of the seeds ($\Theta=90^\circ$) were established in CERR by determining the plane with the highest doses farthest away from the seed (the widest part of the dose distribution shown below). The plane bisecting the dose distribution is clearly visualized through the colorwash corresponding to pixel values in CERR. The transverse plane is also verified by geometrical measurement from the bottom of the channel to the expected midpoint of the seed. Figure 20 below (showing only the center portion of the dosimeter) demonstrates an example of the bisecting plane. The origin of the source is determined using isodose curves on bisecting plane. The dose distribution is assumed to be symmetrical with respect to the longitudinal and transverse axis.

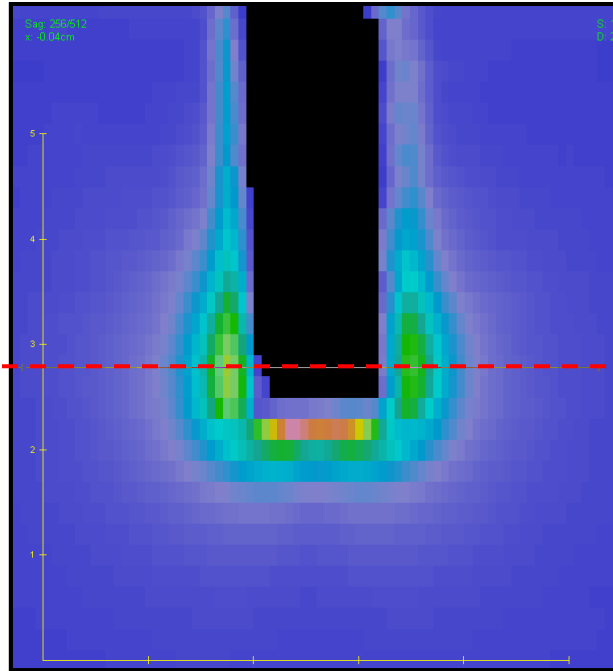


Figure 20. Transverse bisecting plane determined in CERR

2.4.1 Air-kerma Strength

As re-defined in the TG-43U1 report, the radioactive strength of brachytherapy sources is described by S_K , the air-kerma strength in units of U ($1 U = 1 \text{ cGy cm}^2 \text{ h}^{-1}$), and is defined by the following equation:

$$S_K = \dot{K}_\delta(d)d^2$$

$\dot{K}(d)$ is the air-kerma rate corrected for in-air photon attenuation and scattering (for air-kerma “*in vacuo*”) at distance d from the center of the transverse bisecting plane of the source to the point at which the air-kerma was measured. δ is the lower bound energy cutoff for air-kerma rate measurement and is typically set at $\delta = 5 \text{ keV}$. Photons below this energy are usually created through interactions with the titanium seed capsule and do not contribute to patient dose beyond $r = 0.1 \text{ cm}$. The air-kerma strength values are typically reported by

the manufacturer or calibrated by an Accredited Dosimetry Calibration Laboratory (ADCL) and are traceable to the 1999 National Standards Institute of Technology (NIST) standard.

The air-kerma strengths of the brachytherapy seeds used in this study were calibrated by the ADCL at the MD Anderson Cancer Center. Since ADCLs have direct traceability to the NIST primary standards, using the air-kerma strength provided by the ADCL reduces the uncertainty in dose measurements.

2.4.2 Dose rate

The 2D dose-rate ($cGy h^{-1}$) to water equation is specified in the TG-43 protocol:

$$\dot{D}(r, \theta) = S_K \cdot \Lambda \cdot \frac{G_L(r, \theta)}{G_L(r_0, \theta_0)} \cdot g_L(r) \cdot F(r, \theta)$$

This 2D dose rate equation was used to calculate dose rates to water for comparison with the measured dose rates in PRESAGE[®]. The consensus dose rates ($cGy h^{-1} U^{-1}$) as a function of radial distance (r) for each of the source models are shown in the tables below.

r (cm)	1.0	1.5	2.0	3.0	4.0	5.0
Dose rate ($cGy h^{-1} U^{-1}$)	0.9650	0.3910	0.1975	0.0681	0.0301	0.0141

Table 4. Dose rate using 2D formalism for the Amersham 6711

r (cm)	1.0	1.5	2.0	3.0	4.0	5.0
Dose rate ($cGy h^{-1} U^{-1}$)	0.9530	0.3862	0.1950	0.0673	0.0297	0.0140

Table 5. Dose rates using 2D formalism for the AgX100

Twelve separate dose values were measured in PRESAGE[®] for each point of interest, $P(r, \theta)$. For example, if the point of interest is at $P(r = 1 \text{ cm}, \theta = 90^\circ)$, twelve measurements (equally spaced 30° from each other) were taken and an averaged value was calculated. The figure below illustrates this example.

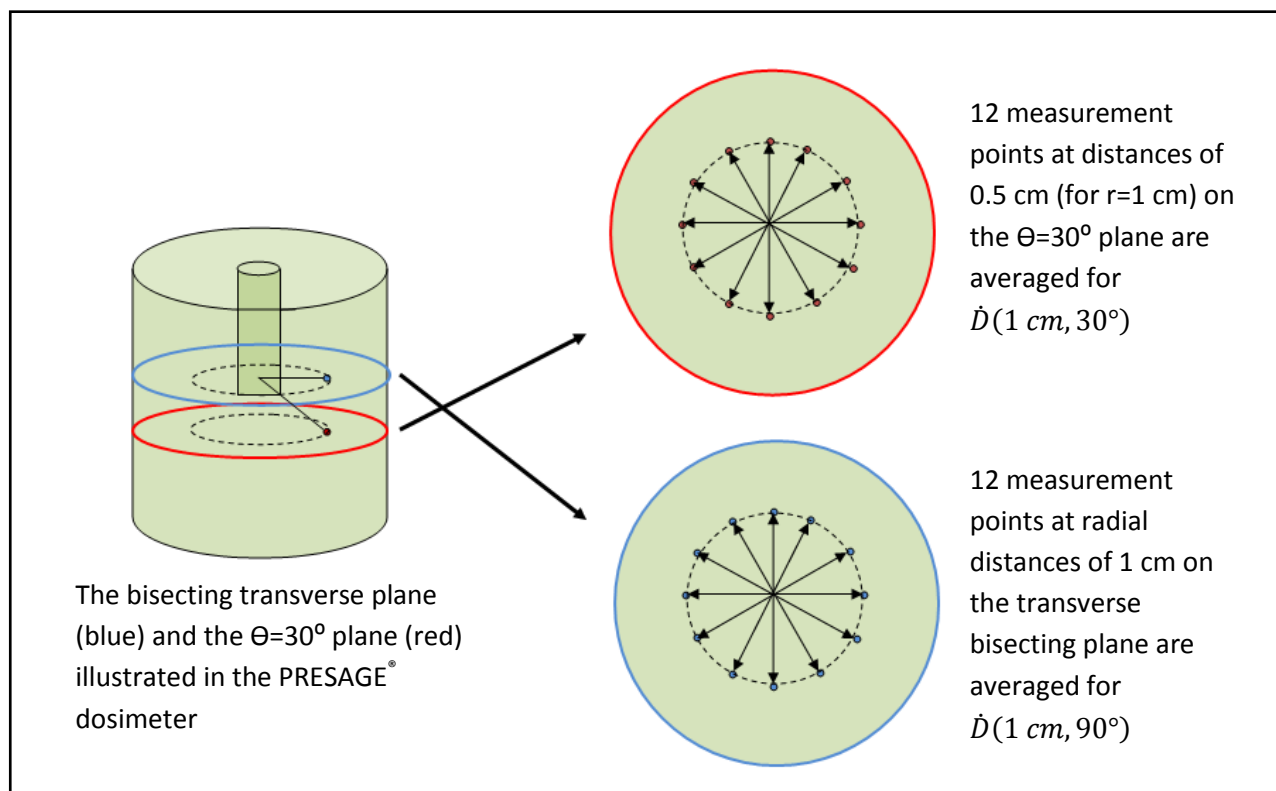


Figure 21. Diagram illustrating the 12 measurement points in PRESAGE[®] for each point of interest for dose rate, anisotropy function, and radial dose function calculations

The dose measurements within the range of $r = 1 \text{ cm}$ to $r = 1.5 \text{ cm}$ were measured in PRESAGE[®] dosimeters with 0.4 cm diameter channels. Dose values within the range of $r = 1.5 \text{ cm}$ to $r = 5 \text{ cm}$ were measured in PRESAGE[®] dosimeters with 1.5 cm diameter channels. The doses were normalized to the dose at $r = 1.5 \text{ cm}$ for both dosimeters. To calculate dose rate values in PRESAGE[®], the dose values were divided by the corresponding total irradiation time (in hours) and the source air kerma strength. Since the irradiation times

for the larger dosimeters were up to almost 10 days, a decay correction was included in the dose calculations for cumulated dose. The total cumulative dose for a “temporary implant” in brachytherapy can be calculated using the equation below[47] .

$$D_{cumulative} = \dot{D}_0 \cdot T_{av} (1 - e^{-\frac{t}{T_{av}}})$$

Therefore, the equation to calculate the dose rate ($\text{cGy h}^{-1} \text{U}^{-1}$) at each radial distance from the mean dose measurements, $\overline{D}(r, \theta)$, in PRESAGE[®] is shown in the equation below.

$$\dot{D}_0(r, \theta) = \frac{\overline{D}(r, \theta)}{S_K \cdot T_{av} (1 - e^{-\frac{t}{T_{av}}})} = \frac{\overline{D}(r, \theta)}{S_K \cdot 1.44 \cdot 59.4 \text{ d} (1 - e^{-\frac{t}{1.44 \cdot 59.4 \text{ d}}})}$$

2.4.3 Dose Rate Constant

The dose rate constant in water, Λ , has the units of $\text{cGy h}^{-1} \text{U}^{-1}$ and is defined as the ratio of the dose rate at the reference point to the air-kerma strength:

$$\Lambda = \frac{\dot{D}(r_0, \theta_0)}{S_K}$$

The dose rate constant is dependent on the source model design. The consensus dose rate constant values reported in TG-43U1 (including the value for the Amersham 6711) were derived by taking the equally-weighted average of the experimentally measured dose rate constants and the Monte Carlo calculated dose rate constants. Since the AgX100 seed is new, a consensus dose rate constant recommended by a consensus value recommended by an AAPM task group is not yet available. However, Theragenics uses the equally-weighted mean of the dose rate constants measured through Monte Carlo calculations and

experimental methods from the studies mentioned previously. The dose rate constants for the two ^{125}I seed models used in this study are as follows:

	Amersham 6711	AgX100
Dose rate constant (cGy h⁻¹ U⁻¹)	0.965	0.953

Table 6. Dose rate constants for both ^{125}I seed models

2.4.4 Geometry Function

The geometry function, $G_L(r, \theta)$, describes the dose falloff as a function of distance. For a point-source approximation (1D formalism), the dose decreases as a function of the inverse square of distance from the source. However, since the physical lengths of the sources are 4.5 mm and the dose measurements in PRESAGE[®] are within relatively close proximity from the source, the line-source approximation (2D formalism) is desired. The line-source approximation more accurately describes the 2D distribution of radioactivity of the source evenly distributed within the active length (L) of the seed. The geometry function using the line-source approximation defined by TG-43U1 is:

$$G_L(r, \theta) = \beta \cdot (L \cdot r \cdot \sin\theta)^{-1} \text{ when } \theta \neq 0^\circ$$

$$G_L(r, \theta) = (r^2 - L^2/4)^{-1} \text{ when } \theta = 0^\circ$$

β is the angle created by hypothetical lines extended from each end of the line source to the point of interest (see Figure 17). The geometry factors were calculated for the polar angles $\theta = 0^\circ$ up to $\theta = 90^\circ$, and for radial distances from $r = 0.5$ cm up to $r = 5$ cm for both the Amersham 6711 and the AgX100 source dosimetry calculations. Since the active lengths of

the 6711 and AgX100 source models are 3 mm and 3.5 mm respectively, two different sets of geometry factors were calculated and used for dosimetry. The tables below show the geometry factors calculated for active lengths of 3 mm and 3.5 mm.

Θ (deg)	$G(r, \Theta)$						
	r=0.5 cm	r=1.0 cm	r=1.5 cm	r=2.0 cm	r=3.0 cm	r=4.0 cm	r=5.0 cm
0	1.099	1.023	1.010	1.006	1.003	1.001	1.001
5	1.098	1.023	1.010	1.006	1.003	1.001	1.001
10	1.094	1.022	1.010	1.005	1.003	1.001	1.001
20	1.081	1.019	1.008	1.005	1.003	1.001	1.001
30	1.062	1.015	1.007	1.004	1.003	1.001	1.001
40	1.039	1.010	1.004	1.003	1.003	1.001	1.001
50	1.018	1.005	1.002	1.001	1.003	1.001	1.001
60	0.998	1.000	1.000	1.000	1.003	1.001	1.001
70	0.984	0.996	0.998	0.999	1.003	1.001	1.001
80	0.975	0.993	0.997	0.998	1.003	1.001	1.001
90	0.972	0.993	0.997	0.998	0.999	1.000	1.000

Table 7. Geometry Factors for L=3 mm

Θ (deg)	$G(r, \Theta)$						
	r=0.5 cm	r=1.0 cm	r=1.5 cm	r=2.0 cm	r=3.0 cm	r=4.0 cm	r=5.0 cm
0	1.140	1.032	1.008	1.003	1.002	1.001	1.140
5	0.941	0.877	0.862	0.859	0.858	0.858	0.941
10	0.926	0.874	0.861	0.859	0.858	0.858	0.926
20	1.081	1.019	1.005	1.003	1.001	1.001	1.081
30	0.910	0.870	0.860	0.859	0.858	0.858	0.910
40	0.891	0.866	0.859	0.859	0.858	0.858	0.891
50	0.872	0.861	0.858	0.859	0.858	0.858	0.872
60	0.856	0.857	0.857	0.859	0.858	0.858	0.856
70	0.843	0.854	0.856	0.859	0.858	0.858	0.843
80	0.835	0.852	0.856	0.859	0.858	0.858	0.835
90	0.833	0.851	0.856	0.856	0.857	0.857	0.833

Table 8. Geometry Factors for L=3.5 mm

2.4.5 Anisotropy Function

The anisotropy function describes the change in dose as the polar angle varies with reference to the transverse ($\Theta_0 = 90^\circ$) plane. This function is dependent on radial distance

away from the source, the polar angle, thickness of the seed encapsulation material, and the photon energies emitted by the source from radioactive decay[14]. The 2D anisotropy function is defined by TG-43U1 as

$$F(r, \theta) = \frac{\dot{D}(r, \theta)}{\dot{D}(r, \theta_0)} \cdot \frac{G_L(r, \theta_0)}{G_L(r, \theta)}$$

The 2D anisotropy functions for the Amersham 6711 have been characterized and the consensus values published in TG-43U1 are based on Monte Carlo-determined values. The agreement between Monte Carlo determined values and experimentally determined values was found to be $\pm 10\%$ [14]. Experimentally derived anisotropy functions were not included in the consensus dataset because the range of values was less complete compared to the Monte Carlo studies. The following table (Table 9) from TG-43U1 lists the anisotropy functions for the Amersham 6711:

		F(r, θ)					
θ ($^\circ$)		r=0.5	r=1	r=2	r=3	r=4	r=5
0		0.333	0.370	0.442	0.488	0.520	0.550
5		0.400	0.429	0.497	0.535	0.561	0.587
10		0.519	0.537	0.580	0.609	0.630	0.645
20		0.716	0.705	0.727	0.743	0.752	0.760
30		0.846	0.834	0.842	0.846	0.848	0.852
40		0.926	0.925	0.926	0.926	0.928	0.928
50		0.972	0.972	0.970	0.969	0.969	0.969
60		0.991	0.991	0.987	0.987	0.987	0.987
70		0.996	0.996	0.996	0.995	0.995	0.995
80		1	1	1	0.999	0.999	0.999
$\Phi_{an}(r)$		0.973	0.944	0.941	0.942	0.943	0.944

Table 9. Anisotropy Function Table for Amersham 6711

The anisotropy functions for both ^{125}I sources were measured in PRESAGE[®] using the measured dose rate values and calculated geometry factor values listed in Table 7. Similar to

the measurements for the dose rates in PRESAGE[®], twelve separate point dose values were measured in PRESAGE[®] for each anisotropy function and the mean of the dose values was converted to dose rate and used to calculate the mean anisotropy function for each point of interest. For example, to calculate $F(r = 2 \text{ cm}, \theta = 30^\circ)$, twelve points (30° apart) on the $P(r = 2 \text{ cm}, \theta = 30^\circ)$ plane were measured and averaged. The dose rate ($\text{cGy h}^{-1} \text{ U}^{-1}$) was determined from the mean dose value by dividing by the total irradiation time in hours and the air kerma strength (corrected for the radioactive decay). The mean dose rate, $\dot{D}(r = 2 \text{ cm}, \theta = 30^\circ)$, was then divided by the mean dose rate on the transverse plane $\dot{D}(r = 2 \text{ cm}, \theta = 90^\circ)$, and multiplied by the ratio of geometry factors to obtain the anisotropy function $F(r = 2 \text{ cm}, \theta = 30^\circ)$ measured in PRESAGE[®]. The measured anisotropy functions for the Amersham 6711 were compared to the Monte Carlo anisotropy functions to evaluate the accuracy of brachytherapy dose measurements in PRESAGE[®] dosimeters.

2.4.6 Radial Dose Function

The radial dose function describes the change in radiation dose due to scattering and attenuation of photons on the transverse plane, excluding the dose fall-off due to the inverse square law (already accounted for by the geometry function)[14]. The 2D equation for the radial dose function using the line-source approximation is:

$$g_L(r) = \frac{\dot{D}(r, \theta_0)}{\dot{D}(r_0, \theta_0)} \cdot \frac{G_L(r_0, \theta_0)}{G_L(r, \theta_0)}$$

Monte Carlo derived values and experimentally measured values of the radial dose function show an average agreement of $\pm 10\%$ [14]. The consensus values recommended by TG-43U1 include datasets mostly from Monte Carlo calculations for radial dose values, especially at

closer distances to the source ($r < 1$ cm) although values at a few radial distances with more complete experimentally derived data sets are included in the consensus values as well. The radial dose functions recommended in TG-43U1 for the Amersham 6711 ($L = 3$ mm) are shown in Table 10 below.

Line source approximation	
r (cm)	g(r)
0.1	1.055
0.15	1.078
0.25	1.082
0.5	1.071
0.75	1.042
1	1.000
1.5	0.908
2	0.814
3	0.632
4	0.496
5	0.364
6	0.270
7	0.199
8	0.148
9	0.109
10	0.080

Table 10. Radial Dose Functions for the Amersham 6711

The radial dose functions were calculated in PRESAGE[®] using the dose rates measured and calculated on the transverse bisecting plane as previously described. Twelve dose measurements (30° apart) for each point of interest were averaged and the radial dose functions within the measurable and accurate range of the PRESAGE[®] dosimeters were calculated. The radial dose functions measured for the Amersham 6711 seed were compared with the consensus values to evaluate of the accuracy of PRESAGE[®] dosimetry with

brachytherapy sources. The radial dose functions measured for the AgX100 seed were compared to the Monte Carlo and experimentally derived values.

3 Results and Discussion for the Amersham 6711

3.1 Dose Rate

Table 11 below shows the mean of the measured dose rates in PRESAGE[®] and the consensus values. The dose rate constant values are in **bold** text. The relative differences of the dose rates between the measured and consensus values are expressed as a percentage of the consensus values. The standard deviations ($k=1$) of the twelve dose rate measurements and the coefficients of variation (expressed in percentage) are also listed. Figure 22 is a graphical comparison of the mean measured dose rate values and consensus values from Table 11.

Dose Rate Comparison	1	1.5	2	3	4	5
PRESAGE [®] measured Dose Rates (cGy h ⁻¹ U ⁻¹)	0.976	0.391	0.193	0.068	0.033	0.021
Consensus Values (cGy h ⁻¹ U ⁻¹)	0.965	0.391	0.198	0.068	0.030	0.014
Relative Difference (%)	1.2	0.0	-2.4	0.2	10.6	50.8
Standard deviation	0.003	0.006	0.011	0.005	0.002	0.004
COV (%)	0.3	1.6	5.8	7.2	7.5	19.2

Table 11. Amersham 6711: Dose Rate Comparison

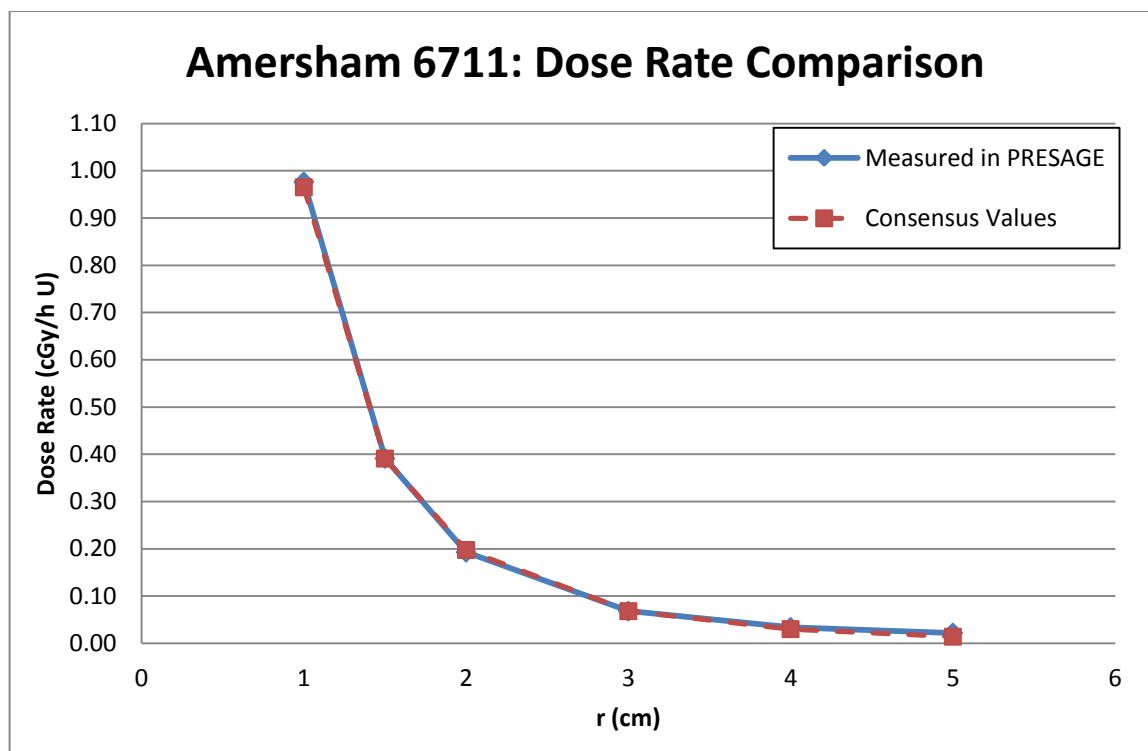


Figure 22. Amersham 6711: Dose Rate Comparison

The dose rates measured in PRESAGE[®] in the $r = 1$ cm to $r = 3$ cm range demonstrated excellent agreement (less than 3% relative difference) with the consensus values from TG-43U1. The coefficient of variation for the dose rates measured was the lowest (0.32%) for the dose rate at $r = 1$ cm and increased with larger radial distances. The gradual increase in standard deviations at larger radial distances is most likely due to the lower doses. The mean dose measurements at each radial distance used to calculate the dose rates are seen in Table 12. The expected doses calculated using TG-43U1 parameters and the relative differences (%) are shown in the second and third lines.

r (cm)	1	1.5	2	3	4	5
Measured Dose (Gy)	2.18	4.49	2.21	0.78	0.38	0.24
Expected Dose (Gy)	2.15	4.49	2.27	0.78	0.35	0.16
Relative Difference (%)	1.2	0.0	-2.4	0.1	10.6	50.8

Table 12. Amersham 6711: Comparison of the doses delivered

The data demonstrate that for doses below 1 Gy, the coefficient of variation increases to above 5%. This suggests that dose response is more stable above 1 Gy in PRESAGE[®].

Figure 23 shows the isodose lines for 2.154 Gy, 4.49 Gy, 2.27 Gy, 0.78 Gy, 0.35 Gy, and 0.16 Gy. The instability of dose response lines at low doses (below 1 Gy) can be observed through the increasing amount of noisiness in the isodose curves.

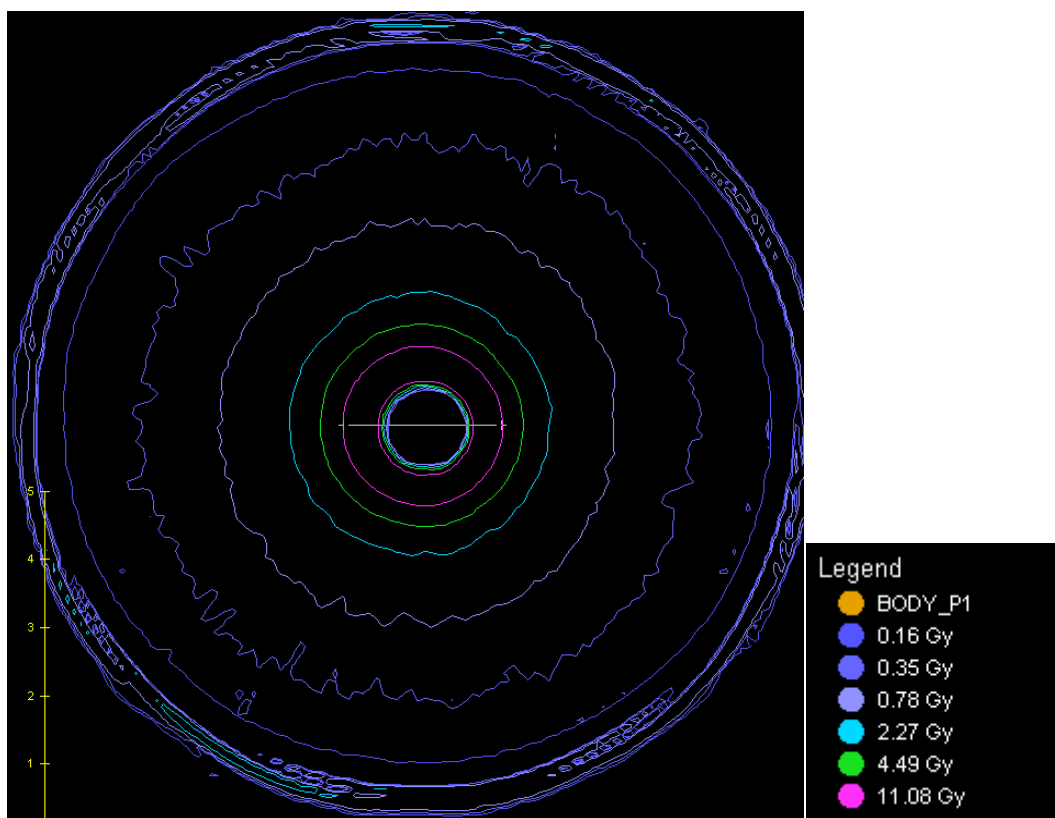


Figure 23. Isodose lines in a large dosimeter displayed in CERR.

The dose rates measured at $r = 4$ cm and $r = 5$ cm demonstrated an over-response of 11% and 51% respectively. The over-responses at these measurement points are likely due to two main reasons: 1. The doses at these radial distances are below 50 cGy and may be below the dynamic range of PRESAGE[®] 2. PRESAGE[®] dose response at low doses (below 1 Gy) undergoes faster rates of OD increase post-irradiation compared to the rate of OD change in dose response at higher doses (above 1 Gy). To irradiate to 78 cGy at 5 cm with a high air kerma strength source of 9 U would take approximately 25 days, which is an impractical amount of time to wait for dosimetry calculations in PRESAGE[®]. The effects of dose response in PRESAGE[®] over long periods of time were evaluated and are discussed in Chapter 5.

3.2 Dose Rate Constant

The dose rate constant (Λ) measured in PRESAGE[®] for the Amersham 6711 seed was 0.976 ± 0.003 cGy h⁻¹ U⁻¹ as seen in Table 13. Following the methods of TG-43U1, the average of the Monte Carlo derived dose rate constant ($\Lambda_{MC} = 0.950$ cGy h⁻¹ U⁻¹) and the PRESAGE[®] measured value is 0.963 cGy h⁻¹ U⁻¹. This dose rate constant differs by less than 0.3% from the TG-43U1 consensus value ($\Lambda = 0.965$ cGy h⁻¹ U⁻¹).

	Λ , dose rate constant (cGy h ⁻¹ U ⁻¹)
PRESAGE[®] measured	0.976
Monte Carlo derived	0.950
Average	0.963
TG-43U1 consensus value	0.965

Table 13. Amersham 6711: Comparison of the dose rate constant

3.3 Anisotropy Function

Table 14 below shows the resulting anisotropy functions measured in PRESAGE[®]. Values in the $r = 1$ cm to $r = 2$ cm range were measured in a small channel dosimeter while the rest of the values were measured in a large channel dosimeter. The values not shown in Table 11 were not measured because the points of interest were either within the channel (which is removed post-irradiation), within the 4 mm of the edge of the dosimeter (edge artifact region), or beyond the physical depth of the dosimeter.

θ (°)	r (cm)				
	r=1	r=2	r=3	r=4	r=5
0					
5			0.526	0.457	
10		0.594	0.574	0.593	
20	0.725	0.722	0.853	0.902	
30	0.792	0.845	0.915	1.034	
40	0.890	0.913	0.954	1.130	1.351
50	0.956	0.978	0.990	1.120	1.257
60	0.953	0.961	1.026	1.052	1.096
70	1.022	0.982	1.026	1.042	1.055
80	1.019	0.972	0.969	0.978	1.123

Table 14. Amersham 6711: Anisotropy Functions measured in PRESAGE[®]

Table 15 shows the percent differences relative to the consensus 2D anisotropy functions for the Amersham 6711.

θ (°)	r (cm)				
	r=1	r=2	r=3	r=4	r=5
0					
5			-1.7	-18.5	
10		2.4	-5.7	-5.8	
20	2.8	-0.7	14.8	19.9	
30	-5.0	0.4	8.2	21.9	
40	-3.8	-1.4	3.1	21.8	45.6
50	-1.7	0.8	2.2	15.6	29.7
60	-3.8	-2.6	4.0	6.5	11.1
70	2.6	-1.4	3.2	4.7	6.0
80	1.9	-2.8	-3.1	-2.1	12.4

Table 15. Amersham 6711 Anisotropy Functions: Relative Differences (%)

For most values in the $r = 1$ to 3 cm range, disagreement between the measured anisotropy values and the consensus values is less than 5%, with a few exceptions. The largest differences are in the $r = 4$ and $r = 5$ cm range, which included over-responses of up to 30%. This was expected since the measured dose rates on the $\theta=90^\circ$ plane showed large relative differences at those distances. Again, these inaccuracies may be due to low doses and nonlinear changes in OD response post-irradiation. The standard deviations and coefficients of variation for the anisotropy values were comparable to the dose rates and can be found in Appendix A. Figures 24-28 display the Amersham 6711 anisotropy functions plotted for each radial distance for the measured and consensus values.

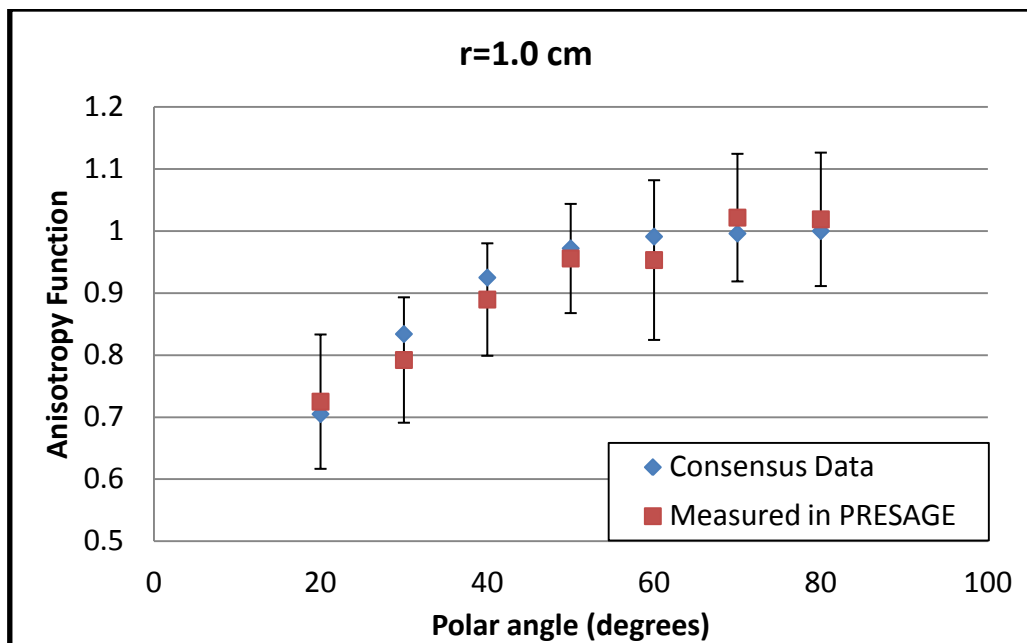


Figure 24. AgX100 Anisotropy functions for $r = 1$ cm: The TG-43U1 values (blue) are plotted with the values measured in PRESAGE[®] (blue). Error bars show one standard deviation above and below the mean dose value measured in PRESAGE[®]. The averaged relative difference was $\pm 3\%$.

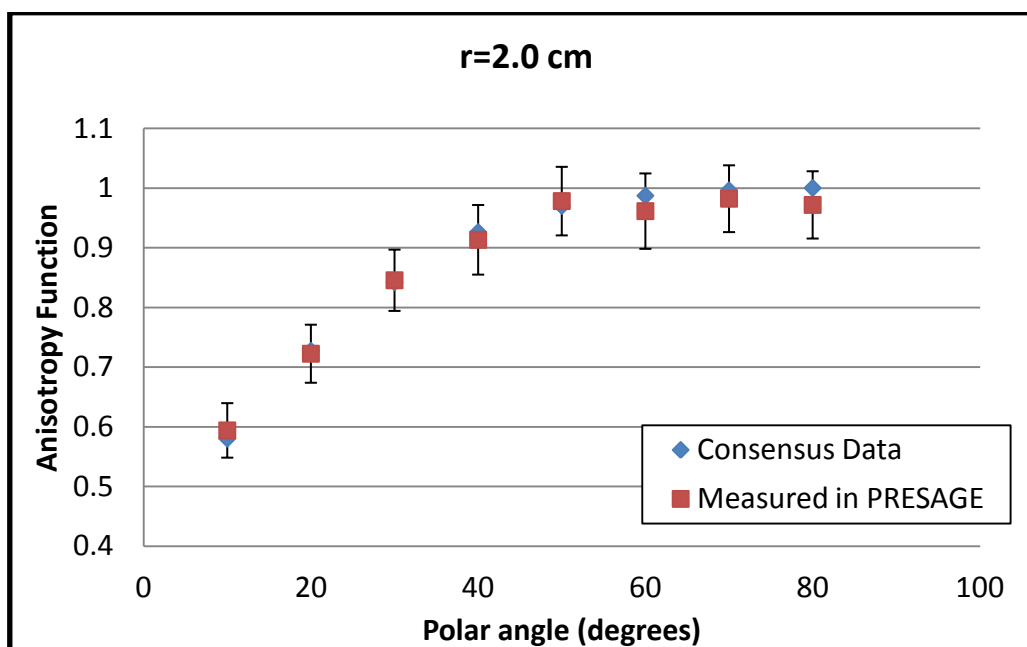


Figure 25. AgX100 Anisotropy functions for $r = 2$ cm: The TG-43U1 values (blue) are plotted with the values measured in PRESAGE[®] (blue). Error bars show one standard deviation above and below the mean dose value measured in PRESAGE[®]. The averaged relative difference was $\pm 2\%$.

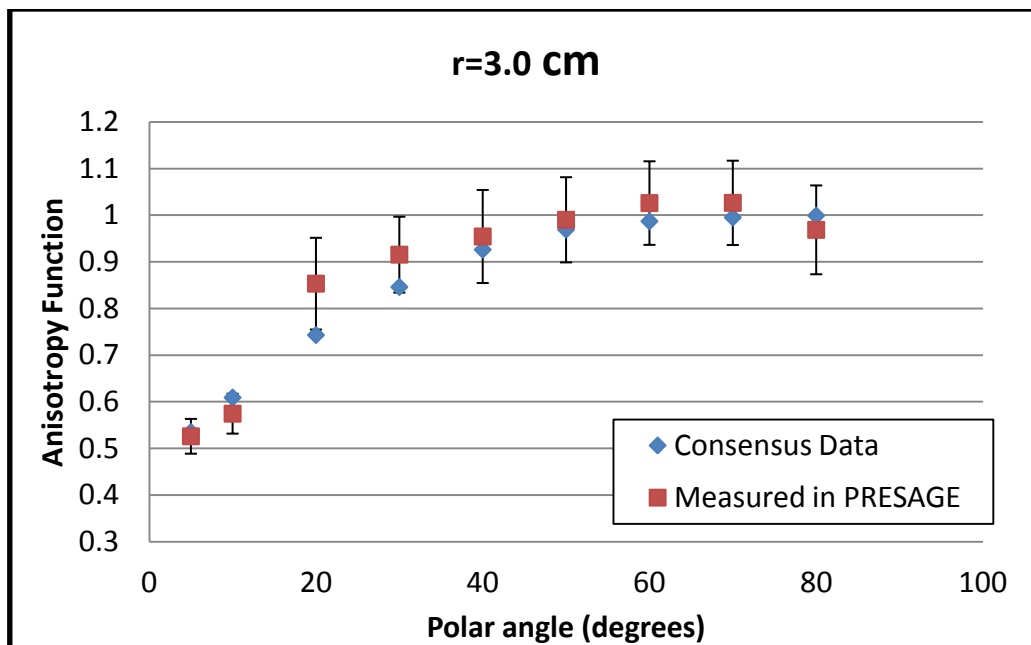


Figure 26. AgX100 Anisotropy functions for $r = 3$ cm: The TG-43U1 values (blue) are plotted with the values measured in PRESAGE[®] (red). Error bars show $\pm 1\sigma$ of the mean dose value measured in PRESAGE[®]. The averaged relative difference was $\pm 5\%$.

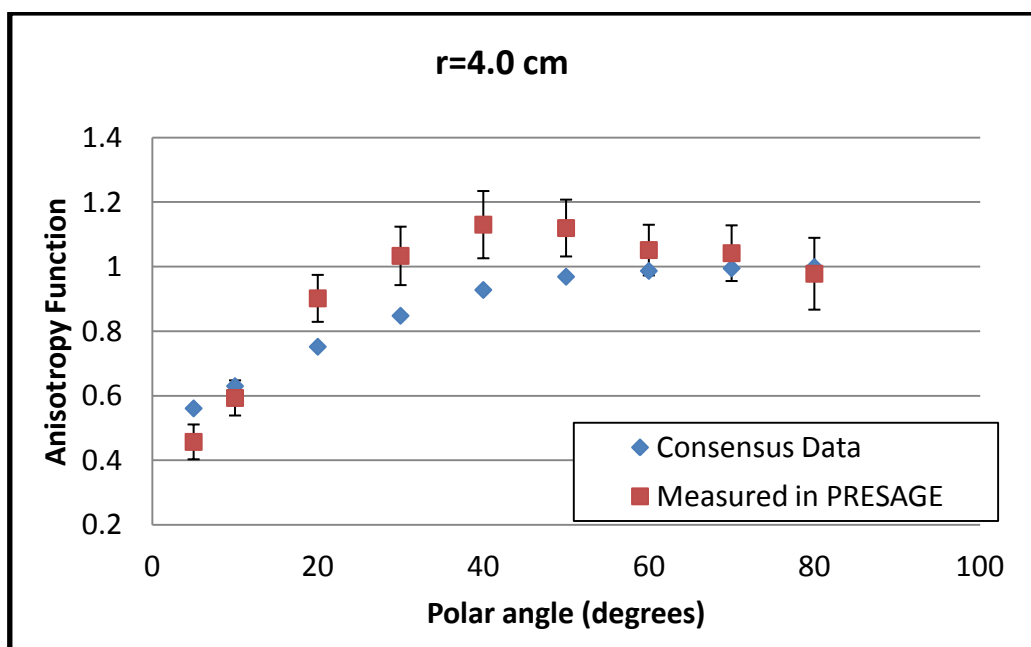


Figure 27. AgX100 Anisotropy functions for $r = 4$ cm: The TG-43U1 values (blue) are plotted with the values measured in PRESAGE[®] (red). Error bars show $\pm 1\sigma$ of the mean dose value measured in PRESAGE[®]. The averaged relative difference was $\pm 13\%$.

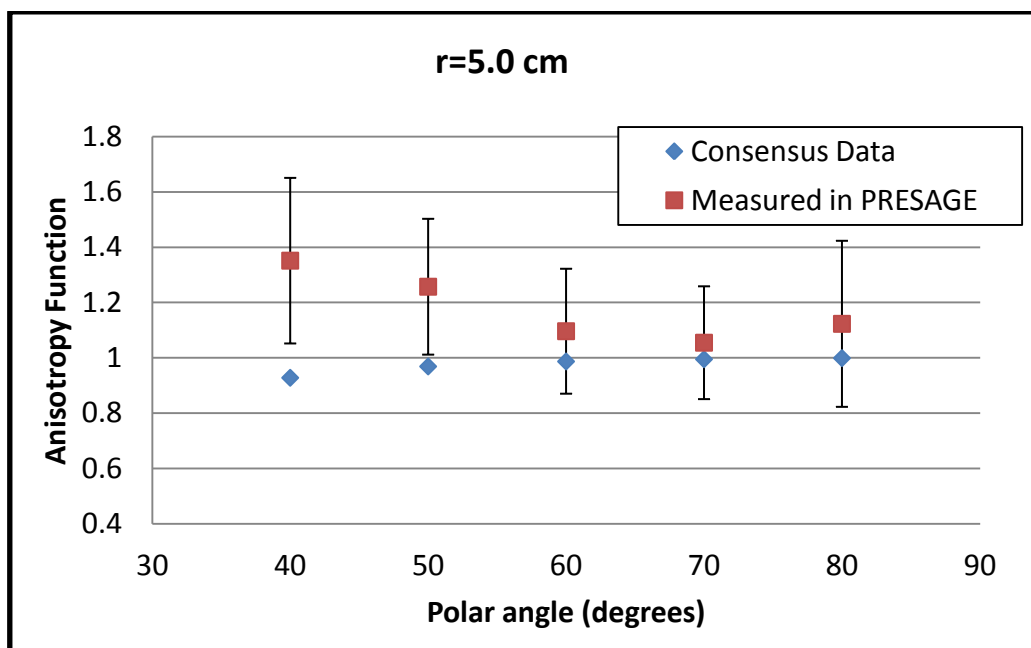


Figure 28. AgX100 Anisotropy functions for $r = 5$ cm: The TG-43U1 values (blue) are plotted with the values measured in PRESAGE[®] (red). Error bars show $\pm 1\sigma$ of the mean dose value measured in PRESAGE[®]. The averaged relative difference was $\pm 21\%$.

3.4 Radial Dose Function

The radial dose functions measured in PRESAGE[®] are displayed below in Table 16.

The dose rate value at $r = 1$ cm, $\theta = 90^\circ$ was measured in a 0.4 cm diameter channel

dosimeter. The rest of the dose rate values from $r = 1.5$ cm to $r = 5$ cm were measured in the

1.5 cm diameter channel.

r (cm)	TG-43U1 value	Measured in PRESAGE	Standard deviation	Relative difference (%)	COV (%)
1	1	1.000		0.0	
1.5	0.908	0.894	0.022	-1.6	2.4
2	0.814	0.782	0.048	-3.9	6.1
3	0.632	0.622	0.046	-1.7	7.4
4	0.496	0.528	0.041	6.4	7.8
5	0.364	0.555	0.104	52.5	18.7

Table 16. Amersham 6711: Radial Dose Function Comparison

The measured and consensus radial dose functions for $r = 1.5$ cm to $r = 3$ cm agree within 4%. Since the radial dose functions are approximately the ratios of the dose rates on the $\theta=90^\circ$ plane, the relative differences are comparable to the relative differences for the dose rates in Section 5.1. The measured radial dose functions at $r = 4$ cm and $r = 5$ cm show an over-response of 6% and 52%, respectively. The standard deviation of the radial dose function was greatest at $r = 5$ cm, with a large coefficient of variation of 18.7%. This suggests that the dose values at 5 cm are too low, resulting in inconsistent dose values that may be affected by noise. Figure 29 shows a graphical representation of the radial dose functions plotted with error bars showing ± 1 standard deviation.

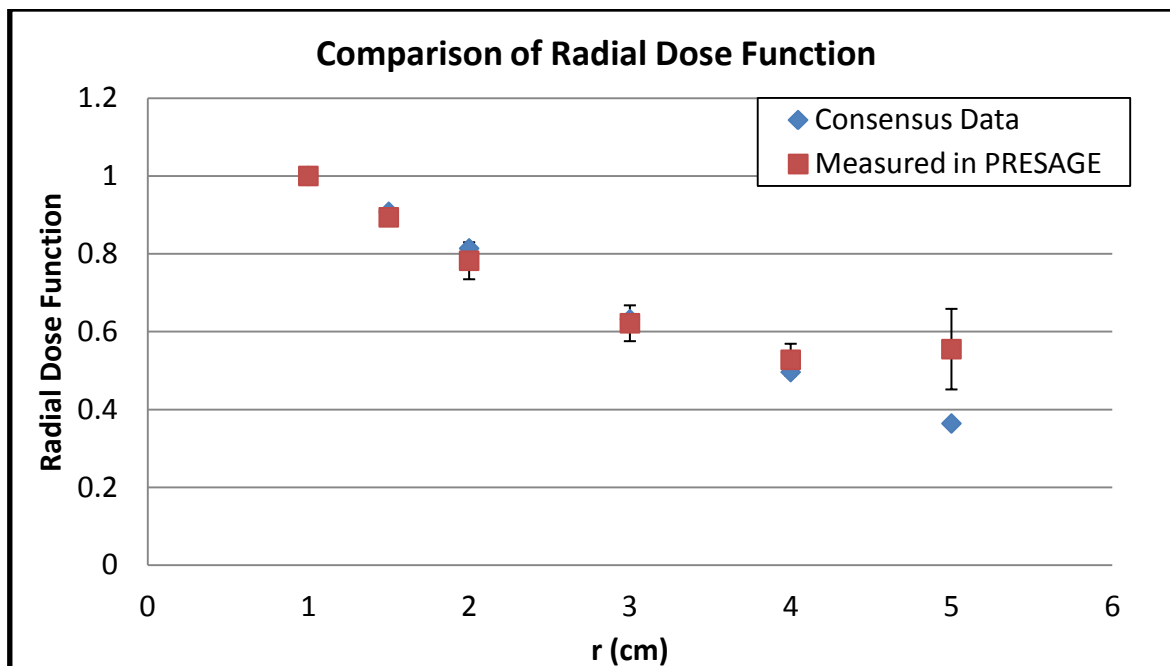


Figure 29. Comparison of AgX100 radial dose functions: The TG-43U1 consensus values (blue) are plotted with the PRESAGE[®] measured values (red) with error bars showing $\pm 1\sigma$.

4 Results and Discussion for the AgX100

4.1 General discussion of results

The experimental set-up and dosimetry analysis for the AgX100 were performed using the same methods as for the Amersham 6711 irradiations and analysis. Tables 17 and 18 display the measured and expected mean doses from the small and large channel dosimeters, respectively. The mean doses were then used to calculate the dose rate at each radial distance.

r(cm)	1	1.5	2	2.5	3
Measured Dose (Gy)	3.612	1.468	0.755	0.424	0.256
Expected Dose (Gy)	3.622	1.468	0.741	0.416	0.256
Relative Difference (%)	-0.3	0.0	1.8	2.0	0.1

Table 17. Dose Comparison in 0.4 cm channel dosimeter

r(cm)	1.5	2	2.5	3	4	5
Measured Dose (Gy)	5.06	2.51	1.49	0.96	0.54	0.25
Expected Dose (Gy)	5.05	2.55	1.43	0.88	0.39	0.18
Relative Difference (%)	0.0	-1.7	4.1	8.7	39.1	35.1

Table 18. Dose Comparison in 1.5 cm channel dosimeter

The measured doses demonstrated excellent agreement with the calculated doses in the 0.4 cm diameter channel dosimeter with the maximum relative difference of 2% at $r = 2.5$ cm. The dose increase from 2 Gy to 3.6 Gy in the small channel dosimeter allowed for dose measurements up to $r = 3$ cm. However, the dose measurements in the large channel dosimeter showed significant over-response in the $r = 3$ cm to $r = 5$ cm range. The relative differences were as high as 39% compared to the expected doses, as shown in Table 18. These results from the large dosimeter are unexpected, because both the large channel dosimeter for the 6711 seed irradiation and the small channel AgX100 seed irradiation demonstrated agreement with 5% of the calculated doses.

Especially with a higher radiation dose of 12.5 Gy at 1 cm, the dose response in the large dosimeter was expected to improve and become more consistent, instead of a resulting increased over-response. The most significant difference in the AgX100 large dosimeter irradiation compared to the 6711 large dosimeter irradiation was the much longer irradiation time of 10 days. It seemed highly possible that longer irradiation times may have played an important role in the dose response accuracy in PRESAGE[®], as previously mentioned in the discussion of the results for the Amersham 6711 irradiations. Therefore, dose response changes in PRESAGE[®] over long periods of time post-irradiation were evaluated. The results are presented in Chapter 5. The dose measurements in the small channel dosimeter were used to characterize the dosimetry parameters of the AgX100 seed.

4.2 Dose Rate

The dose rates ($\text{cGy h}^{-1} \text{U}^{-1}$) measured in PRESAGE[®] with the AgX100 seed are shown in Table 19. The expected dose rates were calculated from the dose rate constant provided by the manufacturer. The measured dose rates were calculated from the mean measured dose (cGy) at each radial distance divided by the irradiation time (hours) and the decay-corrected air kerma strength (U).

r (cm)	1	1.5	2	2.5	3
PRESAGE[®] measured ($\text{cGy h}^{-1} \text{U}^{-1}$)	0.950	0.386	0.199	0.112	0.067
Expected values ($\text{cGy h}^{-1} \text{U}^{-1}$)	0.953	0.386	0.195	0.110	0.067
Relative Difference (%)	-0.3	0.0	1.8	2.0	0.1
Standard deviation	0.022	0.008	0.008	0.008	0.005
COV (%)	2.3	2.2	3.8	7.2	8.1

Table 19. AgX100: Dose Rate Comparison

The measured dose rates from $r = 1$ cm to $r = 3$ cm showed excellent agreement with the expected dose rate values, calculated from the manufacturer-given dose rate constant. All dose rate values agreed within 2%. The standard deviations of the dose rates were comparable to the standard deviations from the 6711 dose rate measurements, although the standard deviation of the measured AgX100 dose rate constant was not quite as low as the standard deviation of the measured 6711 dose rate constant. The coefficient of variation were within 4% from $r = 1$ cm to $r = 2$ cm, and increase to 7-8% for dose rates at $r = 2.5$ cm and $r = 3$ cm. The higher percent differences at these radial distances were most likely due to dose measurements below 50 cGy, which may be low enough to be affected by noise. Figure 30 below is a graphical representation of the measured vs. expected dose rates plotted with error bars of ± 1 standard deviation.

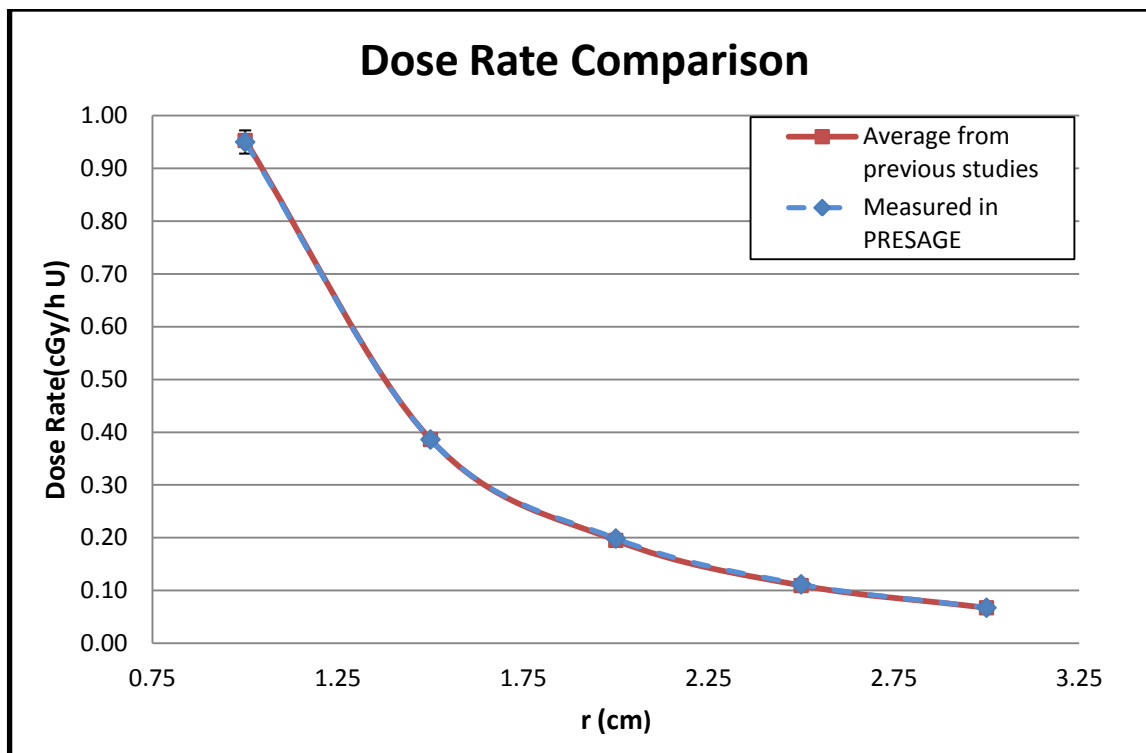


Figure 30. AgX100 Dose Rate Comparison: The dose rates averaged from the previously published Monte Carlo-derived[1] and TLD-measured values[2] (red) plotted with the dose rates measured in PRESAGE[®]. Error bars show $\pm 1\sigma$ from the measured doses at each point.

4.3 Dose Rate Constant

The dose rate constant provided by the manufacturer is $0.9530 \text{ cGy h}^{-1} \text{ U}^{-1}$. This value is the average of the dose rate constant values derived from previous Monte Carlo studies by Mourtada *et al.* and TLD and photon spectrometry measurements in an experimental study by Chen *et al.* Table 20 shows the derived dose rate constants from the studies and the mean value[1,2].

	Dose Rate Constant
Λ_{MCNPX}	0.943 cGy h ⁻¹ U ⁻¹
Λ_{MCNPX}	0.918 cGy h ⁻¹ U ⁻¹
Λ_{TLD}	0.995 cGy h ⁻¹ U ⁻¹
Λ_{PST}	0.957 cGy h ⁻¹ U ⁻¹
Mean Λ=	0.953 cGy h⁻¹ U⁻¹

Table 20. Dose Rate constants of the AgX100

Table 21 shows the dose rate constant comparison from this study with the mean value.

	Dose Rate Constant (cGy h⁻¹ U⁻¹)
Λ measured in this study	0.950
Mean Λ from previous studies	0.953
Relative Difference	-0.3%

Table 21. Dose Rate Constant Comparison

The agreement between the dose rate constant measured in this study to the mean value was less than 0.5%. Although this demonstrates excellent agreement, it is important to note that PRESAGE[®] dose values are relative to the dose at 1.5 cm. Since the dose at 1.5 cm was calculated using the manufacturer provided mean dose rate constant, the value measured in PRESAGE[®] gives a comparison of the measured values relative to the current mean value.

4.4 Anisotropy Function

The anisotropy functions measured in PRESAGE[®] are shown in Table 22 below, measured in the small channel dosimeter. The values missing were measurement points in

the PRESAGE[®] plug and therefore were not analyzed. Tables 23-24 display the anisotropy functions measured from previous studies.

		r (cm)			
θ (°)		r=0.5	r=1	r=2	r=3
0					
5					0.584
10			0.533	0.605	0.667
20			0.7204	0.745	0.781
30	0.751	0.826	0.839	0.864	
40	0.868	0.912	0.933	0.854	
50	0.967	0.973	0.928	0.919	
60	1.021	0.961	0.971	0.914	
70	0.979	1.057	1.017	0.980	
80	0.962	1.033	1.030	0.976	

Table 22. AgX100: Anisotropy Function measured in PRESAGE[®]

		r (cm)		
θ (°)		r=1	r=2	r=3
0		0.354	0.427	0.554
5		--	--	--
10		0.498	0.588	0.651
20		0.671	0.752	0.753
30		0.790	0.859	0.841
40		0.892	0.945	0.908
50		0.955	0.972	0.946
60		0.975	1.009	0.971
70		0.992	1.011	1.023
80		0.994	1.052	1.009

Table 23. AgX100: TLD-measured Anisotropy Functions[2]

θ (°)	r (cm)			
	r=0.5	r=1	r=2	r=3
0	0.217	0.294	0.4	0.462
5	0.314	0.4	0.493	0.548
10	0.404	0.49	0.577	0.624
20	0.652	0.688	0.736	0.761
30	0.813	0.817	0.841	0.852
40	0.916	0.904	0.912	0.915
50	0.986	0.963	0.961	0.961
60	1.028	1.007	0.999	0.994
70	0.987	1.036	1.025	1.017
80	0.995	1.002	1.031	1.028

Table 24. AgX100: Monte-Carlo calculated Anisotropy Functions[1]

For a quantitative comparison, the anisotropy functions measured in this study were compared to the Monte Carlo derived values[1]. Values at $\leq 30^\circ$ demonstrated slightly larger relative differences of up to $\pm 9\%$. Anisotropy functions $\geq 30^\circ$ generally agreed with the previous averaged values within $\pm 5\%$. Figures 31-33 are graphical comparisons of the anisotropy functions between the PRESAGE[®]-measured vs. Monte Carlo calculated values. Further detailed comparisons and standard deviations in the anisotropy function measurements are presented in Appendix A.

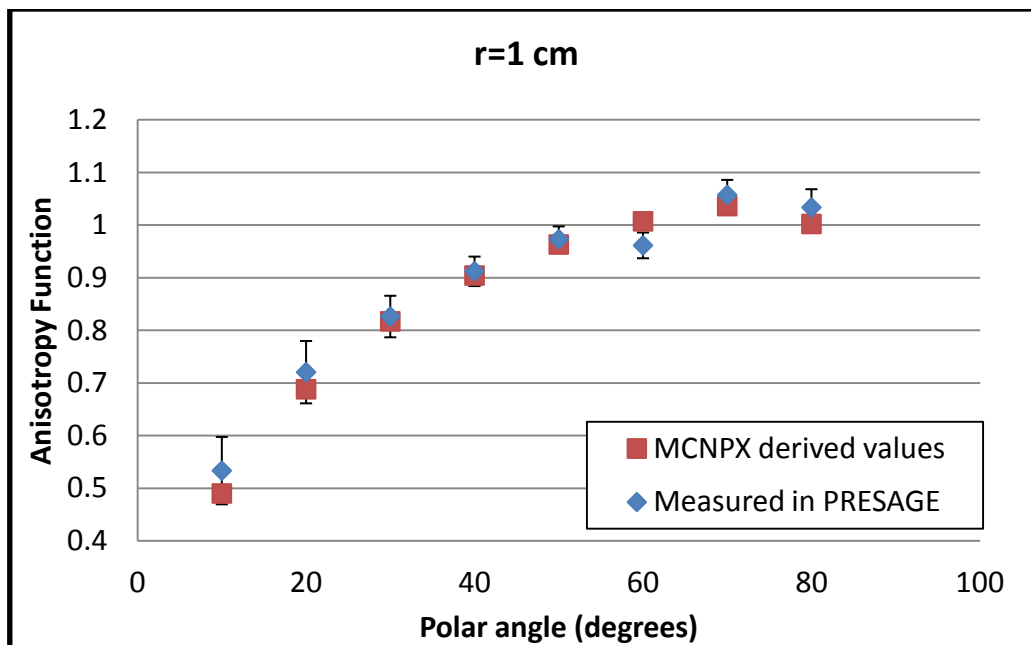


Figure 31. AgX100 Anisotropy Function at $r = 1$ cm: The MCNPX derived values (red) are plotted with the anisotropy function values measured in PRESAGE[®] (blue). Error bars show $\pm 1\sigma$ of the measured values.

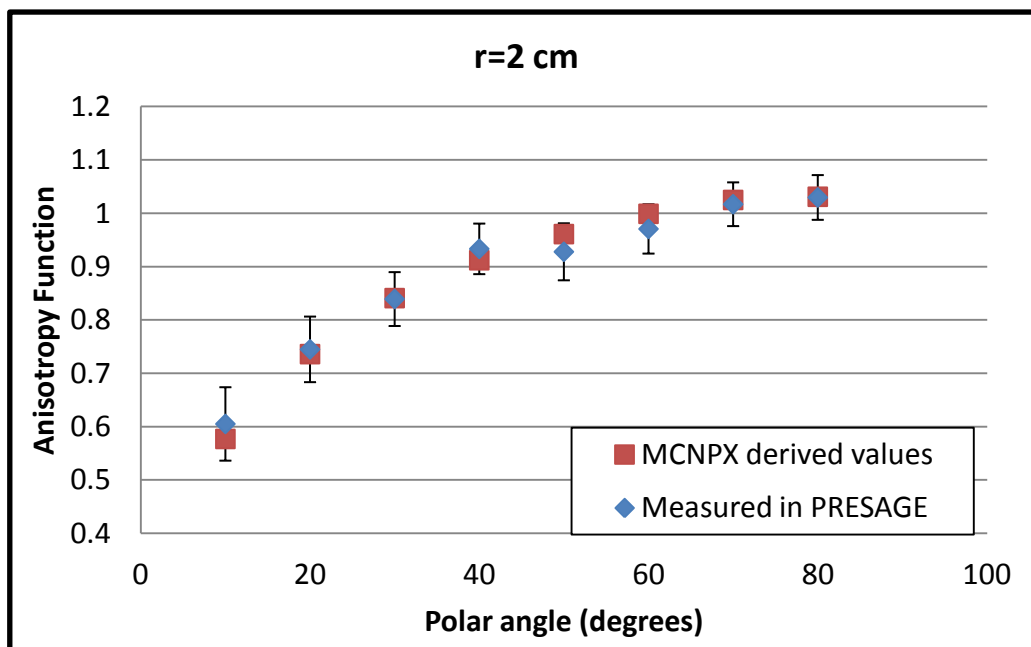


Figure 32. AgX100 Anisotropy Function at $r = 2$ cm: The MCNPX derived values (red) are plotted with the anisotropy function values measured in PRESAGE[®] (blue). Error bars show $\pm 1\sigma$ of the measured values.

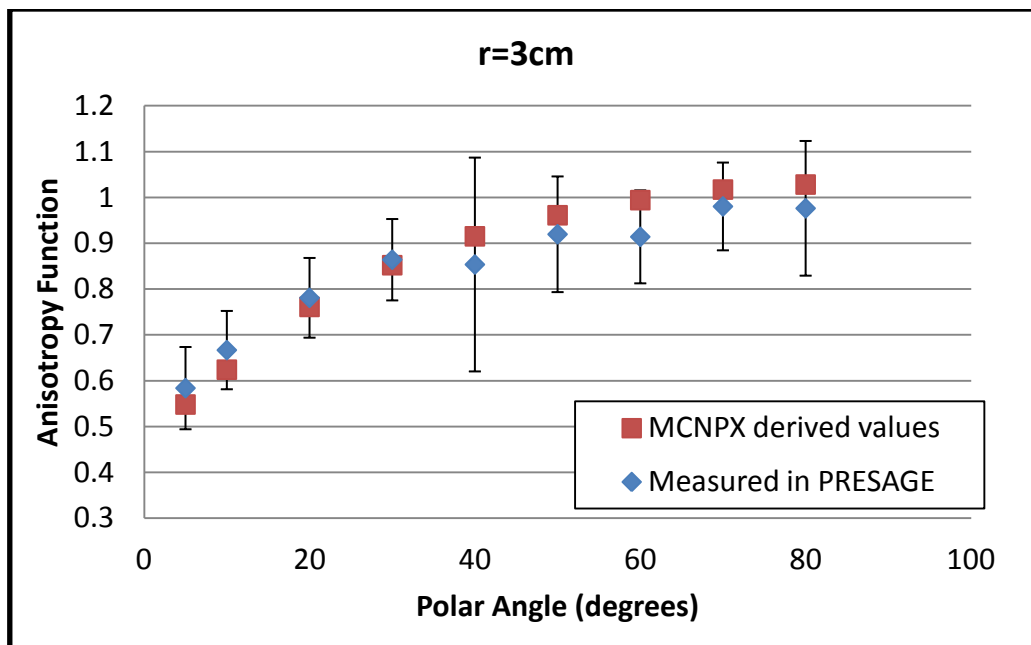


Figure 33. AgX100 Anisotropy Function at $r = 3$ cm: The MCNPX derived values (red) are plotted with the anisotropy function values measured in PRESAGE[®] (blue). Error bars show $\pm 1\sigma$ of the measured values.

4.5 Radial Dose Functions

The radial dose functions measured in previous publications and in this study are shown in Table 27 below. For a quantitative comparison, the PRESAGE[®] measured radial dose functions were compared to the Monte Carlo calculated values.

r (cm)	MCNPX derived	PRESAGE [®] measured	Relative difference (%)	1σ	COV (%)
1	1.000	1.000	--	--	--
1.5	0.908	0.911	0.3	0.029	3.2
2	0.813	0.831	2.2	0.037	4.5
2.5	0.720	0.729	1.3	0.055	7.5
3	0.633	0.634	0.2	0.053	8.4

Table 25. AgX100- Radial Dose Function Comparison

The PRESAGE[®]-measured values agreed with the averaged values within 2.5%. Similar to the pattern observed in the dose rate measurements, the coefficient of variation gradually increased at larger radial distances, which is most likely due to doses that are too low (less than 50 cGy) for the imaging system to capture. Such low doses produce minimal OD change in PRESAGE[®], which may be difficult to capture through the DMOS and would be influenced by background noise. As seen in Figure 23, the lower dose values resulted in jagged isodose lines or dose measurements that were less consistent, thus increasing the standard deviations in the dose measurements. Figure 37 is the graphical representation of the radial dose function values. The PRESAGE[®] measured values were plotted with error bars of ± 1 standard deviation.

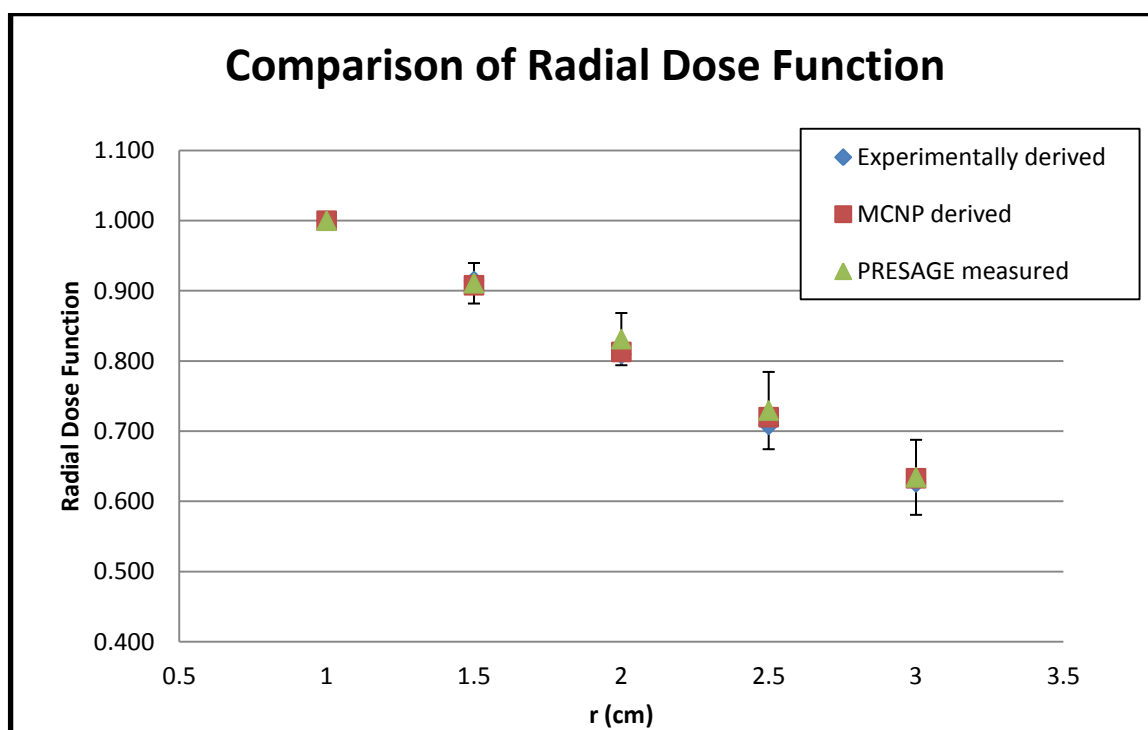


Figure 34. AgX100: Radial Dose Function Comparison: Experimentally derived (TLT) values are shown in blue, MCNPX calculated values are shown in red, and the PRESAGE[®] measured values are shown in green with error bars showing $\pm 1\sigma$.

5 Discussion of the over-response in PRESAGE® at low doses

5.1 Post-irradiation OD change over time

Previous work with PRESAGE® dosimetry has consistently involved external radiation beams only. The irradiation times for external beams are short, ranging from a few seconds to a few minutes depending on the number of beams used and the complexity of the treatment plan. The dose response in PRESAGE® over long periods of irradiation times (several days) has not yet been evaluated and potential changes in dose response as result of long exposure times are unknown. Optical density change in response to radiation dose in PRESAGE® at different dose ranges was suspected to contribute to the over-response observed at the 4-5 cm radial distances in the Amersham 6711 and AgX100 large channel irradiations. An experiment to evaluate the dose response changes over a long period of time was performed for a potential method of correcting the over-response observed at low doses.

Four PRESAGE® cuvettes were irradiated with a 75 kVp photon beam to 1, 3, 5, and 7 Gy. One cuvette was left unirradiated (0 Gy) to observe the background OD change in PRESAGE® over several days at room temperature. After irradiation, the cuvettes were stored in the dark at room temperature, similar to the environment of the dosimeters during irradiations. The OD of each cuvette was determined at several different time points post-irradiation from 1 hour up to 8 days. Tables 28-29 show the change in OD at each read-out. The PRESAGE® dose response to radiation was found to be consistently linear regardless of the time duration post-irradiation, as shown in Figure 35.

Dose	Hours post-irradiation							
	1	2	3	4	5	6	22	31
0	0.000	0.000	0.000	0.000	0.001	0.001	0.001	0.003
1	0.033	0.034	0.034	0.034	0.035	0.036	0.041	0.046
3	0.092	0.094	0.095	0.096	0.098	0.098	0.102	0.104
5	0.145	0.148	0.150	0.152	0.152	0.153	0.157	0.156
7	0.213	0.220	0.218	0.220	0.221	0.222	0.225	0.226

Table 26. OD change at several time points post-irradiation

Dose	Hours post-irradiation							
	48	78	94	104	123	144	170	192
0	0.010	0.007	0.008	0.008	0.010	0.011	0.013	0.013
1	0.045	0.045	0.044	0.045	0.045	0.046	0.047	0.045
3	0.105	0.105	0.103	0.103	0.102	0.101	0.101	0.098
5	0.154	0.150	0.149	0.147	0.145	0.144	0.142	0.137
7	0.222	0.217	0.215	0.214	0.210	0.207	0.204	0.198

Table 27. OD change at several time points post-irradiation (continued)

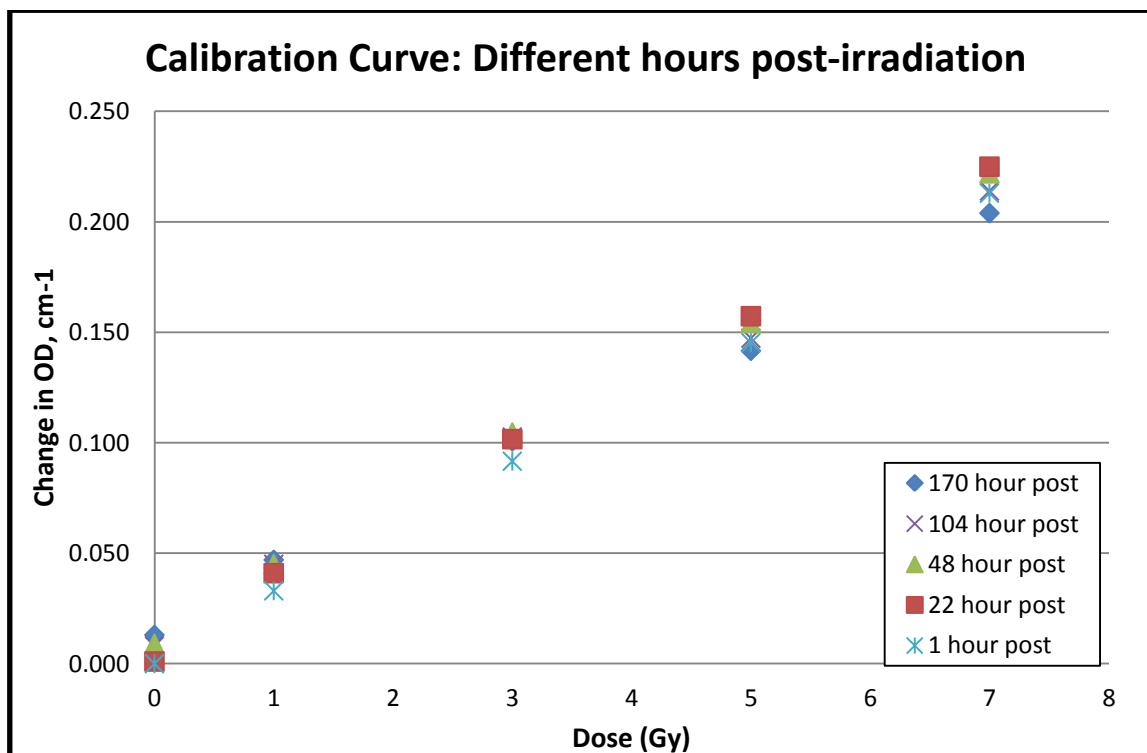


Figure 35. Calibration curve demonstrating linearity in dose response

The change in OD over time post-irradiation was found to be non-linear at each dose level and is dependent on the dose the PRESAGE® cuvette was irradiated to. Figures 36-40 graphically show the trends in OD change at each dose level.

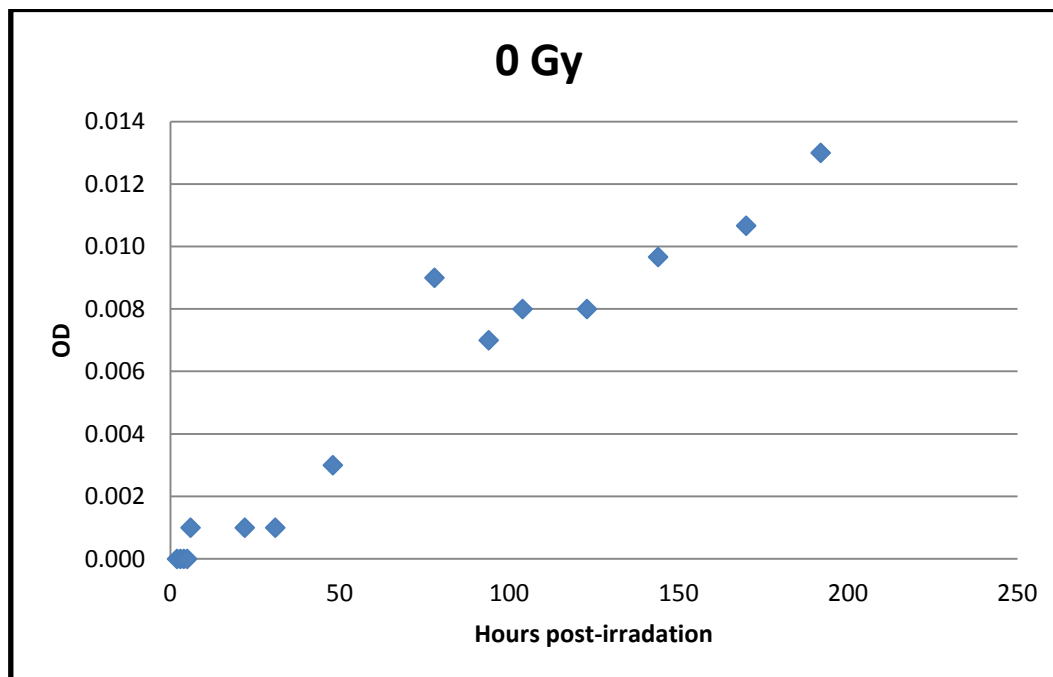


Figure 36. OD change over time for PRESAGE® at 0 Gy

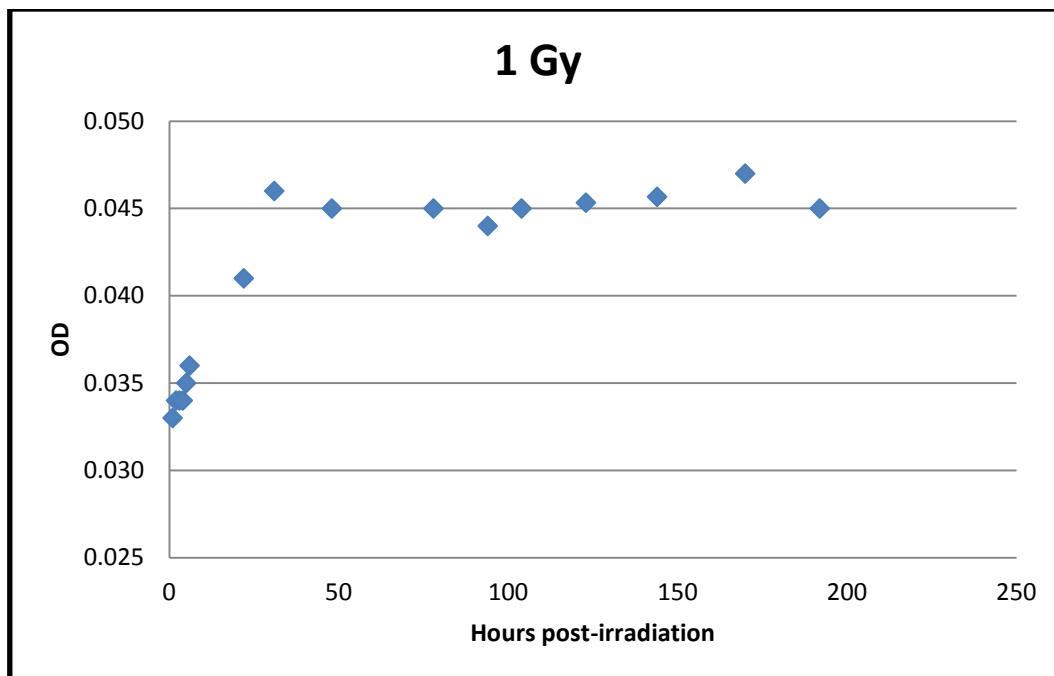


Figure 37. OD change over time for PRESAGE® at 1 Gy

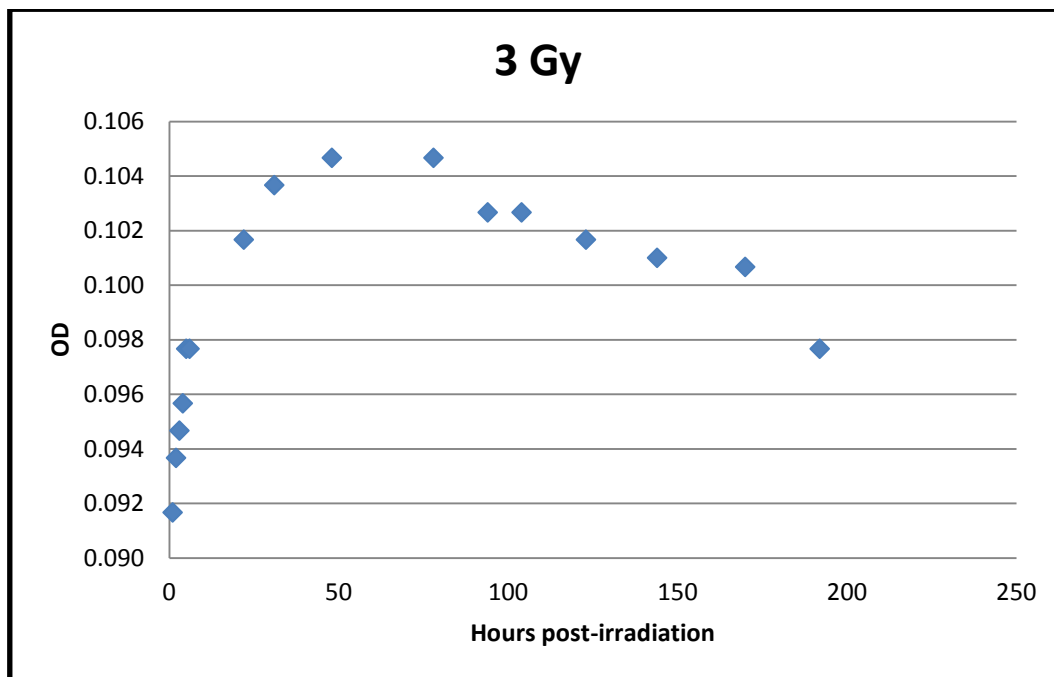


Figure 38. OD change over time for PRESAGE® at 3 Gy

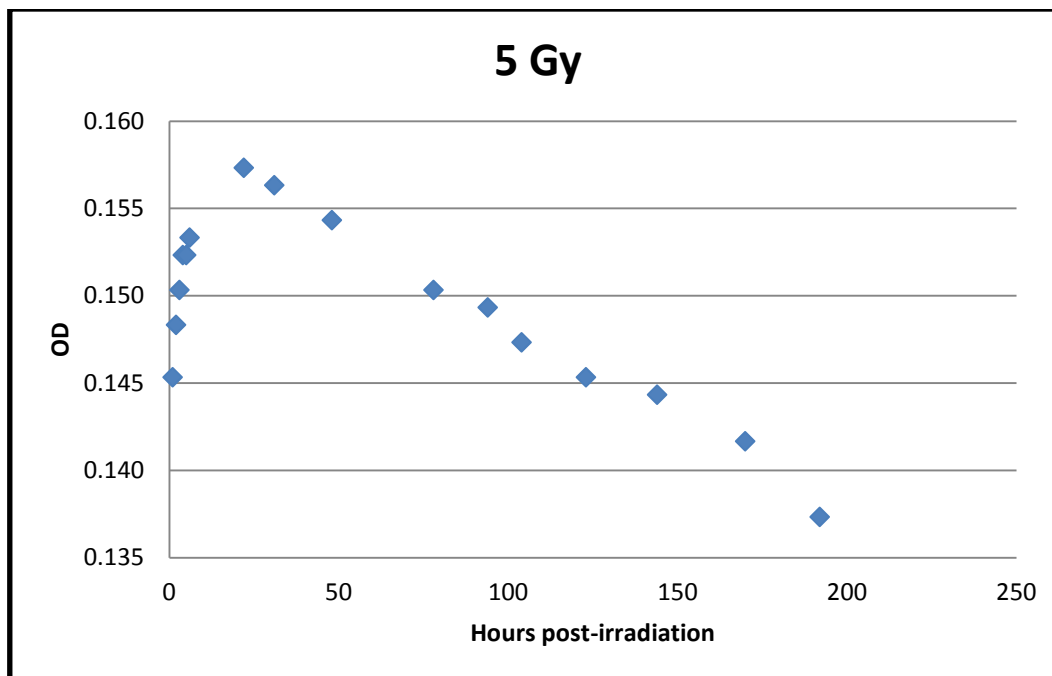


Figure 39. OD change over time for PRESAGE® at 5 Gy

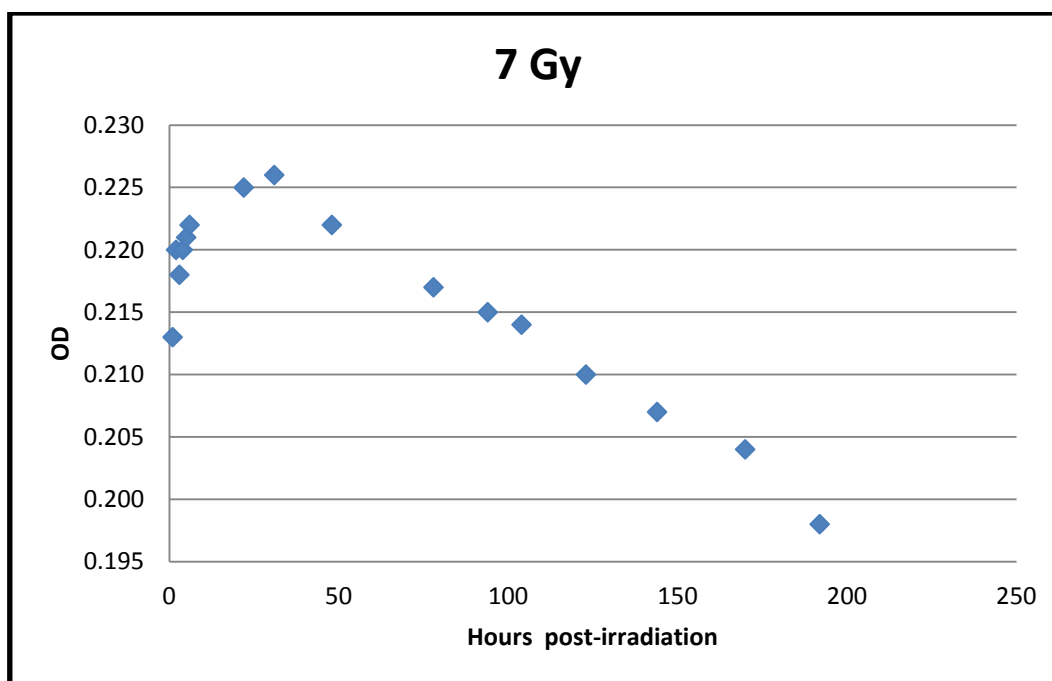


Figure 40. OD change over time for PRESAGE® at 7 Gy

This study shows that OD changes in PRESAGE[®] over time can vary drastically depending on the dose deposited in the dosimeter. With no dose deposited, the OD change in PRESAGE[®] increases relatively linearly over time. This was expected, since PRESAGE[®] is known to darken at a faster rate at room temperature. For higher doses of 3 Gy, 5 Gy and 7 Gy, the OD response increases until approximately 31-50 hours post-irradiation, then consistently decreases with time. Unexpectedly, the change in OD beyond 100 hours post-irradiation fell below the initial OD response at 5 Gy and 7 Gy. This phenomenon of the fading of signal at different rates for different doses in PRESAGE[®] suggests that the post-irradiation optical-CT scan for dosimeters should be held within 48 hours after irradiation. The OD response to 1 Gy continually increased until approximately 48 hours and then maintained a relatively constant response from 48-192 hours. Since the over-response measurements were in regions of dose levels below 1 Gy, the results at 1 Gy was the best approximation for the dose levels at $r = 4$ to 5 cm in the Amersham 6711 large channel dosimeter and $r = 2.5$ to 5 cm in the AgX100 large channel dosimeter.

The change in response at 1 Gy was the greatest compared to the rest of the dose responses at higher doses. While the higher doses eventually began to decrease in response, the response at 1 Gy did not follow the same trend. Since the irradiation times for the large channel dosimeters ranged from approximately 5 to 10 days, the OD response to the doses deposited within the first few days of the irradiation were likely to have changed drastically by the time of the post-irradiation optical-CT scan. The OD at larger distances from the source (smaller doses) did not experience the drastic decrease in OD at smaller distances (larger doses) from the source. Therefore, after the irradiation duration of 5-10 days and the dose values were captured and normalized to the dose at 1.5 cm, the non-linear changes over

the irradiation period resulted in dose values much higher than expected at the larger distances.

Figure 44 below shows the isodose lines on the transverse bisecting plane of the large channel dosimeter irradiated with the AgX100. The isodose lines represent the doses expected (calculated using the dose rate constant), where the pink line represents the calculated dose at 1.5 cm, the green represents the calculated dose at 2 cm, blue represents the calculated dose at 3 cm, and so forth. By measuring the diameters of each isodose curve (distances are displayed in the figure), it was determined that the expected doses at $r = 3$ cm, $r = 4$ cm, $r = 5$ cm actually ended up at $r = 3.07$ cm, $r = 4.44$ cm, and $r = 5.25$ cm. The isodose curves for doses at $r = 1.5$ cm and $r = 2$ cm were accurate in measurement. This proved to be a visual confirmation of the over-response farther away from the source at doses below 1 Gy. The jaggedness of the isodose lines beyond 2.552 Gy also suggests that the OD response was unstable and was perhaps changing, or that the small dose values resulted in larger statistical variations.

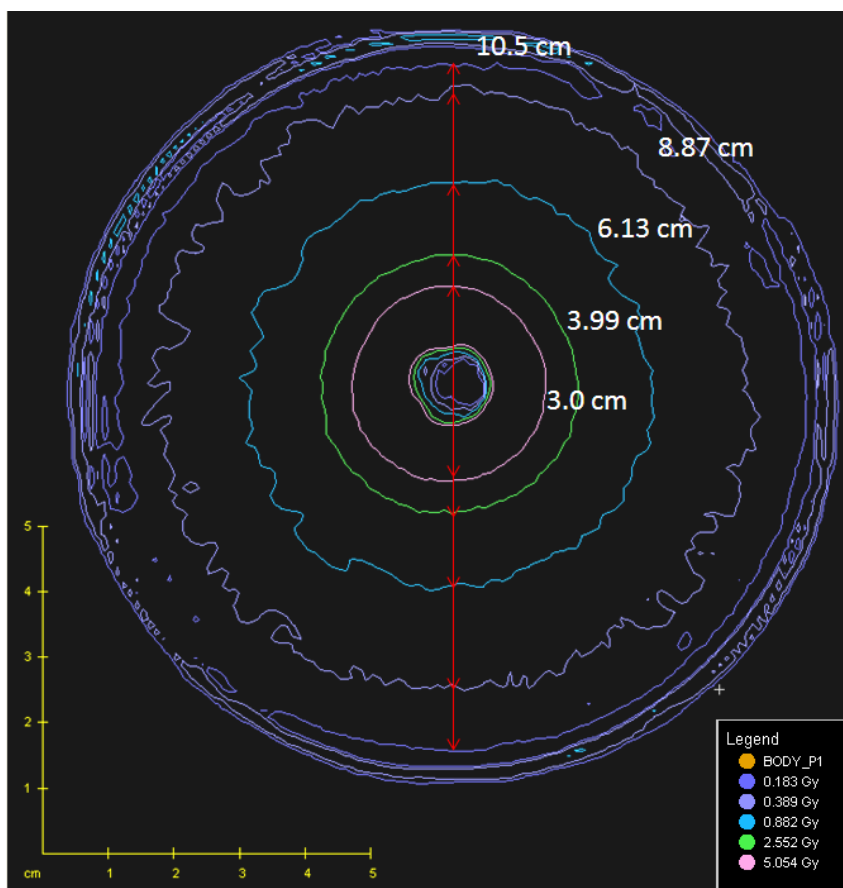


Figure 41. Isodose lines of AgX100-irradiated large channel dosimeter

5.2 Method of correction

An attempt was made to quantify this over-response and to determine correction values for the doses at larger distances from the source. The most straightforward method to account for the non-linear changes in OD response over time was to determine the dose deposited on each day of the irradiation at each radial distance. A correction factor could then be applied to the dose from each day using the ratio of the OD change at the time points post-irradiation to the post-irradiation optical-CT scan time point. A more detailed explanation of this method is described through the following example for the correction factor at $r = 4$ cm in the Amersham 6711-irradiated large channel dosimeter.

The large channel dosimeter was irradiated for a total of 137.83 hours. The dose deposited per day calculated from the decay-corrected air kerma strength of the source was determined and is shown in the Table 30. The “OD-Ratio” was determined by dividing the OD at the post-irradiation time by the OD measured at the time of the optical-CT scan. The four hour post-irradiation OD measurement was chosen as the reference OD since the dosimeter was scanned 4 hours after the removal of the seed. The dose delivered on Day 1 of the irradiation was calculated to be 6.22 cGy at 4 cm. According to the experimental data from Section 5.1 Table 29, the OD response measured at a dose of 1 Gy, 123 hours (the closest time duration to 118.3 hours) post-irradiation is 0.045. Table 28 from Section 5.1 shows that the OD response measured at a dose of 1 Gy 4 hours post-irradiation is 0.034. Therefore, the OD-Ratio of 1.32 gives an estimate of the amount of over-response from the dose deposited on day 1.

Source Strength		Dose on Day 1	
Source Calibration Date	4/17/2013	Irradiation start date	5/23/2013
Calibration Time	2:12 PM	Irradiation start time	4:10 PM
Calibration Strength (U)	13.1229	Irradiation end date	5/24/2013
Today's Date	5/23/2013	Irradiation end time	4:10 PM
Time	4:10 PM	Irradiation duration (h)	24.00
Half-Life of Source (days)	59.43	Dose to 4 cm (cGy)	6.224
Total Time Duration (days)	36.08	Post-irradiation time	118.33
Source strength on Day 1	8.6152	OD-Ratio	1.32

Table 28. Table describing dose deposited on Day 1 at r=4cm and the calculated OD-Ratio

The OD-Ratios were calculated for the dose deposited on each day, and the weighted-mean of the OD-Ratios was determined to be the factor the doses were scaled to over the post-irradiation time. The mean OD-Ratios for doses at r = 4 cm was determined to be 1.259. The mean OD-Ratios for doses at r = 1.5 cm was determined to be 0.991. Since the dose values were normalized to the dose at r = 1.5, the final correction factor for the dose at

$r = 4$ cm was determined by taking the ratio of the weighted-mean OD-Ratio for $r = 4$ cm to $r = 1.5$ cm: $\frac{1.258}{0.994} = 1.266$. Using this approximation of over-response over time, the originally measured dose value of 0.38 Gy at $r = 4$ cm is adjusted to 0.30 Gy. Table 31 below shows the estimated “corrected” doses at each radial distance using the method just described. For the detailed calculation data at each radial distance, please refer to Appendix B.

r (cm)	1.5	2	3	4	5
Measured Dose (original)	4.491	2.211	0.784	0.382	0.244
Weighted mean OD-Ratio	0.994	1.068	1.259	1.258	1.259
Final Correction Factor	1.000	1.074	1.267	1.266	1.267
"Corrected" Dose	4.491	2.059	0.619	0.302	0.193
Expected Dose	4.491	2.268	0.782	0.346	0.162

Table 29. “Corrected” doses at each radial distance for the 6711-irradiated dosimeter

Unfortunately, this method does not seem to accurately correct for the dose response changes over time. This “correction” method resulted in an under-response at all radial distances except at $r = 5$ cm. There were several main reasons for the inaccuracy of this method. Firstly, the change in dose response values used to calculate the weighted-mean OD-Ratios were derived from OD changes at 1 Gy. The doses below 1 Gy may have caused different OD response changes. Secondly, the values used to determine the correction factor were derived from PRESAGE[®] cuvettes that were irradiated with external beam radiation. The behavior of the dose response for continuous exposure in brachytherapy may be different, especially since the OD is continuously increasing from dose. Furthermore, PRESAGE[®] is known to have volume effects. The OD changes in a PRESAGE[®] cuvette

may not accurately represent the changes that would be observed in a large volume PRESAGE[®].

6 Uncertainty Analysis

6.1 Uncertainty in the Dose Rate Constant

As recommended by TG-43U1, the uncertainty in the brachytherapy dosimetry in PRESAGE[®] dosimeters was thoroughly evaluated. The uncertainty analysis follows the recommended protocol set forth in AAPM TG-138[15]. The summary of the Type A and Type B uncertainties for the Amersham 6711 and the AgX100 dose measurements are listed in Table 32 with the final estimation of the total expanded uncertainty ($k=2$) for a 95% confidence limit. The total standard uncertainty ($k=1$) for the dose rates measured in PRESAGE[®] was estimated to be 3.0% and the expanded uncertainty ($k=2$) was 6.0%.

Type A uncertainties in this project were the statistical uncertainties of repeated point-dose measurements in PRESAGE[®]. This uncertainty was analyzed through multiple measurements of the same dose line profile on one plane in the dose cube. The uncertainty was estimated to be 0.3% ($k=1$). The type B uncertainties in this study include several factors. The seed calibration of each source used in this project was calibrated by the ADCL at M.D. Anderson Cancer Center. The uncertainties in the source strength calibration include the NIST WAFAC calibration uncertainty, the ADCL chamber calibration, and the reproducibility of the ADCL air kerma strength measurements of the sources. The total uncertainty was estimated to be 0.9% ($k=1$), as listed in Table 32. The uncertainty in the OD-to-dose conversion lies in the fitting of the dose calibration curve and was estimated to be 0.3%.

The uncertainty dose due to positioning of the seed was estimated to be 2.0%, since the diameter of the catheter was 0.02 cm wider than the diameter of the seeds and there was a potential 0.01 cm shift in the center position (seed diameter = 0.08 cm). The uncertainty in the water equivalency of PRESAGE[®] material for accurate dose to water dosimetry was evaluated. Gorjiara et al. thoroughly investigated the radiological water equivalence of different formulations of PRESAGE[®] at energies ranging from 50 kVp to 6 MV x-ray beams[45]. The authors measured the maximum (k=2) uncertainty to be approximately 4% for photons in the 10-100 keV energy range. This large uncertainty is mainly due to the dominant interaction of photoelectric effect in the ¹²⁵I emitted energy spectrum, which results in higher absorbed dose in PRESAGE[®] than in water because of the slightly higher effective Z of 7.6 in PRESAGE[®] (effective Z of water is 7.42).

The quadrature sum was determined from all of the Type A and Type B uncertainties listed below for the total standard uncertainty (k=1). The expanded relative uncertainty (k=2) is simply double the total standard uncertainty value.

Uncertainty Component	Type A (k=1)	Type B (k=1)
OD from measurement point selection	0.3%	
Seed Calibration (NIST + ADCL)		0.9%
OD-to-Dose Conversion (fitting)		0.3%
Dose at r = 1 cm from seed positioning in catheter (± 0.01 cm)		2.0%
Water-equivalency of PRESAGE [®]		2.0%
Total standard uncertainty (k=1)	3.0%	
Expanded relative uncertainty (k=2)	6.0%	

Table 30. Uncertainty in PRESAGE[®] measurements of the dose rate constant

6.2 Uncertainty in Anisotropy Function

By definition, anisotropy is a ratio between two doses. As such, error (uncertainty) in seed calibration and uncertainty due to water equivalency would cancel out. Source positioning uncertainty (± 0.01 cm) would also have somewhat compensatory effects for anisotropy calculation. The resulting uncertainty from source positioning was estimated to be 1.0%. Therefore, resulting dose uncertainty for anisotropy would reduce to 1.1%. Thus, uncertainty ($k=1$) in measured anisotropy values would be 1.5%. The expanded relative uncertainty ($k=2$) would be 3.0%.

6.3 Uncertainty in the Radial Dose Function

Like anisotropy, radial dose function values are ratios of two doses. Therefore, the uncertainty arguments stated for dose anisotropy would apply for radial dose function as well. However, source position uncertainty (± 0.01 cm) may have a higher impact at shorter radial distances. The uncertainty ($k=1$) in measured radial dose values would be 1.5% and the expanded relative uncertainty ($k=2$) would be 3.0%.

7 Conclusion

The hypothesis for this project was accepted for dose measurements up to $r=3$ cm. The dosimetric parameters measured in PRESAGE[®] using the Amersham 6711 seed model were within $\pm 5\%$ of the TG-43U1 values for dosimetry parameters measured in the range of $r = 1$ to $r = 3$ cm. The AgX100 seed model was successfully characterized using PRESAGE[®] from $r = 1$ to $r = 3$ cm.

The results of this study demonstrate great potential in use of PRESAGE[®] for brachytherapy dosimetry. For both the Amersham 6711 and AgX100 seed irradiations, the measured dose rates up to distances 3 cm away from the source were within $\pm 3\%$ of the consensus values. The radial functions and the anisotropy functions measured in PRESAGE[®] also agreed well with values in TG-43U1 and previous publications. The AgX100 seed was successfully characterized, and the resulting dosimetric parameters agreed with Monte Carlo derived values within $\pm 9\%$.

However, there are several factors to be aware of for future work. First of all, the issue with the rate of OD change with time in different dose ranges needs to be addressed for more accurate dosimetry in the future. This can be done either by using high air kerma strength sources to keep irradiation times low and dose values high, or by finding a way to correct for the dose response changes. As shown in Chapter 5, finding an appropriate method to accurately correct for the OD change at different doses over different post-irradiation time periods can be a difficult and complicated task. To avoid dealing with this phenomenon in PRESAGE[®], it would be best to keep the time between seed placement in the dosimeter to the post-irradiation optical-CT scan within 48 hours. Secondly, the doses used for dosimetry measurements should be at a minimum of 20 cGy. For a coefficient of variation under 3%, doses should be at a minimum of 1 Gy.

As with every research project, there is always much room for improvements. To continue with this work, it would be strongly beneficial for a more advanced method of dose analysis. The dose measurements in this project were acquired manually through dose line profiles in CERR and the calculated dosimetric parameters were computationally intensive

and time-consuming. A more automatic method of analysis- perhaps similar to a 3D gamma analysis- would be more efficient. Furthermore, the effective Z of PRESAGE[®] is water-equivalent for MV energy radiation beams. Although the PRESAGE[®] formulations are continuously improving and the effective Z of the O-MeO-LMG formulation used in this study is even lower than the effective Z of the formulations previously evaluated by Gorjiara et al., it is possible that a small correction factor may still be needed for the low energy emitted by ¹²⁵I sources.

The findings in this study help to pave the way for 3D brachytherapy dosimetry in PRESAGE[®], which would greatly improve the general knowledge and confidence in the 3D dosimetry of sources used in brachytherapy and also advance quality assurance methods. Despite the limitations described previously, PRESAGE[®] can serve as a reliable dosimetry tool, especially for high activity irradiations. Future work in dosimetry evaluations for HDR devices or the COMS eye plaque (consisting of multiple seeds for a higher total activity) in PRESAGE[®] are likely to produce promising results and may be the start of the new 3D dosimetry era for brachytherapy.

Appendix A

Anisotropy Function data for the Amersham 6711-

PRESAGE: Anisotropy Function Table

θ (°)	r (cm)					
	r=0.5	r=1	r=2	r=3	r=4	r=5
0						
5				0.526	0.457	
10			0.594	0.574	0.593	
20		0.725	0.722	0.853	0.902	
30	0.589	0.792	0.845	0.915	1.034	
40	0.819	0.890	0.913	0.954	1.130	1.351
50	0.828	0.956	0.978	0.990	1.120	1.257
60	0.900	0.953	0.961	1.026	1.052	1.096
70	0.940	1.022	0.982	1.026	1.042	1.055
80	0.957	1.019	0.972	0.969	0.978	1.123

Relative differences

θ (°)	r (cm)					
	r=0.5	r=1	r=2	r=3	r=4	r=5
0						
5				-1.69	-18.50	
10			2.37	-5.68	-5.81	
20		2.83	-0.66	14.83	19.94	
30	-30.35	-5.02	0.39	8.20	21.88	
40	-11.56	-3.83	-1.39	3.05	21.81	45.62
50	-14.83	-1.67	0.82	2.18	15.56	29.74
60	-9.21	-3.81	-2.62	3.95	6.54	11.07
70	-5.59	2.58	-1.41	3.16	4.72	6.00
80	-4.32	1.89	-2.84	-3.05	-2.08	12.42

Standard Deviations

θ (°)	r (cm)					
	r=0.5	r=1	r=2	r=3	r=4	r=5
0						
5				0.04	0.05	
10			0.05	0.04	0.05	
20		0.11	0.05	0.10	0.07	
30	0.15	0.10	0.05	0.08	0.09	
40	0.21	0.09	0.06	0.10	0.10	0.30
50	0.21	0.09	0.06	0.09	0.09	0.25
60	0.24	0.13	0.06	0.09	0.08	0.23
70	0.28	0.10	0.06	0.09	0.09	0.20
80	0.30	0.11	0.06	0.10	0.11	0.30

COV (%)

θ (°)	r (cm)					
	r=0.5	r=1	r=2	r=3	r=4	r=5
0						
5				7.08	11.81	
10			7.69	7.44	9.17	
20		14.94	6.73	11.53	8.07	
30	26.22	12.76	6.07	8.89	8.76	
40	25.61	10.19	6.39	10.45	9.22	22.15
50	25.67	9.21	5.87	9.22	7.86	19.52
60	26.86	13.50	6.58	8.73	7.46	20.60
70	29.75	10.07	5.70	8.81	8.28	19.33
80	31.59	10.55	5.80	9.83	11.38	26.73

Anisotropy Function Data for the AgX100-

Measured values

Θ (°)	r (cm)			
	r=0.5	r=1	r=2	r=3
0				
5	--	--		0.583755
10	--	0.53343	0.605138	0.666755
20	--	0.720448	0.744928	0.780834
30	0.751427	0.826172	0.839246	0.86397
40	0.868119	0.91206	0.933323	0.853528
50	0.966869	0.972967	0.927848	0.919498
60	1.021487	0.961308	0.970709	0.913896
70	0.979447	1.057201	1.017008	0.980228
80	0.962204	1.033441	1.029704	0.976139

Relative differences (%) between measured and 6711 anisotropy functions:

Θ (deg)	r (cm)			
	0.5	1	2	3
0				
5				9.11
10		-0.66	4.33	9.48
20		2.19	2.47	5.09
30	-11.18	-0.94	-0.33	2.12
40	-6.25	-1.40	0.79	-7.83
50	-0.53	0.10	-4.35	-5.11
60	3.08	-3.00	-1.65	-7.41
70	-1.66	6.14	2.11	-1.48
80	-3.78	3.34	2.97	-2.29

Relative differences (%) between measured and TLD-measured values:

θ (deg)	r (cm)		
	1	2	3
0			
5			na
10	7.11	2.91	2.42
20	7.37	-0.94	3.70
30	4.58	-2.30	2.73
40	2.25	-1.24	-6.00
50	1.88	-4.54	-2.80
60	-1.40	-3.79	-5.88
70	6.57	0.59	-4.18
80	3.97	-2.12	-3.26

Relative differences between measured and Monte Carlo-derived values:

θ (deg)	r (cm)			
	0.5	1	2	3
0				
5				6.52
10		8.86	4.88	6.85
20		4.72	1.21	2.61
30	-7.57	1.12	-0.21	1.40
40	-5.23	0.89	2.34	-6.72
50	-1.94	1.03	-3.45	-4.32
60	-0.63	-4.54	-2.83	-8.06
70	-0.77	2.05	-0.78	-3.62
80	-3.30	3.14	-0.13	-5.04

Appendix B

Data for correction method for over-response regions-

Amersham 6711 Large channel dosimeter:

Pre-scan	5/21/2013	5:00 PM
Irradiation start time:	5/23/2013	4:10 PM
Irradiation end time:	5/29/2013	10:00 AM
Post-scan	5/29/2013	2:30 PM
Total duration	137.83	

r = 1 cm			
Delivered Dose per day		Dose on Day 1	
Calibration Date	4/17/2013	Irradiation start date	5/23/2013
Calibration Time	2:12 PM	Irradiation start time	4:10 PM
Calibration Strength (U)	13.1229	Irradiation end date	5/24/2013
Today's Date	5/23/2013	Irradiation end time	4:10 PM
Actual Time	4:10 PM	Irradiation duration	24.00
Half-Life of Source (days)	59.43	Dose to 1 cm (cGy)	199.5275991
Total Time Duration (days)	36.08194444	time post-irradiation	118.33
Source strength on Day 1	8.61518131	OD-Ratio	0.954545455
Delivered Dose per day		Dose on Day 2	
Calibration Date	4/17/2013	Irradiation start date	5/24/2013
Calibration Time	2:12 PM	Irradiation start time	4:10 PM
Calibration Strength (U)	13.1229	Irradiation end date	5/25/2013
Today's Date	5/24/2013	Irradiation end time	4:10 PM
Actual Time	4:10 PM	Irradiation duration	24.00
Half-Life of Source (days)	59.43	Dose to 1 cm (cGy)	197.2139765
Total Time Duration (days)	37.08194444	time post-irradiation	94.33
Source strength on Day 2	8.51528396	OD-Ratio	0.977272727
Delivered Dose per day		Dose on Day 3	
Calibration Date	4/17/2013	Irradiation start date	5/25/2013
Calibration Time	2:12 PM	Irradiation start time	4:10 PM
Calibration Strength (U)	13.1229	Irradiation end date	5/26/2013
Today's Date	5/25/2013	Irradiation end time	4:10 PM
Actual Time	4:10 PM	Irradiation duration	24.00
Half-Life of Source (days)	59.43	Dose to 1 cm (cGy)	194.9271815
Total Time Duration (days)	38.08194444	time post-irradiation	70.33
Source strength on Day 3	8.416544969	OD-Ratio	0.986363636
Delivered Dose per day		Dose on Day 4	
Calibration Date	4/17/2013	Irradiation start date	5/26/2013
Calibration Time	2:12 PM	Irradiation start time	4:10 PM
Calibration Strength (U)	13.1229	Irradiation end date	5/27/2013
Today's Date	5/26/2013	Irradiation end time	4:10 PM
Actual Time	4:10 PM	Irradiation duration	24.00
Half-Life of Source (days)	59.43	Dose to 1 cm (cGy)	192.666903
Total Time Duration (days)	39.08194444	time post-irradiation	46.33

Source strength on Day 4	8.318950906	OD-Ratio	1.009090909
Delivered Dose per day			
Calibration Date		Dose on Day 5	
Calibration Date	4/17/2013	Irradiation start date	5/27/2013
Calibration Time	2:12 PM	Irradiation start time	4:10 PM
Calibration Strength (U)	13.1229	Irradiation end date	5/28/2013
Today's Date	5/27/2013	Irradiation end time	4:10 PM
Actual Time	4:10 PM	Irradiation duration	24.00
Half-Life of Source (days)	59.43	Dose to 1 cm (cGy)	190.4328336
Total Time Duration (days)	40.08194444	time post-irradiation	22.33
Source strength on Day 5	8.222488496	OD-Ratio	1.022727273
Delivered Dose per day			
Calibration Date		Dose on Day 6	
Calibration Date	4/17/2013	Irradiation start date	5/28/2013
Calibration Time	2:12 PM	Irradiation start time	4:10 PM
Calibration Strength (U)	13.1229	Irradiation end date	5/29/2013
Today's Date	5/28/2013	Irradiation end time	10:00 AM
Actual Time	4:10 PM	Irradiation duration	17.83
Half-Life of Source (days)	59.43	Dose to 1 cm (cGy)	139.8613862
Total Time Duration (days)	41.08194444	time post-irradiation	4.50
Source strength on Day 6	8.127144615	OD-Ratio	1
		Total Dose (cGy)	1114.630
		Weighted mean of factor	0.991
		Dose in PRESAGE (cGy)	1104.500
		Correction factor	1.009

r = 2 cm			
Delivered Dose per day		Dose on Day 1	
Calibration Date	4/17/2013	Irradiation start date	5/23/2013
Calibration Time	2:12 PM	Irradiation start time	4:10 PM
Calibration Strength (U)	13.1229	Irradiation end date	5/24/2013
Today's Date	5/23/2013	Irradiation end time	4:10 PM
Actual Time	4:10 PM	Irradiation duration	24.00
Half-Life of Source (days)	59.43	Dose to 1.5 cm (cGy)	80.84486142
Total Time Duration (days)	36.0819444	time post-irradiation	118.33
Source strength on Day 1	8.61518131	OD-Ratio	0.95404814
Delivered Dose per day			
		Dose on Day 2	

Calibration Date	4/17/2013	Irradiation start date	5/24/2013
Calibration Time	2:12 PM	Irradiation start time	4:10 PM
Calibration Strength (U)	13.1229	Irradiation end date	5/25/2013
Today's Date	5/24/2013	Irradiation end time	4:10 PM
Actual Time	4:10 PM	Irradiation duration	24.00
Half-Life of Source (days)	59.43	Dose to 1.5 cm (cGy)	79.90742468
Total Time Duration (days)	37.0819444	time post-irradiation	94.33
Source strength on Day 2	8.51528396	OD-Ratio	0.980306346
Delivered Dose per day			
Calibration Date		Dose on Day 3	
Calibration Date	4/17/2013	Irradiation start date	5/25/2013
Calibration Time	2:12 PM	Irradiation start time	4:10 PM
Calibration Strength (U)	13.1229	Irradiation end date	5/26/2013
Today's Date	5/25/2013	Irradiation end time	4:10 PM
Actual Time	4:10 PM	Irradiation duration	24.00
Half-Life of Source (days)	59.43	Dose to 1.5 cm (cGy)	78.98085799
Total Time Duration (days)	38.0819444	time post-irradiation	70.33
Source strength on Day 3	8.41654497	OD-Ratio	0.986870897
Delivered Dose per day			
Calibration Date		Dose on Day 4	
Calibration Date	4/17/2013	Irradiation start date	5/26/2013
Calibration Time	2:12 PM	Irradiation start time	4:10 PM
Calibration Strength (U)	13.1229	Irradiation end date	5/27/2013
Today's Date	5/26/2013	Irradiation end time	4:10 PM
Actual Time	4:10 PM	Irradiation duration	24.00
Half-Life of Source (days)	59.43	Dose to 1.5 cm (cGy)	78.0650353
Total Time Duration (days)	39.0819444	time post-irradiation	46.33
Source strength on Day 4	8.31895091	OD-Ratio	1.013129103
Delivered Dose per day			
Calibration Date		Dose on Day 5	
Calibration Date	4/17/2013	Irradiation start date	5/27/2013
Calibration Time	2:12 PM	Irradiation start time	4:10 PM
Calibration Strength (U)	13.1229	Irradiation end date	5/28/2013
Today's Date	5/27/2013	Irradiation end time	4:10 PM
Actual Time	4:10 PM	Irradiation duration	24.00
Half-Life of Source (days)	59.43	Dose to 1.5 cm (cGy)	77.15983204
Total Time Duration (days)	40.0819444	time post-irradiation	22.33
Source strength on Day 5	8.2224885	OD-Ratio	1.032822757
Delivered Dose per day			
Calibration Date		Dose on Day 6	
Calibration Date	4/17/2013	Irradiation start date	5/28/2013
Calibration Time	2:12 PM	Irradiation start time	4:10 PM

Calibration Strength (U)	13.1229	Irradiation end date	5/29/2013
Today's Date	5/28/2013	Irradiation end time	10:00 AM
Actual Time	4:10 PM	Irradiation duration	17.83
Half-Life of Source (days)	59.43	Dose to 1.5 cm (cGy)	56.66922488
Total Time Duration (days)	41.0819444	time post-irradiation	4.50
Source strength on Day 6	8.12714462	OD-Ratio	1
		Total Dose (cGy)	451.627
		Weighted mean of factor	0.994
		Dose in PRESAGE (cGy)	448.859
		Correction factor	1.006

r = 3 cm			
Delivered Dose per day		Dose on Day 1	
Calibration Date	4/17/2013	Irradiation start date	5/23/2013
Calibration Time	2:12 PM	Irradiation start time	4:10 PM
Calibration Strength (U)	13.1229	Irradiation end date	5/24/2013
Today's Date	5/23/2013	Irradiation end time	4:10 PM
Actual Time	4:10 PM	Irradiation duration	24.00
Half-Life of Source (days)	59.43	Dose to 2 cm (cGy)	40.83595941
Total Time Duration (days)	36.0819444	time post-irradiation	118.33
Source strength on Day 1	8.61518131	OD-Ratio	1.06271777
Delivered Dose per day		Dose on Day 2	
Calibration Date	4/17/2013	Irradiation start date	5/24/2013
Calibration Time	2:12 PM	Irradiation start time	4:10 PM
Calibration Strength (U)	13.1229	Irradiation end date	5/25/2013
Today's Date	5/24/2013	Irradiation end time	4:10 PM
Actual Time	4:10 PM	Irradiation duration	24.00
Half-Life of Source (days)	59.43	Dose to 2 cm (cGy)	40.36244597
Total Time Duration (days)	37.0819444	time post-irradiation	94.33
Source strength on Day 2	8.51528396	OD-Ratio	1.073170732
Delivered Dose per day		Dose on Day 3	
Calibration Date	4/17/2013	Irradiation start date	5/25/2013
Calibration Time	2:12 PM	Irradiation start time	4:10 PM
Calibration Strength (U)	13.1229	Irradiation end date	5/26/2013
Today's Date	5/25/2013	Irradiation end time	4:10 PM

Actual Time	4:10 PM	Irradiation duration	24.00
Half-Life of Source (days)	59.43	Dose to 2 cm (cGy)	39.89442315
Total Time Duration (days)	38.0819444	time post-irradiation	70.33
Source strength on Day 3	8.41654497	OD-Ratio	1.094076655
Delivered Dose per day			
Calibration Date	4/17/2013	Dose on Day 4	
Calibration Time	2:12 PM	Irradiation start date	5/26/2013
Calibration Strength (U)	13.1229	Irradiation start time	4:10 PM
Today's Date	5/26/2013	Irradiation end date	5/27/2013
Actual Time	4:10 PM	Irradiation end time	4:10 PM
Half-Life of Source (days)	59.43	Irradiation duration	24.00
Total Time Duration (days)	39.0819444	Dose to 2 cm (cGy)	39.4318273
Source strength on Day 4	8.31895091	time post-irradiation	46.33
		OD-Ratio	1.094076655
Delivered Dose per day			
Calibration Date	4/17/2013	Dose on Day 5	
Calibration Time	2:12 PM	Irradiation start date	5/27/2013
Calibration Strength (U)	13.1229	Irradiation start time	4:10 PM
Today's Date	5/27/2013	Irradiation end date	5/28/2013
Actual Time	4:10 PM	Irradiation end time	4:10 PM
Half-Life of Source (days)	59.43	Irradiation duration	24.00
Total Time Duration (days)	40.0819444	Dose to 2 cm (cGy)	38.97459547
Source strength on Day 5	8.2224885	time post-irradiation	22.33
		OD-Ratio	1.06271777
Delivered Dose per day			
Calibration Date	4/17/2013	Dose on Day 6	
Calibration Time	2:12 PM	Irradiation start date	5/28/2013
Calibration Strength (U)	13.1229	Irradiation start time	4:10 PM
Today's Date	5/28/2013	Irradiation end date	5/29/2013
Actual Time	4:10 PM	Irradiation end time	10:00 AM
Half-Life of Source (days)	59.43	Irradiation duration	17.83
Total Time Duration (days)	41.0819444	Dose to 2 cm (cGy)	28.6244806
Source strength on Day 6	8.12714462	time post-irradiation	4.50
		OD-Ratio	1
		Total Dose (cGy)	228.124
		Weighted mean of factor	1.068
		Dose in PRESAGE (cGy)	243.545
		Correction factor	0.937

r = 4 cm			
Delivered Dose per day		Dose on Day 1	
Calibration Date	4/17/2013	Irradiation start date	5/23/2013
Calibration Time	2:12 PM	Irradiation start time	4:10 PM
Calibration Strength (U)	13.1229	Irradiation end date	5/24/2013
Today's Date	5/23/2013	Irradiation end time	4:10 PM
Actual Time	4:10 PM	Irradiation duration	24.00
Half-Life of Source (days)	59.43	Dose to 3 cm (cGy)	14.08065233
Total Time Duration (days)	36.08194444	time post-irradiation	118.33
Source strength on Day 1	8.61518131	OD-Ratio	1.333333333
<hr/>			
Delivered Dose per day		Dose on Day 2	
Calibration Date	4/17/2013	Irradiation start date	5/24/2013
Calibration Time	2:12 PM	Irradiation start time	4:10 PM
Calibration Strength (U)	13.1229	Irradiation end date	5/25/2013
Today's Date	5/24/2013	Irradiation end time	4:10 PM
Actual Time	4:10 PM	Irradiation duration	24.00
Half-Life of Source (days)	59.43	Dose to 3 cm (cGy)	13.9173801
Total Time Duration (days)	37.08194444	time post-irradiation	94.33
Source strength on Day 2	8.51528396	OD-Ratio	1.294117647
<hr/>			
Delivered Dose per day		Dose on Day 3	
Calibration Date	4/17/2013	Irradiation start date	5/25/2013
Calibration Time	2:12 PM	Irradiation start time	4:10 PM
Calibration Strength (U)	13.1229	Irradiation end date	5/26/2013
Today's Date	5/25/2013	Irradiation end time	4:10 PM
Actual Time	4:10 PM	Irradiation duration	24.00
Half-Life of Source (days)	59.43	Dose to 3 cm (cGy)	13.7560011
Total Time Duration (days)	38.08194444	time post-irradiation	70.33
Source strength on Day 3	8.416544969	OD-Ratio	1.323529412
<hr/>			
Delivered Dose per day		Dose on Day 4	
Calibration Date	4/17/2013	Irradiation start date	5/26/2013
Calibration Time	2:12 PM	Irradiation start time	4:10 PM
Calibration Strength (U)	13.1229	Irradiation end date	5/27/2013
Today's Date	5/26/2013	Irradiation end time	4:10 PM
Actual Time	4:10 PM	Irradiation duration	24.00
Half-Life of Source (days)	59.43	Dose to 3 cm (cGy)	13.59649336

Total Time Duration (days)	39.08194444	time post-irradiation	46.33
Source strength on Day 4	8.318950906	OD-Ratio	1.323529412
Delivered Dose per day			
Calibration Date		Dose on Day 5	
Calibration Date	4/17/2013	Irradiation start date	5/27/2013
Calibration Time	2:12 PM	Irradiation start time	4:10 PM
Calibration Strength (U)	13.1229	Irradiation end date	5/28/2013
Today's Date	5/27/2013	Irradiation end time	4:10 PM
Actual Time	4:10 PM	Irradiation duration	24.00
Half-Life of Source (days)	59.43	Dose to 3 cm (cGy)	13.4388352
Total Time Duration (days)	40.08194444	time post-irradiation	22.33
Source strength on Day 5	8.222488496	OD-Ratio	1.205882353
Delivered Dose per day			
Calibration Date		Dose on Day 6	
Calibration Date	4/17/2013	Irradiation start date	5/28/2013
Calibration Time	2:12 PM	Irradiation start time	4:10 PM
Calibration Strength (U)	13.1229	Irradiation end date	5/29/2013
Today's Date	5/28/2013	Irradiation end time	10:00 AM
Actual Time	4:10 PM	Irradiation duration	17.83
Half-Life of Source (days)	59.43	Dose to 3 cm (cGy)	9.870010778
Total Time Duration (days)	41.08194444	time post-irradiation	4.50
Source strength on Day 6	8.127144615	OD-Ratio	1
		Total Dose (cGy)	78.659
		Weighted mean of factor	1.259
		Dose in PRESAGE (cGy)	99.062
		Correction factor	0.794

r = 4 cm			
Delivered Dose per day		Dose on Day 1	
Source Calibration Date	4/17/2013	Irradiation start date	5/23/2013
Calibration Time	2:12 PM	Irradiation start time	4:10 PM
Calibration Strength (U)	13.1229	Irradiation end date	5/24/2013
Today's Date	5/23/2013	Irradiation end time	4:10 PM
Time	4:10 PM	Irradiation duration	24.00
Half-Life of Source (days)	59.43	Dose to 4 cm (cGy)	6.224
Total Time Duration (days)	36.0819444	post-irradiation time	118.33
Source strength on Day 1	8.61518131	OD-Ratio	1.32
Delivered Dose per day		Dose on Day 2	

Calibration Date	4/17/2013	Irradiation start date	5/24/2013
Calibration Time	2:12 PM	Irradiation start time	4:10 PM
Calibration Strength (U)	13.1229	Irradiation end date	5/25/2013
Today's Date	5/24/2013	Irradiation end time	4:10 PM
Actual Time	4:10 PM	Irradiation duration	24.00
Half-Life of Source (days)	59.43	Dose to 4 cm (cGy)	6.151441132
Total Time Duration (days)	37.0819444	time post-irradiation	94.33
Source strength on Day 2	8.51528396	OD-Ratio	1.294117647
Delivered Dose per day			
Calibration Date		Dose on Day 3	
Calibration Date	4/17/2013	Irradiation start date	5/25/2013
Calibration Time	2:12 PM	Irradiation start time	4:10 PM
Calibration Strength (U)	13.1229	Irradiation end date	5/26/2013
Today's Date	5/25/2013	Irradiation end time	4:10 PM
Actual Time	4:10 PM	Irradiation duration	24.00
Half-Life of Source (days)	59.43	Dose to 4 cm (cGy)	6.080112085
Total Time Duration (days)	38.0819444	time post-irradiation	70.33
Source strength on Day 3	8.41654497	OD-Ratio	1.323529412
Delivered Dose per day			
Calibration Date		Dose on Day 4	
Calibration Date	4/17/2013	Irradiation start date	5/26/2013
Calibration Time	2:12 PM	Irradiation start time	4:10 PM
Calibration Strength (U)	13.1229	Irradiation end date	5/27/2013
Today's Date	5/26/2013	Irradiation end time	4:10 PM
Actual Time	4:10 PM	Irradiation duration	24.00
Half-Life of Source (days)	59.43	Dose to 4 cm (cGy)	6.009610135
Total Time Duration (days)	39.0819444	time post-irradiation	46.33
Source strength on Day 4	8.31895091	OD-Ratio	1.323529412
Delivered Dose per day			
Calibration Date		Dose on Day 5	
Calibration Date	4/17/2013	Irradiation start date	5/27/2013
Calibration Time	2:12 PM	Irradiation start time	4:10 PM
Calibration Strength (U)	13.1229	Irradiation end date	5/28/2013
Today's Date	5/27/2013	Irradiation end time	4:10 PM
Actual Time	4:10 PM	Irradiation duration	24.00
Half-Life of Source (days)	59.43	Dose to 4 cm (cGy)	5.939925689
Total Time Duration (days)	40.0819444	time post-irradiation	22.33
Source strength on Day 5	8.2224885	OD-Ratio	1.205882353
Delivered Dose per day			
Calibration Date		Dose on Day 6	
Calibration Date	4/17/2013	Irradiation start date	5/28/2013
Calibration Time	2:12 PM	Irradiation start time	4:10 PM

Calibration Strength (U)	13.1229	Irradiation end date	5/29/2013
Today's Date	5/28/2013	Irradiation end time	10:00 AM
Actual Time	4:10 PM	Irradiation duration	17.83
Half-Life of Source (days)	59.43	Dose to 4 cm (cGy)	4.362515777
Total Time Duration (days)	41.0819444	time post-irradiation	4.50
Source strength on Day 6	8.12714462	OD-Ratio	1
		Total Dose (cGy)	34.767
		Weighted mean of factor	1.258
		Dose in PRESAGE (cGy)	43.727
		Correction factor	0.795

r = 5 cm			
Delivered Dose per day		Dose on Day 1	
Calibration Date	4/17/2013	Irradiation start date	5/23/2013
Calibration Time	2:12 PM	Irradiation start time	4:10 PM
Calibration Strength (U)	13.1229	Irradiation end date	5/24/2013
Today's Date	5/23/2013	Irradiation end time	4:10 PM
Actual Time	4:10 PM	Irradiation duration	24.00
Half-Life of Source (days)	59.43	Dose to 5 cm (cGy)	2.915377355
Total Time Duration (days)	36.08194444	time post-irradiation	118.33
Source strength on Day 1	8.61518131	OD-Ratio	1.333333333
Delivered Dose per day		Dose on Day 2	
Calibration Date	4/17/2013	Irradiation start date	5/24/2013
Calibration Time	2:12 PM	Irradiation start time	4:10 PM
Calibration Strength (U)	13.1229	Irradiation end date	5/25/2013
Today's Date	5/24/2013	Irradiation end time	4:10 PM
Actual Time	4:10 PM	Irradiation duration	24.00
Half-Life of Source (days)	59.43	Dose to 5 cm (cGy)	2.881572092
Total Time Duration (days)	37.08194444	time post-irradiation	94.33
Source strength on Day 2	8.51528396	OD-Ratio	1.294117647
Delivered Dose per day		Dose on Day 3	
Calibration Date	4/17/2013	Irradiation start date	5/25/2013
Calibration Time	2:12 PM	Irradiation start time	4:10 PM
Calibration Strength (U)	13.1229	Irradiation end date	5/26/2013
Today's Date	5/25/2013	Irradiation end time	4:10 PM
Actual Time	4:10 PM	Irradiation duration	24.00
Half-Life of Source (days)	59.43	Dose to 5 cm (cGy)	2.848158817

Total Time Duration (days)	38.08194444	time post-irradiation	70.33
Source strength on Day 3	8.416544969	OD-Ratio	1.323529412
Delivered Dose per day			
		Dose on Day 4	
Calibration Date	4/17/2013	Irradiation start date	5/26/2013
Calibration Time	2:12 PM	Irradiation start time	4:10 PM
Calibration Strength (U)	13.1229	Irradiation end date	5/27/2013
Today's Date	5/26/2013	Irradiation end time	4:10 PM
Actual Time	4:10 PM	Irradiation duration	24.00
Half-Life of Source (days)	59.43	Dose to 5 cm (cGy)	2.815132987
Total Time Duration (days)	39.08194444	time post-irradiation	46.33
Source strength on Day 4	8.318950906	OD-Ratio	1.323529412
Delivered Dose per day			
		Dose on Day 5	
Calibration Date	4/17/2013	Irradiation start date	5/27/2013
Calibration Time	2:12 PM	Irradiation start time	4:10 PM
Calibration Strength (U)	13.1229	Irradiation end date	5/28/2013
Today's Date	5/27/2013	Irradiation end time	4:10 PM
Actual Time	4:10 PM	Irradiation duration	24.00
Half-Life of Source (days)	59.43	Dose to 5 cm (cGy)	2.782490107
Total Time Duration (days)	40.08194444	time post-irradiation	22.33
Source strength on Day 5	8.222488496	OD-Ratio	1.205882353
Delivered Dose per day			
		Dose on Day 6	
Calibration Date	4/17/2013	Irradiation start date	5/28/2013
Calibration Time	2:12 PM	Irradiation start time	4:10 PM
Calibration Strength (U)	13.1229	Irradiation end date	5/29/2013
Today's Date	5/28/2013	Irradiation end time	10:00 AM
Actual Time	4:10 PM	Irradiation duration	17.83
Half-Life of Source (days)	59.43	Dose to 5 cm (cGy)	2.043570513
Total Time Duration (days)	41.08194444	time post-irradiation	4.50
Source strength on Day 6	8.127144615	OD-Ratio	1
		Total Dose (cGy)	16.286
		Weighted mean of factor	1.259
		Dose in PRESAGE (cGy)	20.511
		Correction factor	0.794

References

- [1] J.M. F. Mourtada, G. Ibbott, Monte Carlo calculations of AAPM Task Group Report No. 43 dosimetry parameters for the I-125 I-seed AgX100 source model, *Brachytherapy* 11 (2012) 237-244.
- [2] P.B. Z. Chen, R. Nath, Experimental Characterization of the Dosimetric Properties of a newly designed I-Seed model AgX100 I-125 interstitial brachytherapy source, *Brachytherapy* 11 (2012) 476-482.
- [3] S. Webb, The physical basis of IMRT and inverse planning, *The British Journal of Radiology* 76 (2003) 678-689.
- [4] J.A. M. Oldham and H. Sakhalkar and P. Guo, An investigation of the accuracy of an IMRT dose distribution using two- and three-dimensional dosimetry techniques, *Medical Physics* 35 (2008) 2072-2080.
- [5] e.a. L. M. Jampol, The COMS randomized trial of iodine 125 brachytherapy for choroidal melanoma, *Ophthalmology* 109 (2002) 2197-2206.
- [6] e.a. C. M. Yashar, Initial Clinical Experience with the Strut-Adjusted Volume Implant (SAVI) Breast Brachytherapy Device for APBI: First 100 Patients with more than 1 year of follow-up, *International Journal of Radiation Oncology* 80 (2011) 765-770.
- [7] W.F.H. A. K. Krintz, G. S. Ibbott, D. S. Followill, A reanalysis of the Collaborative Ocular Melanoma Study Medium Tumor Trial eye plaque dosimetry, *International Journal of Radiation Oncology* 56 (2003) 889-896.
- [8] K.L.L. N. L. Gagne, M. J. Rivard, Radiobiology for eye plaque brachytherapy and evaluation of implant duration and radionuclide choice using an objective function, *Medical Physics* 39 (2012) 3332-3342.

- [9] P.M. Devlin, *Brachytherapy Applications and Techniques*, Lippincott Williams & Wilkins, Philadelphia, 2007, pp. 1-5.
- [10] L.S. D. Bates, N. Zamboglou, *Medical Physics and Biomedical Engineering*, Taylor & Francis Group, LLC, Boca Raton, 2007.
- [11] J.F. Williamson, Brachytherapy technology and physics practice since 1950: a half-century of progress, *Physics in Medicine and Biology* 51 (2006) R303-R325.
- [12] J.A.L. S. W. Chen, S. N. Yang, H.L Ko, F. J. Lin, The adverse effect of treatment prolongation in cervical cancer by high dose rate intracavitary brachytherapy, *Radiotherapy and Oncology* 67 (2003) 69-76.
- [13] I. 38, Dose and volume specifications for reporting intracavitary therapy in gynecology, International Commission on Radiation Units and Measurements, Bethesda, MD, 1985, pp. 1-23.
- [14] B.M.C. M. J. Rivard, L.A. DeWerd, et al., Update of AAPM Task Group No. 43 Report: A revised AAPM protocol for brachytherapy dose calculations, *Med Phys* 31 (2004) 633-674.
- [15] G.S.I. L. A. DeWerd, A. S. Meigooni, M. G. Mitch, M. J. Rivard, K. E. Stump, B. R. Thomadsen, J. L. M. Venselaar, A dosimetric uncertainty analysis for photon-emitting brachytherapy sources: Report of AAPM Task Group No. 138 and GEC-ESTRO, *Medical Physics* 38 (2011) 782-801.
- [16] J.A.P. S.H. Levitt, C.A. Perez, S. vijayakumar, *Technical Basis of Radiation Therapy*, Springer-Verlag Berlin Heidelberg, 2006.
- [17] I.J.S. C. C. Ling, J. Mitchell, R. Stickler, The Variation of OER with Dose Rate, *International Journal of Radiation Oncology* 11 (1985) 1367-1373.

- [18] P.M. Devlin, *Brachytherapy Applications and Techniques*, Lippincott Williams & Wilkins, Philadelphia, 2007, pp. 52.
- [19] S. Nag, *High Dose Rate Brachytherapy: a textbook*, Futura, New York.
- [20] I. Medi-Physics, OncoSeed Iodine-125 Seeds, in: O.b.G. Healthcare (Ed.), 2009.
- [21] R.E.M. H.L. Andrews, E. J. LeBrun, Gel Dosimeter for Depth-Dose Measurements, *Review of Scientific Instruments* 28 (1957) 329-332.
- [22] Y.S.K. J. C. Gore, R. J. Schulz, Measurement of radiation dose distributions by nuclear magnetic resonance (NMR) imaging, *Physics in Medicine and Biology* 29 (1984) 1189-1197.
- [23] B.A.W. L. E. Olsson, A. Fransson, B. Nordell, Diffusion of ferric ions in agarose dosimeter gels *Physics in Medicine and Biology* 37 (1992) 2243-2252.
- [24] P.J.H. C. Baldock, A. R. Piercy, B. Healy, Experimental determination of the diffusion coefficient in two-dimensions in ferrous sulphate gels using the finite element method., *Australasian Physical & Engineering Sciences in Medicine* 24 (2001) 19-30.
- [25] J.C.G. M. J. Maryanski, R. P. Kennan, R. J. Shulz, NMR Relaxation Enhancement in gels polymerized and cross-linked by ionizing radiation: a new approach to 3D dosimetry by MRI *Magnetic Resonance Imaging* 11 (1993) 253-258.
- [26] Y.D.D. C Baldock, S. Doran, G. Ibbott, A. Jirasek, M. Lepage, K. B. McAuley, M. Oldham, L. J. Schreiner, Polymer Gel Dosimetry, *Physics in Medicine and Biology* 55 (2010) R1-R63.

- [27] R.J.S. M. J. Maryanski, G. S. Ibbott, J. C. Gatenbym J. Xie, D. Horton, J. C. Gore, Magnetic Resonance Imaging of Radiation Dose Distribution using a polymer-gel dosimeter, *Physics in Medicine and Biology* 39 (1994) 1437-1455.
- [28] M.R. J. C. Gore, M. J. Maryanski, R. J. Schulz, Radiation dose distributions in three dimensions from tomographic optical density scanning of polymer gels: I. Development of an optical scanner, *Physics in Medicine and Biology* 41 (1996) 2695-2704.
- [29] Y.Z.Z. M. J. Maryanski, J. C. Gore, Radiation dose distributions in three dimensions from tomographic optical density scanning of polymer gels: II. Optical properties of the BANG polymer gel, *Physics in Medicine and Biology* 41 (1996) 2705-2717.
- [30] J.H.S. M. Oldham, S. Kumar, J. Wong, D. A. Jaffray, Optical-CT gel-dosimetry I: Basic investigations, *Medical Physics* 30 (2003) 623-635.
- [31] L.K. M. Oldham, Optical-CT gel-dosimetry II: Optical artifacts and geometrical distortion, *Medical Physics* 31 (2004) 1093-1205.
- [32] J.A. P. Guo, M. Oldham, A practical three-dimensional dosimetry system for radiation therapy, *Med Phys* 33 (2006) 3962-3972.
- [33] M.J.M. J. Adamovics, New 3D radiochromic solid polymer dosimeter from leuco dyes and a transparent polymeric matrix, *Medical Physics* 30 (2003) 1349-1349.
- [34] M.J.M. J. Adamovics, Characterisation of PresageTM: A New 3-D Radiochromic Solid Polymer Dosemeter for Ionising Radiation, *Radiation Protection Dosimetry* 120 (2006) 107-112.
- [35] J.A.A. P.Y. Guo, M. Oldham, Characterization of a new radiochromic three-dimensional dosimeter, *Med Phys* 33 (2006) 1338-1345.

- [36] J.A. H.S. Sakhalkar, G. Ibbott, M. Oldham, A comprehensive evaluation of the PRESAGE/optical-CT 3D dosimetry system, *Medical Physics* 36 (2008) 71-82.
- [37] M.O. A. Thomas, Fast, large field-of-view, telecentric optical-CT scanning system for 3D radiochromic dosimetry, *Journal of Physics: Conference Series* 250 (2010).
- [38] J.A. A. Thomas and J. Newton, M. Oldham, Commissioning and benchmarking a 3D dosimetry system for clinical use, *Med Phys* 38 (2011) 4846-4857.
- [39] K.J. J. Adamovics, J. Dietrich, PRESAGE- Development and optimization studies of a 3D radiochromic plastic dosimeter- Part 1, *Journal of Physics: Conference Series* 56 (2006) 172-175.
- [40] J.A. H. Sakhalkar and D. Sterling, G. Ibbott, M. Oldham, Investigation of the feasibility of relative 3D dosimetry in the Radiologic Physics Center Head and Neck IMRT phantom using Presage/optical-CT, *Medical Physics* 36 (2009) 3371-3377.
- [41] A.T. C. Clift, J. Adamovics, Z. Chang, I. Das, M. Oldham, Toward Acquiring Comprehensive Radiosurgery Field Commissioning Data using the PRESAGE/optical-CT 3D Dosimetry System, *Institute of Physics and Engineering in Medicine* 55 (2010) 1279-1293.
- [42] J.A. M. Heard, G. S. Ibbott, Measurement of a 200 MeV proton beam using a polyurethane dosimeter, *Journal of Physics: Conference Series* 56 (2006).
- [43] S.D. S. Al-Nowais, A. Kacperek, N. Krstajic, J. Adamovics, D. Bradley, A preliminary analysis of LET effects in the dosimetry of proton beams using PRESAGE and optical CT, *Applied Radiation and Isotopes* 67 (2009) 415-418.

- [44] J.A. P. Wai, N. Krstajic, A. Ismail, A. Nisbet, S. Doran, Dosimetry of the microSelectron-HDR Ir-192 source using PRESAGE and optical CT, *Applied Radiation and Isotopes* 67 (2009) 419-422.
- [45] R.H. T. Gorjiara, J. K. Kim, Z. Kuncic, J. Adamovics, C. Baldock, Study of dosimetric water equivalency of PRESAGE for megavoltage and kilovoltage x-ray beams, *Journal of Physics: Conference Series* 250 012053 (2010).
- [46] A.I.B. J. O. Deasy, V. H. Clark, CERR: A computational environment for radiotherapy research, *Medical Physics* 30 (2003) 979-987.
- [47] F.M. Khan, *The Physics of Radiation Therapy*, 4 ed., Lippincott Williams & Wilkins, Baltimore, 2010.

Olivia Huang was born in Columbia, Missouri on December 4, 1987 to the parents of Wei-an and Meng-fen Huang. After completing her Human Biology Degree at the University of California, San Diego in 2010, she entered the Medical Physics program at the University of Texas-Houston M.D. Anderson Cancer Center. She completed her research project and the Specialized Masters Degree in Medical Physics in August 2013.

Permanent Address:

20488 Chalet Lane

Saratoga, CA 95070

Email:

oli.huang@gmail.com